PhD THESIS

Department of Chemistry
Università degli Studi di Torino

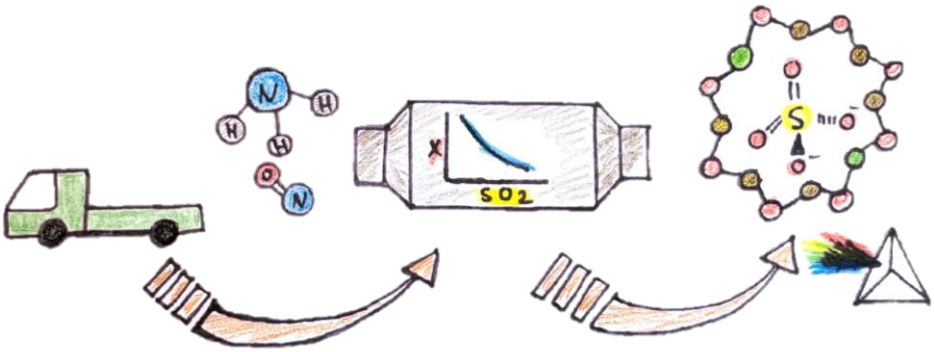

Characterization and Testing of SO_2 Poisoning Effect on Cu-CHA Zeolites

REZA KHALEGHI ABASABADI

Doctoral School of the University of Torino
PhD Program in Chemical and Materials Sciences - XXXVII cycle
www.unito.it

“This being human is a guest house.
Every morning a new arrival.

A joy, a depression, a meanness,
some momentary awareness comes
as an unexpected visitor.

Welcome and entertain them all...”

Jalal al-Din Rumi

Università degli Studi di Torino
Doctoral School of the University of Torino
PhD Program in Chemical and Materials Sciences - XXXVII cycle

Characterization and testing of SO_2 poisoning effect on Cu-CHA zeolites

Candidate: **Reza Khaleghi Abasabadi**

Supervisors: Prof.ssa **Gloria Berlier**

Dr. **Ton V. W. Janssens**

Prof.ssa **Elisa Borfecchia** – Co-supervisor

Jury Members: Prof. **Marco Daturi**
University of Caen

Prof. **Anker Degn Jensen**
Technical University of Denmark

Dr. **Matteo Signorile**
University of Turin

Head of the Doctoral School: Prof. Eleonora Bonifacio

PhD programme Coordinator: Prof. Bartolomeo Civalleri

Preface

This PhD thesis represents my academic and industrial exploration and research in the field of catalysis, with a focus on a deactivation of Cu-chabazite (Cu-CHA) zeolite catalyst by SO_2 in the ammonia-assisted selective catalytic reduction (NH_3-SCR) of nitrogen oxides (NOx) from diesel exhaust systems. In this study I have investigated a catalytic behavior under different operating conditions, including exposure to SO_2, using spectroscopic techniques, characterization and catalytic testing.

The research is presented in four main chapters. **Chapter 1** provides a literature review about the mechanism of Cu-CHA catalyst in NH_3-SCR reaction and the deactivation of the catalyst by SO_2. **Chapter 2** shows how SO_2 affects the Cu-CHA catalyst in the NH_3-SCR reaction at 200 ºC, using *in situ* diffuse reflectance UV-vis spectroscopy, SO_2 uptake measurements, and catalytic testing. The reactivity of SO_2 with several Cu species, which are formed under specific treatment conditions, was examined at 200 ºC. By examining the UV-vis spectra and the first-order rate constant, we investigated the effect of Si/Al ratio on the activity of Cu-CHA catalyst and its reactivity to SO_2. The measured deactivation and quantified UV-vis spectra changes are analyzed in terms of a proposed reaction mechanism, also considering the impact of the zeolite Si/Al ratio.

Chapter 3 explores the impact of water on Cu-CHA catalyst behavior during SO_2 exposure in the NH_3-SCR reaction. The observations of catalytic testing and SO_2 uptake measurements clarify the different influence of O_2 or H_2O on catalyst deactivation by SO_2. Through techniques such as *in situ* FT-IR spectroscopy, temperature-programmed desorption and Raman spectroscopy, the study examines the effects of combined SO_2/H_2O exposure on catalyst deactivation. Through systematic experimentation and analysis, a mechanism for wet SO_2 poisoning is proposed.

Chapter 4 focuses on the SO_2 sensitivity of Cu-CHA catalysts, introducing a formalism to quantify the deactivation in terms of the sensitivity for SO_2 without relying on kinetic assumptions. By applying this methodology to catalysts with different Cu loadings and Si/Al ratios, the study identifies high SO_2 sensitivity at the beginning of SO_2 exposure. This chapter provides a

model based on a quadratic equation which allows to predict the decrease of the activity as a function of the uptake of SO_2 for different catalyst composition.

This work was carried out as part of a collaborative effort between the Department of Chemistry of University of Turin and Umicore Aps Denmark under the Marie Skłodowska-Curie Innovative Training Networks (ITN) project, "CHASS". The characterization part was performed at the University of Turin over 18 months. The catalytic testing and kinetic study were carried out at Umicore Aps Denmark through 18 months, as well.

This thesis would not have been possible without the guidance, support, and encouragement of several individuals and institutions. I express my deepest gratitude to my supervisors, Prof.ssa Gloria Berlier and Dr. Ton V. W. Janssens whose expertise and mentorship were invaluable throughout this journey. I am equally thankful to my colleagues, especially from CHASS group for their collaboration and stimulating discussions, and to the technical staff for their assistance with experimental setups and data acquisition both at the University of Turin and Umicore Aps Denmark.

I am also deeply grateful to my family and friends in Italy, Iran and Denmark for their unwavering support and understanding during the demanding phases of my research. Their encouragement has been a source of strength and inspiration.

Finally, I acknowledge the financial and logistical support provided by the European Union's Horizon 2020 research and innovation program under the Marie Sklodowska-Curie grant agreement No. 955839 (CHASS), which enabled the successful execution of this project.

I hope that this thesis will serve as a meaningful contribution to the field of catalysis and inspire further research in developing sustainable solutions for environmental challenges.

Table of contents

I Chapter I: Literature review

The term 'nitrogen oxides' (NOx) usually refers to NO and NO_2 which have significant effect on human health and the enviroment.[1] The main responsible for the anthropogenic emission of NOx in the atmosphere are the combustion processes in plants, incinerators and vehicles, where NOx is formed by reaction of N_2 and O_2 at high temperature. The emission from road transport is considered as one of the significant sources of NOx pollution, [2] with a particular focus on heavy-duty diesel vehicles for freight transport.[3] The lean conditions used in a diesel engine improve its efficiency but also make the reduction of NOx to N_2 unfavorable, due to the presence of O_2 in the exhaust gases.

Different processes have been proposed to control NOx emission from diesel vehicles. One effective way is the selective catalytic reduction (SCR) with ammonia as reducing agent, generated in situ by thermal decomposition of urea.[4] The main reactions of NH_3-SCR are shown as

$$4\,NH_3 + 4\,NO + O_2 \rightarrow 4\,N_2 + 6\,H_2O \qquad \textit{I.1)}$$

$$2\,NH_3 + NO + NO_2 \rightarrow 2\,N_2 + 3\,H_2O \qquad \textit{I.2)}$$

$$8\,NH_3 + 6\,NO_2 \rightarrow 7\,N_2 + 12\,H_2O \qquad \textit{I.3)}$$

Which Eq.I.1 is considered as the standard SCR reaction.[5] Fast SCR reaction (Eq.I.2) occurs in presence of both NO and NO_2 which, accelerates the reaction. The NO_2-SCR (Slow SCR reaction, Eq.I.3) can take place when NO_2 concentration is higher than NO one.[6] The standard SCR is the main reaction for our studies in this thesis.

I.1 Cu ion-exchanged chabazite zeolites (Cu-CHA)

The most significant SCR catalysts include supported vanadium oxide (typically VOx-TiO_2), iron and copper exchanged zeolites.[5] Among Cu-exchanged zeolites, the Cu-CHA catalyst has shown a good activity at low temperatures and reasonable hydrothermal stability.[7] Thanks to these superior performances it is currently commercialized as catalysts for the NH_3-SCR reaction on diesel exhaust gases treatment systems.[7] The chabazite zeolite (also known as SSZ-13) has a framework structure characterized by 6 and 8-

membered rings, 6MR and 8MR respectively. The 8MRs define access to the chabazite cage, with a diameter of 3.8 Å. The negative charges induced on the framework by the presence of Al^{3+} heteroatoms are balanced by counterions, typically H^+, [8] which in Cu-CHA are partially exchanged with Cu^{II} ions, which can reversibly change their oxidation state between Cu^{II} and Cu^{I} depending on the treatment conditions. [9]

The speciation of framework coordinated Cu ions depends on the zeolite composition, *e.g.* on Cu loading, Si/Al ratio and Al distribution in the framework. The most thermodynamically stable Cu^{II} sites are stabilized by two negative charges in 6MR; these are often referred to as fw-Cu^{II}. If only a negative charge is present, an extra ligand is needed for charge compensation, and fw-$[Cu^{II}(OH)]^+$ are formed in 8MR.[9–11] The relative concentration of fw-Cu^{II} and fw-$[Cu^{II}(OH)]^+$ was computed as a function of Si/Al ratio and Cu/Al ratio, based on the assumption that fw-Cu^{II} are formed first, followed by fw-$[Cu^{II}(OH)]^+$ (Figure I.1). There are many experimental confirmation of this model, so that based on the Cu content and Si/Al ratio of the zeolite, one can prepare and study zeolites with a majority of fw-Cu^{II} or fw-$[Cu^{II}(OH)]^+$ sites. [12–14] Moreover, fw-Cu^{I} sites can be formed by treatment in an inert or reducing atmosphere. [9]

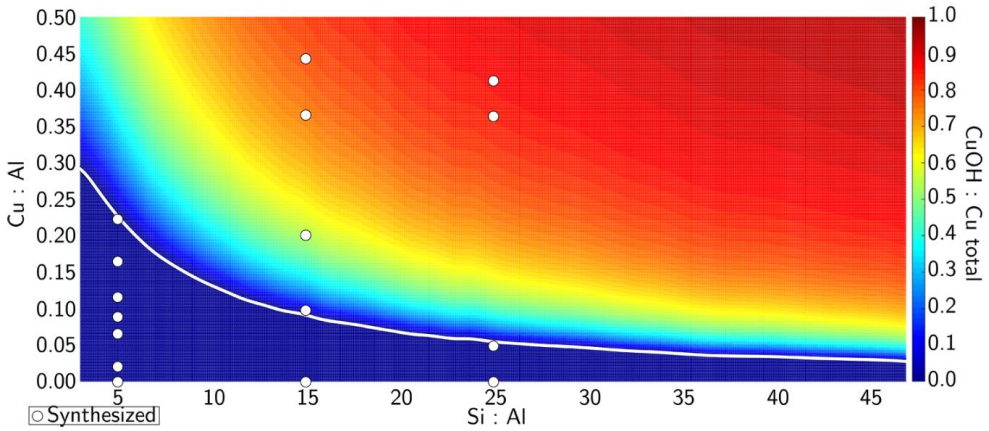

Figure I.1- Distribution of Cu sites on Cu-CHA catalyst as a function of Si/Al and Cu/Al ratios. The blue and red regions indicates a predominance fw-Cu^{II} and fw-$[Cu^{II}(OH)]^+$, respectively.[15]

I.2 NH_3-SCR reaction on Cu-CHA catalysts

Different NH_3-SCR reaction mechanisms have been proposed along the years.

A common understanding is that it is based on a redox cycle between Cu^{II} and Cu^{I} ions, so that it can be divided into an oxidation and reduction half cycles.[10] A lot of attention has been devoted to the oxidation half-cycle, which can be obtained in a NO/O_2 mixture or with O_2 alone. However, more recent studies from the group of Prof Tronconi also focused on the relevance of the reduction half-cycle. This is carried out by exposing the catalyst to an NO/NH_3 mixture. [16,17] Concerning the oxidation half-cycle, the main issue is the reactivity of O_2 with Cu^{I} ions.[10,16,18,19] The oxidation of Cu^{I} is a one electron process, while the reduction of O_2 is a four electrons one.[20–23] It has been proposed that O_2 activation can be favored by the presence of NO, or by pairs of Cu^{I} ions. Multinuclear Cu_xO_y species have been indeed observed in Cu-CHA treated in oxidizing conditions.[13,24,25] However, this possibility is limited by the Al content and distribution in the framework. Some mobility of framework coordinated Cu ions, which could favor the formation of Cu^{I} pairs able to activate O_2 has been reported during thermal treatments, both mildly reducing (self-reduction in inert conditions, favoring migration of Cu^{I} ions from 6MR to 8MR) or in oxidizing conditions, leading to a redistribution of Cu^{II} sites from fw-$[Cu^{II}(OH)]^+$ to fw-Cu^{II}.[26–28]

In NH_3-SCR conditions at low temperature (below 250 °C), Cu sites are coordinated by different ligands like NH_3, NOx^- and OH^-.[10,15,16,29] The formation of mobile complex of Cu^{I} solvated by NH_3 ($[Cu^{I}(NH_3)_2]^+$) has been shown by X-ray absorption spectrsocopy.[10,30,31] The $[Cu^{I}(NH_3)_2]^+$ complex shows a weak interaction with framework and mobility under SCR conditions.[15,32,33] During NH_3-SCR reaction, the $[Cu^{I}(NH_3)_2]^+$ complexes play an important role to activate O_2.[22,34,35] According to a 2nd order dependence to the Cu content for the activity of Cu-CHA catalysts in NH_3-SCR reaction, it is reasonable to consider the oxidation of pairs of $[Cu^{I}(NH_3)_2]^+$ complexes as rate determining. [20,22,23] By decreasing the Cu loading, the possibility of pairing two $[Cu^{I}(NH_3)_2]^+$ complexes becomes lower because of a long average distance between Cu ions.[15,22] A comparison between $[Cu^{I}(NH_3)_2]^+$ complex and fw-Cu^{I} show an increase in the reaction with O_2 for $[Cu^{I}(NH_3)_2]^+$ complex.[36] This changes by increasing temperature above 200 °C, because of the decomposition of $[Cu^{I}(NH_3)_2]^+$ complex and loss of Cu mobility.[37,38] Then, the fw-Cu^{I} becomes more significant and plays an important role for NH_3-

SCR reaction at higher temperatures.[39,40]

A $[Cu_2^{II}(NH_3)_4O_2]^{2+}$ complex has been proposed to be formed from the reaction of two $[Cu^{I}(NH_3)_2]^{+}$ complexes and O_2 at 200 °C. From XAS, DFT and Diffuse reflectance ultraviolet-visible (DR-UV-Vis) studies, it has been suggested that its structure can be described as μ-η^2, η^2-peroxo diamino dicopper(II).[41,42] The spectra of X-ray absorption near edge structure (XANES), Extended X-ray absorption fine structure (EXAFS) and DR-UV-Vis shows that Cu^{II} species after oxidation of $[Cu^{I}(NH_3)_2]^{+}$ complexes are different from Cu^{II} species by heating up at 400 °C. The DR UV-Vis spectrum of $[Cu_2^{II}(NH_3)_4O_2]^{2+}$ exhibits a broad band in d-d transition region centered at 13850 cm^{-1} and a ligand-to-metal charge transition (LMCT) which are different from fw-Cu^{II}.[43] The efficiency of formation of $[Cu_2^{II}(NH_3)_4O_2]^{2+}$ complexes from $[Cu^{I}(NH_3)_2]^{+}$ pairs has been at first rationalized only in terms of Cu density, affecting the Cu-Cu average distance.[22] However, since the process involves charged entities, it is reasonable to expect that the mobility of the $[Cu^{I}(NH_3)_2]^{+}$ complexes and formation of $[Cu_2^{II}(NH_3)_4O_2]^{2+}$ complex is influenced by the zeolite Si/Al ratio. This is in agreement with the observation that Si/Al ratio influences the catalytic activity, at fixed Cu loading.[44,45] The amount of formed $[Cu_2^{II}(NH_3)_4O_2]^{2+}$ complex was found to be higher for Cu-CHA with Si/Al ratio of 5 compared to Si/Al ratio of 29 with similar Cu loading. This also corresponded to a higher activity of the former with respect to the latter at low temperature. [44] The authors also observed an influence of the Si/Al ratio on the structure of the $[Cu_2^{II}(NH_3)_4O_2]^{2+}$ complex, present with a 'planar' and/or 'bent' CuO_2Cu core.[44]

Based on these evidences, the oxidation and reduction half-cycles of the NH_3-SCR reaction at 200 °C can be studied as the oxidation of the $[Cu^{I}(NH_3)_2]^{+}$ complexes with O_2 and reduction of $[Cu_2^{II}(NH_3)_4O_2]^{2+}$ complex with NO/NH_3, respectively. In the latter step, N_2 and H_2O are formed, so that it can inferred that the activity of Cu-CHA in NH_3-SCR at low temperatures depends on the reactivity of $[Cu_2^{II}(NH_3)_4O_2]^{2+}$ complex with NO/NH_3. This has been confirmed by operando XAS studies. Moreover, the reactivity of the $[Cu_2^{II}(NH_3)_4O_2]^{2+}$ complex to NH_3 and NO alone has been studied. The former shows a relatively slow and partial reduction of the complex. The reaction of $[Cu_2^{II}(NH_3)_4O_2]^{2+}$ complex with NO displays a more efficient reduction

accompanied by N_2 production. The reaction stops when the necessary ingredients (NH_3 and O_2 in the complex) are consumed. This furthermore confirms the activity of the $[Cu_2^{II}(NH_3)_4O_2]^{2+}$ complex in the reaction, and the importance of the reduction step.[43]

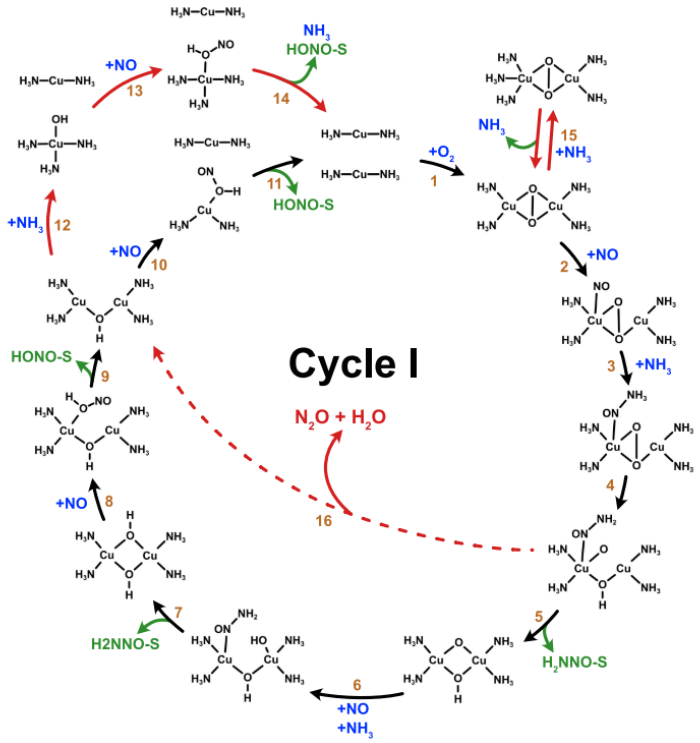

Figure I.2- The cycle of NH_3-SCR reaction on Cu-CHA catalyst at low temperature, proposed on the basis of first-principle calculations.[48] The S represents an Brønsted acid site.

The mechanism of the redox cycle, involving the oxidation of $[Cu^{I}(NH_3)_2]^{+}$ complexes in O_2 and a reduction of $[Cu_2^{II}(NH_3)_4O_2]^{2+}$ complex in NO/NH_3 has been studied by a first-principle microkinetic model (Figure I.2). [46–48] The key point is that it is necessary to have two $[Cu^{I}(NH_3)_2]^{+}$ complexes in one cage to adsorb O_2 which is feasible based on small diffusion barrier in one cage for complexes. Then, two $[Cu^{I}(NH_3)_2]^{+}$ complexes can adsorb O_2 and start the reaction cycle to form the $[Cu_2^{II}(NH_3)_4O_2]^{2+}$ complex. NO adsorb on a Cu atom of the $[Cu_2^{II}(NH_3)_4O_2]^{2+}$ complex which is more reasonable than adsorption on O atom. Then, NH_3 is adsorbed by reaction with NO and formation of H_2NNO which coordinates to a site. Its decomposition to N_2 and

H_2O is proposed to occur over Brønsted acid sites. The second and third NO and NH_3 adsorb and form H_2NNO and HONO which again decompose to NO and H_2O on Brønsted acid sites. HONO needs one NH_3 to form H_2O and H_2NNO which can decompose to N_2 and H_2O. There are two possibilities for the fourth NO and NH_3 adsorption which is shown at the end of cycle. Based on this cycle, 4 NO and 4 NH_3 adsorb and form 4 N_2 and 6 H_2O. Adsorption of NH_3 instead of NO at the beginning of cycle on $[Cu_2^{II}(NH_3)_4O_2]^{2+}$ complex inhibit the cycle of reaction and NO cannot adsorb and react. This side-reaction is in agreement with the observation that NH_3 can block and inhibit the NH_3-SCR reaction at low temperature.[49,50]

I.3 Exposure of Cu-CHA catalyst to SO_2

One significant concern about Cu-CHA catalyst is its loss of activity after a long exposure to SO_2, even in small concentration. This can be seen in Figure I.3, showing that the deactivation is particular important below 350 °C, already after one hour of exposure to SO_2.[51,52] It has been proposed by Hammershøi et al. that the final deactivation (measured at 220 °C) of Cu-CHA catalyst is 0.85-0.95 based on the temperature of SO_2 exposure (200, 300, 400 and 500 °C). Deactivation increases with longer exposures to SO_2, but in a lower degree. SO_2 uptake was measured and expressed as S/Cu molar ratio, ranging from 0.5 to 1. The key point is that a large deactivation is observed in correspondence of a small SO_2 uptake in a short time. The regeneration of catalysts at 550 °C in a flow of 10% O_2, 5% H_2O and N_2 can restore around 80% of the activity. The S/Cu ratio after regeneration did not exceed 0.2 and reached a stable level after 120 hours of regeneration. This could correspond to some Cu-interacting sulfur species which are stable at 550 ºC.[52] Then, the main observation is that Cu-CHA catalyst shows a maximum deactivation of 95% and 20% before and after regeneration, respectively.

The regenerated catalyst was characterized by a 0.2 S/Cu ratio which corresponds to an irreversible deactivation. The irreversible part does not affect the activation energy of Cu-CHA catalysts in NH_3-SCR reaction. It means that the irreversible deactivation corresponds to a stable Cu sulfate formation. The interesting point is that the presence of H_2O always causes higher S/Cu ratio for the irreversible part of the deactivation. In addition, the

irreversible deactivation is higher for sample exposed to SO_2 at a low temperature.[53]

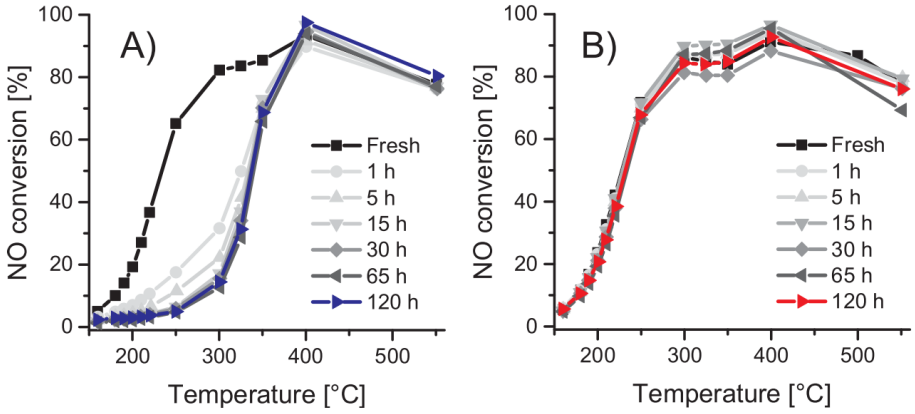

Figure I.3- NO conversion with respect to the temperature in the NH3-SCR reaction. a) the SO2 exposed catalysts at 200 °C, b) the regenerated catalysts after heating at 550 °C for 6 h.[52]

As mentioned, a small amount of SO_2 can deactivate Cu-CHA catalysts severely, particularly in the reversible part. Namely, small SO_2 uptakes in the reversible part (S/Cu ratio of 0.1-0.2) cause a deactivation around 60-80%. The reversible part displays a lower activation energy which can be restored after regeneration at 550 °C. This could be related to an internal diffusion limitation which is important in deactivation process. However, according to the calculation of diffusion coefficient, it was shown that there are no internal diffusion limitations for Cu-CHA catalysts. In this case, the high deactivation with small amount of S/Cu ratio could be correspond to a direct interaction of Cu and sulfur containing species. In addition, a correlation was observed between the activation energy for regenerated catalyst and the diffusion effect on the irreversible deactivation. Based on this, the reversible deactivation with the same SO_2 uptake as the irreversible one cannot confirm an internal diffusion limitation to deactivate the catalyst around 60-80%, as well. It was proposed that the reversible deactivation causes an inhibition of the formation of $[Cu^{I}(NH_3)_2]^+$ complex and a consequent decrease in the mobility of Cu ions.[53]

A mixture of SO_3 and SO_2 was investigated compared to SO_2 only to deal with a most realistic speciation of SOx in an exhaust gas. By adding SO_3,

deactivations were significantly increased at 200, 300 and 400 ºC for Cu/beta zeolite based catalyst. It was shown that the storage and removal of sulfur is different when SO_3 is present with respect to SO_2 only. However, EXAFS results showed that the sulfate formation from SO_2/SO_3 exposure does not change the local structure of Cu sites.[51] The effect of SO_3 caused more severe deactivation at low temperatures which was difficult to reverse. The presence of SO_3 has a bit impact on reversible and irreversible deactivation at high temperatures.[53]

Different mechanisms can take place by adsorption of SO_2/SO_3 species on Cu site at low and high temperatures.[54] The formation of Cu sulfate species is a result of a reaction of SO_3 and Cu^{II} site in wet conditions.[55] A higher S/Cu ratio was measured in presence of H_2O which can be related to access of more Cu sites to SO_3. According to first-principles calculations, bisulfite and bisulfate species are formed from a reaction of monomeric Cu sites and SO_2. However, only bisulfate has been observed after reaction of SO_3 with mono- and dicopper species. In addition, the adsorption of SOx on dicopper is more thermodynamically favored than on monocopper. It means that the Cu species affect the stability of sulfur species which are formed during SOx exposure.[55]

One of the significant parameters for SO_2 exposure is the presence of water vapor in the flow. It was found that the deactivation of Cu-CHA catalysts is more severe under SCR conditions compared to SO_2/H_2O. This observation is referred to a possibility of the formation of ammonium sulfate species on the catalysts.[56–58] Generally speaking, analysis if the literature shows that the effect of SO_2 on the catalytic activity of Cu-CHA in the NH_3-SCR reaction has been studied in a large variety of conditions, such as SO_2 alone, SO_2/O_2, SO_2/SO_3, SO_2/H_2O, $SO_2/O_2/H_2O$, SO_2 in the NH_3-SCR mixture in both dry and wet conditions. Moreover, different effects have been observed when exposure was carried out at low (< 250 °) or high temperature. Concerning the speciation of sulfur-based species formed in this process, there is a general agreement about the formation of sulfates, mainly classified as ammonium sulfate and Cu-based sulfates.[59] This aspect will be dealt with in the introduction of Chapter IV.

I.4 Investigation SO_2 interaction with Cu sites in Cu-CHA catalysts

Different studies have focused on the specificity of SO_2 interaction with the different Cu species present in Cu-CHA. In one contribution, the SO_2 interaction with framework coordinated fw-Cu^{II} and fw-$[Cu^{II}(OH)]^+$ sites was analysed, by considering zeolites with different Si/Al ratio and Cu loading. In Figure I.4, Temperature-programmed desorption (TPD)-SO_2 studies show the formation of more stable sulfate species for Cu-CHA catalyst with low Si/Al ratio, characterized by a relative abundance of fw-Cu^{II} sites. This catalyst showed higher formation of ammonium sulfate species when Cu-CHA was exposed to NH_3/SO_2. On the contrary, the catalyst with higher Si/Al ratio displays a formation of Cu bisulfate species which are more stable during SO_2-TPD (Figure I.4).[60]

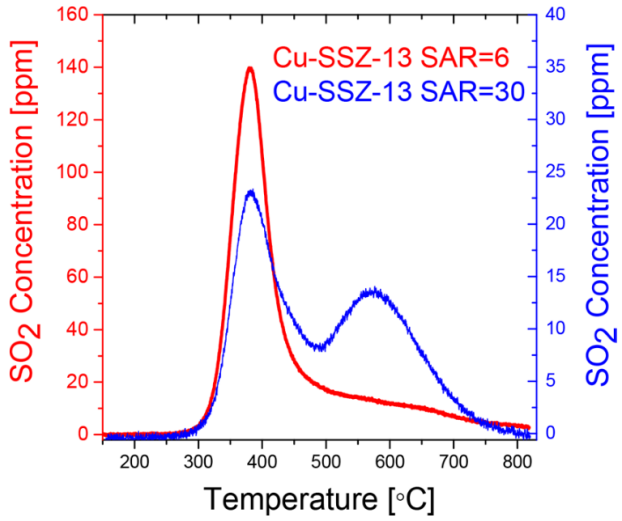

Figure I.4- SO_2 TPD of Cu-CHA with Si/Al ratio of 6 and 30 after exposure to 50 ppm SO_2, 500 ppm NH_3, 10% O_2, 5% H_2O and N_2 at 150 °C, a heating rate of 10 °C/min in N_2.[60]

The fw-Cu^{II} was shown more resistant than fw-$[Cu^{II}(OH)]^+$ after dry SO_2 poisoning of Cu-CHA catalysts. The SCR reaction rate per Cu showed a linear decrease by adding sulfur as mol_S:mol_{Cu} for Cu-CHA with more fw-Cu^{II}. However, apparent activation energy and reaction order did not change after SO_2 exposure. The S/Cu ratio was higher than that measured for Cu-CHA with more fw-$[Cu(OH)]^+$. In this case, the apparent activation energy changed after

SO_2 exposure. The bisulfate species was considered as sulfate species that can bond to Cu sites. Cu sites can bond to one or two HSO_4^- and become mobile which seems more feasible for fw-$[Cu^{II}(OH)]^+$ than for fw-Cu^{II}. Based in these results, it was concluded that Cu-CHA with low Si/Al ratio are more resistant to deactivation.[61]

The different reactivity of fw-Cu^{II} and fw-$[Cu^{II}(OH)]^+$ were also evaluated by EPR after SO_2 exposure of Cu-CHA catalyst with 2.81 Cu wt% and a Si/Al = 15 which form stable species on fw-$[Cu^{II}(OH)]^+$. The fw-Cu^{II} was unaffected by exposure to SO_2 which could be the reason for deactivation levelling off around 90%.[62] It has been shown that H_2-Temperature-programmed reduction (H_2-TPR) can be one of the ways to analzye different Cu species in a CHA zeolite with 2 Cu wt% and a Si/Al = 11.4. Three H_2-TPR peaks were assigned to: i) fw-$[Cu^{II}(OH)]^+$ and fw-$[Cu^{II}OCu^{II}]^{2+}$ at 220 ºC, ii) fw-Cu^{II} and fw$[Cu^{II}HOOHCu^{II}]^{2+}$ at 360 ºC and iii) paired fw-Cu^{II} and fw-$[Cu^{II}OOCu^{II}]^{2+}$ at 500 ºC.[63] A pair of Cu^{II} at hight temperature can form fw-$[Cu^{II}OOCu^{II}]^{2+}$ which is important for the methane-to-methanol reaction.[64] The regeneration of catalysts in SCR gas was followed by SO_2-TPD, showing SO_2 desorption at 400 ºC which is lower compared to 650 ºC, related to regeneration in inert gas. This shows that the gas composition sulfur can affect the regeneration process by formation of different sulfur species.[65]

The effect of SO_2 exposure on different Cu species, including the NH_3-solvated complexes observed at low temperature (200 °C) was studied. It was observed that the $[Cu_2^{II}(NH_3)_4O_2]^{2+}$ complexes, which are relevant intermediates in the NH_3-SCR reaction, are more sensitive to SO_2 than other Cu^{II} and Cu^{I} species. This can be observed by the changes in EXAFS and XANES spectra, and in the higher S/Cu ratio with respect to the other states of the catalysts (Figure I.5, left and right panels, respectively). The uptake of SO_2 and sensitivity to fw-Cu^{I} is negligible after similar SO_2 exposure, while species formed after exposure of fw-Cu^{II} to NH_3 (a combination of $[Cu_2^{II}(NH_3)_4O_2]^{2+}$ and $[Cu^{I}(NH_3)_2]^+$ complexes) show some changes and a relatively high SO_2 uptake. The key point is that the changes of XAS data are approximately correlated with SO_2-TPD results.

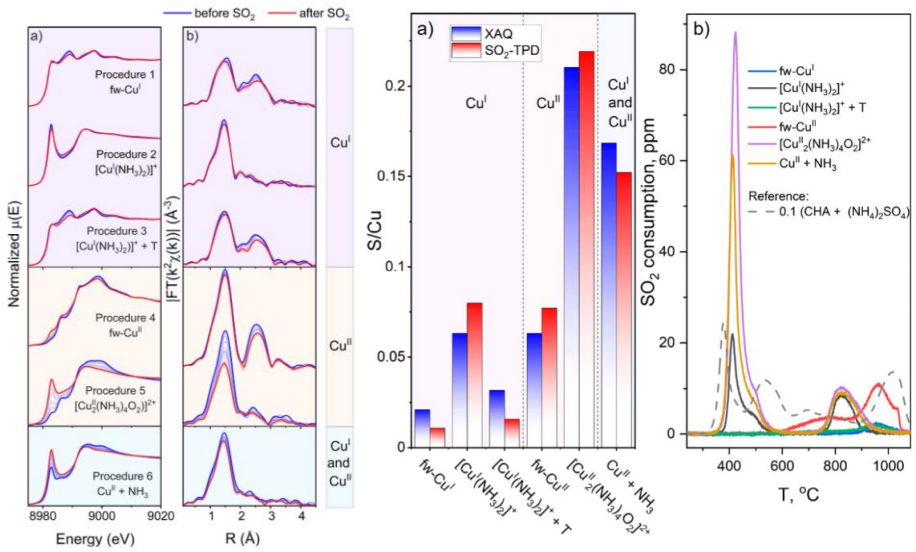

Figure I.5- XANES, EXAFS, SO_2-TPD and S/Cu ratio measurements of SO_2 exposure of different Cu species at 200 °C.[66]

Another important point is the comparison of SO_2-TPD results after SO_2 exposure to the different Cu species and the SO_2-TPD of $(NH_4)_2SO_4$ impregnated in Cu-free chabazite (H-CHA). The temperature of SO_2 desorption is 40 °C lower for H-CHA + $(NH_4)_2SO_4$ (380 °C) compared to the species formed after SO_2 exposure of $[Cu_2^{II}(NH_3)_4O_2]^{2+}$ complex (420 °C), suggesting that the formed sulfate species are not $(NH_4)_2SO_4$. Some reports mention that the desorption of SO_2 at 420 °C is a fingerprint for $(NH_4)_2SO_4$ or NH_4HSO_4 species.[59–61] The difference in desorption temperatures in the two experiments could be related to different experimental conditions, such as temperature ramp. Cu Kβ valence-to-core XES (X-ray emission spectroscopy) showed that Cu does not interact with S, suggesting that the possible SOx binding to the Cu is carried out through an oxygen atom after SO_2 exposure of $[Cu_2^{II}(NH_3)_4O_2]^{2+}$ complex.[66]

The reaction of $[Cu_2^{II}(NH_3)_4O_2]^{2+}$ complex with SO_2 has been investigated by Density Functional Theory (DFT). In Figure I.6, an energy landscape shows the reaction of $[Cu_2^{II}(NH_3)_4O_2]^{2+}$ complex with SO_2. In the first steps SO_2 adsorbs on one of O atoms of the $[Cu_2^{II}(NH_3)_4O_2]^{2+}$ complex and reacts with another O to form a stable sulfate species (III structure in Figure I.6). This sulfated species can react with NO and NH_3 to form N_2, H_2O and H_2SO_4. In

this process H_2NNO is formed, which can desorb and decompose on Brønsted sites to form N_2 and H_2O. One of the Cu atoms in the $[Cu_2^{II}(NH_3)_4O_2]^{2+}$ complex is reduced to Cu^I and form $[Cu^I(NH_3)_2]^+$, while the other Cu is involved in the formation of Cu^{II}-bisulfate with NH_3 (VII). After repeating the adsorption of NO and NH_3, another $[Cu^I(NH_3)_2]^+$ complex and H_2SO_4 are formed (X). In agreement with experiments, it was shown that SO_2 interacts weakly with $[Cu^I(NH_3)_2]^+$ complexes, without formation of chemical bonds.

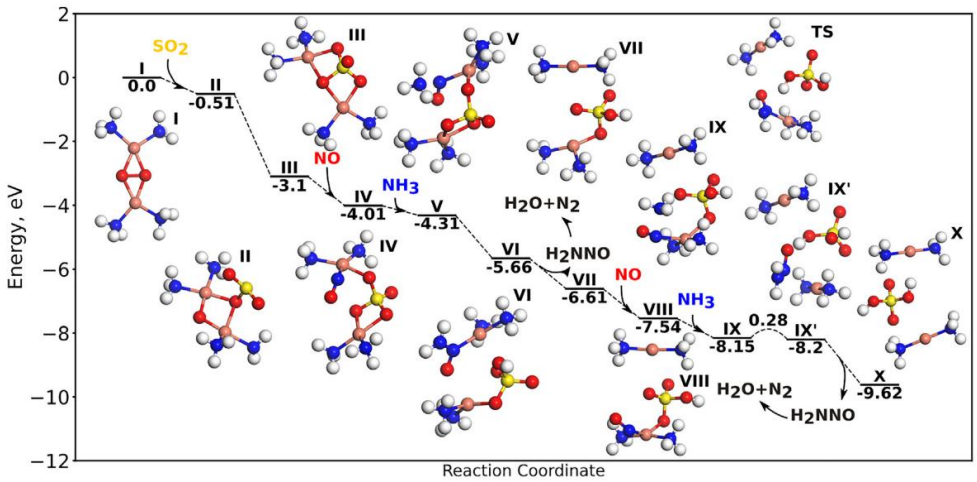

Figure I.6- Energy landscape for SO_2 exposure of $[Cu_2^{II}(NH_3)_4O_2]^{2+}$ complex in presence of NO and NH_3 at low temperatures.[48]

According to the calculation, the barrier for H_2SO_4 diffusion to another cage is around 1.45 eV. This shows that H_2SO_4 cannot move to another cage and this causes an accumulation at low temperatures. The point is that H_2SO_4 can react with NH_3 in an acid-base reaction to form $(NH_4)_2SO_4$ or $(NH_4)HSO_4$. According to a phase diagram evaluation of thermodynamic stability with respect to temperature and NH_3 pressure, HSO_4NH_4 is the most favorable species at 200 °C with the typical NH_3 concentration of SCR conditions. On the contrary, $(NH_4)_2SO_4$ is stable at lower temperature or high concentration of NH_3, and H_2SO_4 is not stable in the conditions considered in the phase diagram. The accumulation of $(NH_4)HSO_4$ species causes an inhibition for two $[Cu^I(NH_3)_2]^+$ complexes to activate O_2. It means that it can be separated two $[Cu^I(NH_3)_2]^+$ complexes which cannot activate O_2 and form the $[Cu_2^{II}(NH_3)_4O_2]^{2+}$ complex necessary for the NO conversion. This would be

the reason for the deactivation of the Cu-CHA catalyst. However, two $[Cu^{I}(NH_3)_2]^+$ complexes could be stabilized in the presence of one $(NH_4)HSO_4$, suggesting that a small uptake of SO_2 should not be detrimental to the activity.[48]

The sensitivity of $[Cu_2^{II}(NH_3)_4O_2]^{2+}$ complex to SO_2 was followed for two Cu-CHA with low and high Cu loading and the same Si/Al ratio of 6.7. It has been shown that the SO_2 interaction has the same mechanism for Cu-CHA catalyst with low and high Cu loading. Sulfur K-edge XANES and Kα XES show that after the reaction sulfur is present as S^{VI} (implying an oxidation of S^{IV} in SO_2), in agreement with the formation of SO_4^{2-} group sulfurs.

Analysis of the EXAFS data indicates that the sulfur atom is located on the second shell of Cu with a distance around 2.6 Å which supports the hypothesis that Cu and S are interacted with O ligands. In this Cu-sulfated compound Cu has a square-planar coordination with mixed NH_3/O ligands. According to a semi-quantitative analysis of the XANES spectra measured during the reaction, a two steps mechanism for the reaction of $[Cu_2^{II}(NH_3)_4O_2]^{2+}$ complex with SO_2 has been proposed. In this mechanism, one $[Cu_2^{II}(NH_3)_4O_2]^{2+}$ complex reacts with one SO_2 and form one $[Cu^{I}(NH_3)_2]^+$, one fw-Cu^{I} and SO_aX which is an intermediate species (Eq.I.4). Then, the second $[Cu_2^{II}(NH_3)_4O_2]^{2+}$ complex reacts with SO_aX to form another $[Cu^{I}(NH_3)_2]^+$ and $Cu^{II}SO_4Z$ which Z contain O, framework O or NH_3 to make Cu with 4 ligands as proven by XANES and EXAFS (Eq.I.5).[67]

$$[Cu_2^{II}(NH_3)_4O_2]^{2+} + SO_2 \rightarrow [Cu^{I}(NH_3)_2]^+ + fw - Cu^{I} + SO_aX \quad \textit{I.4)}$$

$$[Cu_2^{II}(NH_3)_4O_2]^{2+} + SO_aX \rightarrow [Cu^{I}(NH_3)_2]^+ + Cu^{II}SO_4Z \quad \textit{I.5)}$$

As mentioned above, the SO_2-TPD results reported in Ref (Anastasia, SO_2-TPD), are in agreement with the formation of a Cu-sulfated compounds, since the desorption peak of SO_2 does not match that of an H-CHA zeolite impregnated with $(NH_4)_2SO_4$. Ab initio molecular dynamics (AIMD) indicates that oxygen ions in $(NH_4)_2SO_4$ or $(NH_4)HSO_4$ could be coordinated to Cu sites through an electrostatic interaction.[48] This means that it should be possible to have higher decomposition temperature after formation of $SO_4(NH_4)$ or HSO_4NH_4 in Cu-CHA with respect to the $(NH_4)_2SO_4$ impregnated H-CHA.

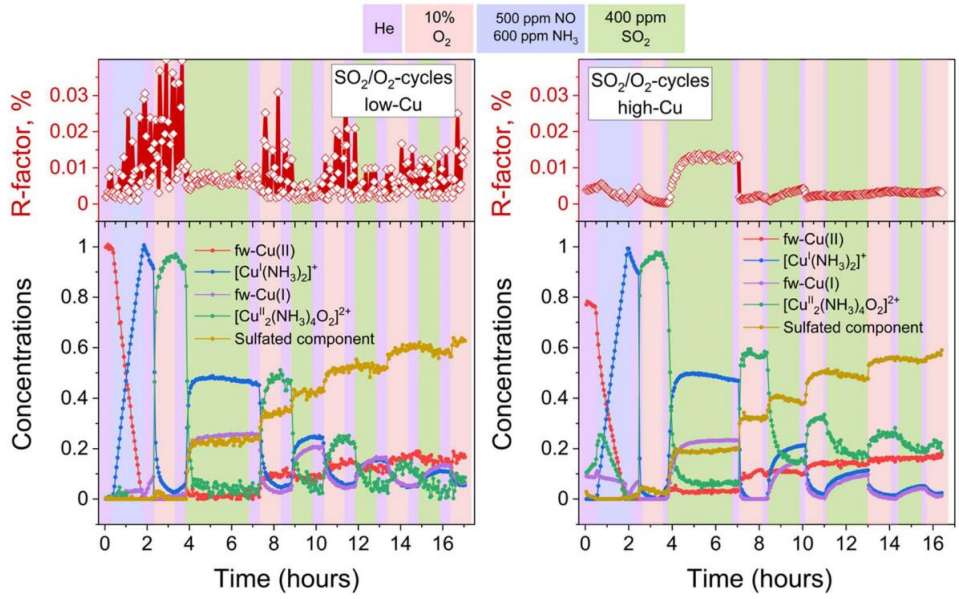

Figure I.7- Quantification of Cu species during SO_2 exposure and Oxidation cycles of $[Cu_2^{II}(NH_3)_4O_2]^{2+}$ complex by in situ XANES spectroscopy. Cu-CHA catalyst with 0.8 Cu wt% (left) and 3.2 wt% (right) with a same Si/Al ratio of 6.7.[67]

The effect of SO_2/O_2 has been shown to cause a higher deactivation with respect to SO_2 alone.[59] The SO_2 uptake is 2-3 times more than when only SO_2 is on the catalyst. The changes of XANES spectra shows an initial increase of $[Cu^I(NH_3)_2]^+$ complexes which are then gradually consumed during SO_2/O_2 exposure to form the $[Cu^I(NH_3)_2]^+$ complexes. Based on Eq.I.4 and I.5, the two $[Cu^I(NH_3)_2]^+$ complexes formed by reaction with SO_2 could react with O_2 in the SO_2/O_2 mixture and form a new $[Cu_2^{II}(NH_3)_4O_2]^{2+}$ complex, which could then react with SO_2. In this case, more SO_2 can be collected to form $Cu^{II}SO_4Z$ complexes until a saturation level.

To have a better understanding of the effect of O_2, cycles of SO_2 exposure followed by O_2 were performed. Figure I.7 shows the results of a linear combination fit of the XANES spectra measured during the different cycles. This allows a semi-quantitative analysis of the different Cu species formed on each step of procedure. For both low and high Cu loadings about 50% of Cu is present as $[Cu^I(NH_3)_2]^+$ complexes, around 25% as fw-Cu^I and Cu-sulfated with a minor amount of $[Cu_2^{II}(NH_3)_4O_2]^{2+}$ after the first SO_2 exposure. The oxidation step after SO_2 causes the formation of new $[Cu_2^{II}(NH_3)_4O_2]^{2+}$

complexes and Cu-sulfated species. The latter steadily increases with every step, finally levelling off, at the expenses of the former. After the fourth cycle of SO_2 exposure and oxidation, there are Cu-sulfated species, fw-Cu^{II} and $[Cu_2^{II}(NH_3)_4O_2]^{2+}$ complex. From the data it is not possible to be sure about the presence of $[Cu_2^{II}(NH_3)_4O_2]^{2+}$ complexes at this step, since the XANES spectrum could correspond to a Cu species which has a similar coordination of Cu (Cu_xO_y) in $[Cu_2^{II}(NH_3)_4O_2]^{2+}$ complex. On the other hand, the observed trend suggests in each step of SO_2 exposure, some $[Cu_2^{II}(NH_3)_4O_2]^{2+}$ complexes could be inaccessible to SO_2 and not react with it, which would explain the remaining activity of Cu-CHA catalyst. [64,67] This remaining fraction of $[Cu_2^{II}(NH_3)_4O_2]^{2+}$ complexes could gradually decrease by repeated exposure to SO_2.

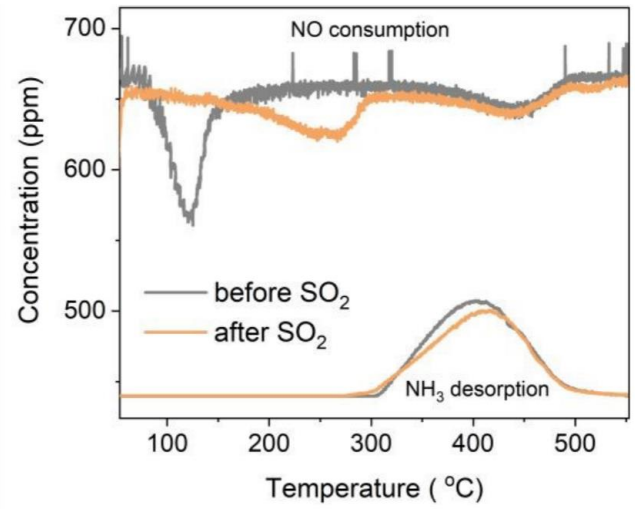

Figure I.8- NO consumption and NH_3 desorption through a reaction of NO with $[Cu_2^{II}(NH_3)_4O_2]^{2+}$ complex with (grey curve) and without (orange curve) SO_2 exposure, Temperature programmed reaction was carried out in NO/N_2 from 50 to 550 °C.[68]

Another important aspect investigated in recent works is the reactivity of NO with the $[Cu_2^{II}(NH_3)_4O_2]^{2+}$ complex, since this is the key point of the reaction cycle which corresponds to the activity of Cu-CHA catalyst. In Figure I.8 (grey curve), a consumption of NO after forming the $[Cu_2^{II}(NH_3)_4O_2]^{2+}$ complex is observed at 120 °C, indicating a reaction between the two. After SO_2 exposure of the $[Cu_2^{II}(NH_3)_4O_2]^{2+}$ complex, the NO consumption exhibits a shift at 250 °C. This means that the reaction of NO and the $[Cu_2^{II}(NH_3)_4O_2]^{2+}$ complex

needs a higher reaction temperature. The observed NH_3 desorption around 300 ^oC could correspond to the decomposition of the $[Cu^I(NH_3)_2]^+$ complexes or the NH_3 desorption from Brøsnted acid sites.[69] The amount of desorbed NH_3 is lower after SO_2 exposure of the $[Cu_2^{II}(NH_3)_4O_2]^{2+}$ complex which shows some NH_3 desorption during SO_2 exposure.

The same experiment was carried out by measuring Cu k-edge XANES spectra, focusing on the intensity of the pre-edge peak at 8982.5 eV, which is a fingerprint of Cu^I. As mentioned above, the reaction of NO with the $[Cu_2^{II}(NH_3)_4O_2]^{2+}$ complex results in a formation of Cu^I. The growing of Cu^I is lower after reaction of NO with the $[Cu_2^{II}(NH_3)_4O_2]^{2+}$ complex after SO_2 exposure at 200 °C. By increasing temperature to 300 ^oC, the intensity of Cu^I becomes comparable to the experiment without SO_2 exposure. Based on multivariate curve resolution (MCR) analysis, it was shown that fw-Cu^I and $[Cu^I(NH_3)_2]^+$ (ratio of 60/35, respectively) are the main species after the reaction of NO with $[Cu_2^{II}(NH_3)_4O_2]^{2+}$ complex. After SO_2 exposure, the ratio is increased to 73/23, indicating a lower amount of $[Cu^I(NH_3)_2]^+$, in agreement with the slightly lower NH_3 desorption of Figure I.8. Based on the gas composition of the outlet of the XAS experiment, the formation of N_2 and H_2O and the NO consumption around 250 ^oC during heating up to 300 ^oC exhibits an agreement with the NO TPD results. However, the rate of reaction of NO with $[Cu_2^{II}(NH_3)_4O_2]^{2+}$ complex becomes slower. Totally, these results indicates that SO_2 changes the chemical properties of Cu in NH_3-SCR reaction.[68]

II Chapter II: Probing the effect of Si/Al ratio in Cu-CHA zeolite catalyst on SO_2 exposure: in situ DR UV-vis spectroscopy and deactivation measurements

The work presented in this chapter is published as a peer-reviewed article in Catal. Sci. Technol. 2024.

Reza K. Abasabadi, Ton V. W. Janssens, Silvia Bordiga and Gloria Berlier. *Probing the effect of the Si/Al ratio in Cu-CHA zeolite catalysts on SO_2 exposure: in situ DR UV-vis spectroscopy and deactivation measurements*. *Catal. Sci. Technol*., 2024, 14, 3076.

II.1 Abstract

Cu-exchanged chabazite zeolite (Cu-HA) is one of the most effective catalysts for ammonia-assisted selective catalytic reduction (NH_3-SCR) in diesel exhaust systems. However, this catalyst is sensitive to small amounts of SO_2 in the exhaust gases, causing a deactivation after prolonged exposure. To have a better understanding of the effect of Si/Al ratio of zeolite on the SO_2 exposure of Cu-CHA catalysts, we measured in situ Diffuse Reflectance UV-vis NIR spectroscopy, SO_2 uptake, and deactivation of SO_2 poisoned Cu-CHA catalysts with the same Cu loading (3.2 wt%) and different Si/Al ratio (6.7, 11 and 15) at 200 ºC. SO_2 selectively reacts with an oxygen-bridged diamine dicopper (II) complex $[Cu^{II}_2(NH_3)_4O_2]^{2+}$, resulting in 50% deactivation in all catalysts, with an SO_2 uptake which varies from 0.2 S/Cu ratio for the catalyst with Si/Al = 6.7, to S/Cu = 0.12 for Si/Al = 15. For the fresh catalysts, the NH_3-SCR activity decreases as the Si/Al ratio increases from 6.7 to 15, as also indicated by the amount of $[Cu^{II}_2(NH_3)_4O_2]^{2+}$ complexes. After exposure of the $[Cu^{II}_2(NH_3)_4O_2]^{2+}$ complex to SO_2, the change in UV-vis spectra correlates well with the SO_2 uptake and the expected Cu-species formed for all three Si/Al ratios. This suggests that, under the applied conditions, the SO_2 reaction with $[Cu^{II}_2(NH_3)_4O_2]^{2+}$ complex in Cu-CHA does not depend on the Si/Al ratio.

II.2 Introduction

Nitrogen oxides (NOx) are harmful byproducts of diesel fuel combustion in automotive engines. The release of nitrogen oxides from diesel exhaust systems into the environment is regulated by various authorities, making it crucial to abate them before they are dispersed.[70] By employing the NH_3-SCR (Selective Catalytic Reduction) reaction, NO_X emissions from diesel exhaust systems can be effectively reduced. In the standard NH_3-SCR reaction, NO is reduced with NH_3 in presence of O_2 to produce N_2 and H_2O with a stoichiometry of $4NO + 4NH_3 + O_2 \rightarrow 4N_2 + 6H_2O$.[71,72] Cu-chabazite (CHA) small pore zeolites are commercialized catalysts for the NH_3-SCR reaction. Cu-CHA catalysts are highly active in the NH_3-SCR reaction, particularly at low temperatures, and demonstrate excellent thermal stability.[73,9]

The Si/Al ratio of zeolite affects the formation of the $[Cu_2^{II}(NH_3)_4O_2]^{2+}$ complex,[44] which is an important intermediate in the NH_3-SCR reaction, highly sensitive to SO_2 in the Cu-CHA catalyst. A high Si/Al ratio resulted in a lower amount of $[Cu_2^{II}(NH_3)_4O_2]^{2+}$ complexes and higher residual amount of $[Cu^{I}(NH_3)_2]^{+}$ after the oxidation part,[44] while catalysts with a low Si/Al ratio showed a higher yield of $[Cu_2^{II}(NH_3)_4O_2]^{2+}$ formation, and higher catalytic activity.[74] These observations point to an influence of Si/Al ratio on the NH_3-SCR reaction.[74]

In this study, the impact of SO_2 on the Cu-CHA catalyst in NH_3-SCR reaction at 200 ºC was investigated by employing in situ Diffuse Reflectance UV-vis-NIR spectroscopy, SO_2 uptake and deactivation measurements for three Cu-CHA catalysts with Si/Al ratios of 6.7, 11 and 15 and 3.2 Cu wt%. By examining the UV-vis spectra in the visible region (Cu^{II} d-d transitions) and the first-order rate constant measured at 200 °C, we investigated the effect of Si/Al ratio on the formation of $[Cu_2^{II}(NH_3)_4O_2]^{2+}$ complex and its reactivity to SO_2. We measured deactivation and quantified the UV-vis absorption in the Cu^{II} d-d region to gain a better understanding of the impact of Si/Al ratio on the SO_2 reaction with the $[Cu_2^{II}(NH_3)_4O_2]^{2+}$ complex.

II.3 Experimental

Three commercial H-CHA zeolites (Si/Al = 6.7, 11 and 15) were used to

prepare the Cu ion-exchanged chabazite zeolite catalysts by incipient wetness impregnation with the appropriate amount of an aqueous solution of Cu-nitrate to obtain 3.2 Cu wt%. The samples were impregnated by spraying the solution under stirring of the powder to get a more even distribution of the Cu. Then, the samples were dried for 2 h at 90 °C, followed by 2 h of calcination at 600 °C in air to decompose the nitrates.

To determine the effect of SO_2 on the Cu-CHA catalysts, four well-defined Cu-species, namely framework-bound Cu^I and Cu^{II} (fw-Cu^I and fw-Cu^{II}), the $[Cu^I(NH_3)_2]^+$ and $[Cu^{II}_2(NH_3)_4O_2]^{2+}$ complexes were prepared in-situ, before exposure to SO_2 (see Figure II.1 in for details). In short, fw-Cu^{II} is produced by oxidation in 10% O_2 at 400 °C, [66,75,76,77] fw-Cu^I by reduction of fw-Cu^{II} in 1% H_2 at 400 °C,[66] the $[Cu^I(NH_3)_2]^+$ complex is formed by exposure of fw-Cu^{II} species to a mixture of 500 ppm NO and 600 ppm NH_3 at 200 °C,[10,78,79,43] and finally the $[Cu^{II}_2(NH_3)_4O_2]^{2+}$ complex is formed by exposure of $[Cu^I(NH_3)_2]^+$ to 10% O_2 at 200 °C.[79,43,66,44,41] The effect of exposure to 100 ppm SO_2 in N_2 on these four Cu-species was then determined by in-situ Diffuse Reflectance (DR) UV-vis-NIR, SO_2 uptake and activity measurements. It has been mentioned below more information about experimental parts.

In all experiments the catalysts were first heated at (400 °C for DR UV-Vis and 550 ºC for SO_2 uptake and catalytic testing) in 10% O_2/N_2 flow and left at this temperature for 1 hour. The following steps are described for the four different procedures:

a) Cooling in 10% O_2/N_2 flow at 200 °C, resulting in the formation of framework coordinated Cu^{II} sites (fw-Cu^{II}).

b) 1% H_2/N_2 flow at 400 °C for 1 hour, followed by cooling in the same atmosphere to 200 °C, resulting in the formation of framework coordinated Cu^I sites (fw-Cu^I).

c) Cooling in 10% O_2/N_2 flow at 200 °C, followed by 20 minutes N_2 purge and subsequent exposure to NO/NH_3 (500 ppm/600 ppm, rest N_2) for 45 min, resulting in the formation of 'mobile' $[Cu^I(NH_3)_2]^+$ complex.

d) The same procedure as in c), followed by N_2 purge and exposure to 10%O_2/N_2 for 30 min, resulting in the formation of $[Cu^{II}_2(NH_3)_4O_2]^{2+}$ complexes.

Then subsequently the catalysts were exposed to 50 ppm SO_2/N_2 followed by the DR UV-Vis experiments and 100 ppm SO_2/N_2 for SO_2 uptake and catalytic testing measurements at 200 ºC.

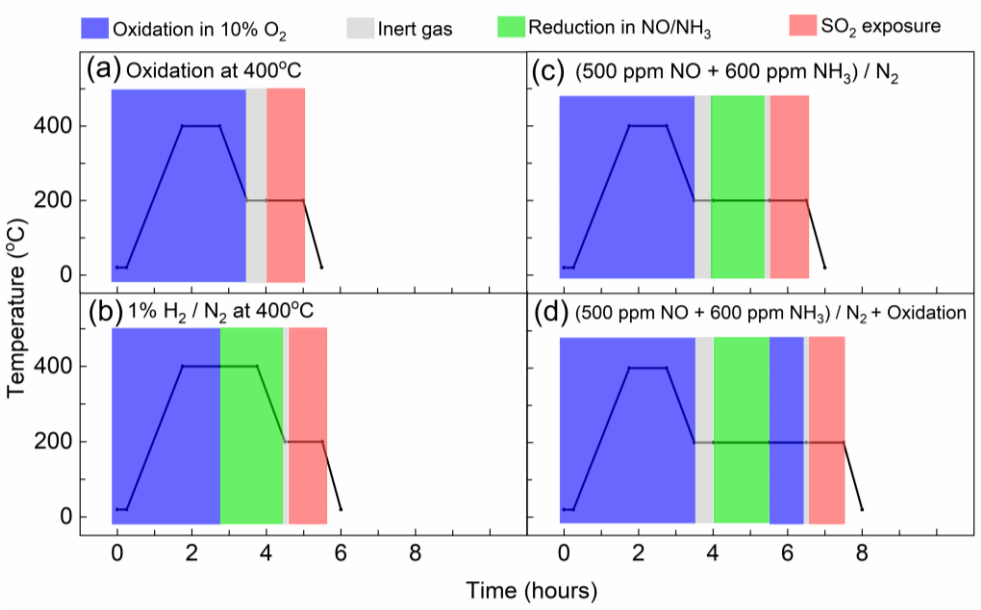

Figure II.1- Schematic representation of the four procedures carried out to obtain (a) framework-Cu^{II}, (b) framework-Cu^{I}, (c) $[Cu^{I}(NH_3)_2]^+$ complex and (d) $[Cu^{II}_2(NH_3)_4O_2]^{2+}$ complex.

For the DR UV-vis-NIR measurements, spectra were recorded with a Varian Cary 5000 spectrophotometer, equipped with a R928 PMT UV-vis detector and a cooled PbS photocell NIR detector. Spectra were collected with a Praying Mantis® element, coupled with a low temperature reaction chamber, connected to a gas manifold system. For all UV-vis measurements, a 40 mg sample of the catalyst (sieve fraction 150-300 µm) was placed in the reaction chamber. Before each specific procedure described above and in Figure II.1, the catalyst was first heated at 400 ºC in 10% O_2 in N_2 with a total flow of 6 NL/h and left at this temperature for 1 hour, before cooling to the desired temperature. Teflon powder was used to measure the reference spectrum needed to determine the relative reflectance (R%):

$$R_{\%} = \frac{R_{sample}}{R_{reference}} \times 100 \qquad \textit{II.1)}$$

The Kubelka Munk function was applied for semiquantitative comparison of the spectra in the region between 8000 and 20000 cm^{-1}, characteristic of d-d transitions of Cu^{II} ions. The reflectance of the samples during the measurements was adjusted in the range 20% - 50% in order to compare the calculated areas without artefacts due to a different vertical offset.[80]

The effect of SO_2 on the catalytic activity was determined using a powder flow reactor setup. The deactivation of the catalyst was determined as the ratio of the activities before and after exposure to 100 ppm SO_2 in N_2 at 200 °C. The entire procedure for the activity measurements is as follows: a sample of 10 mg of the fresh catalyst was diluted with 150 mg silicon carbide and added to a quartz U-tube reactor with inner diameter of 4 mm; quartz wool was used to keep the catalysts as a fixed catalytic bed. The composition of the feed and outlet gases were measured with a Gasmet CX4000 FTIR analyzer. First, the catalyst was subjected to heating at 550^0C in 10% O_2 in N_2 with a total flow of 12 NL/h and maintained at this temperature for 1 hour. To determine the activities, the catalyst was exposed to 500 ppm NO, 600 ppm NH_3, 10% O_2 and 5% H_2O (SCR gases) at 200 ºC. Then, each Cu species was formed by the mentioned procedures and exposed to 100 ppm SO_2 in N_2. Subsequently, the catalyst was exposed to SCR gases to measure the activity of the SO_2 exposed catalyst. The activities are evaluated by determining the first-order rate constants, k (mol/g_{cat}.h) for the fresh and SO_2 exposed catalysts with the following equations:

$$k = -\frac{F}{W} ln\,(1 - X) \qquad \textit{II.2)}$$

where F (mol/h) is the feed flow in reactor, w (g_{cat}) is the mass of catalyst and X is the conversion of NOx, i.e. NO/NO_2.

The ratio of the rate constants after and before the SO_2 exposure are then the measure for the deactivation:

$$Deactivation\ (\%) = \frac{k_{deactivated}}{k_{Fresh}} \times 100 \qquad \textit{II.3)}$$

The SO_2 uptake on the fw-Cu^{I}, fw-Cu^{II}, $[Cu^{I}(NH_3)_2]^+$, $[Cu^{II}_2(NH_3)_4O_2]^{2+}$ complexes were measured in the same flow reactor setup and FTIR analyzer, using a 100 ppm SO_2/N_2 feed gas. After the preparation of the desired Cu species, the SO_2 concentration in the feed gas was measured for 15 min by bypassing the reactor, to obtain a good background. Then, the sample was exposed to 100 ppm SO_2/N_2 for 45 min at 200 °C, resulting in a lower the SO_2 concentration at the outlet. After 45 min, the SO_2 concentration in the outlet reached the feed concentration again, indicating that the SO_2 uptake is complete (see Figure II.2). The SO_2 uptake is then calculated from integration of the SO_2 consumption curve (yellow area in Figure II.2) during the SO_2 exposure.

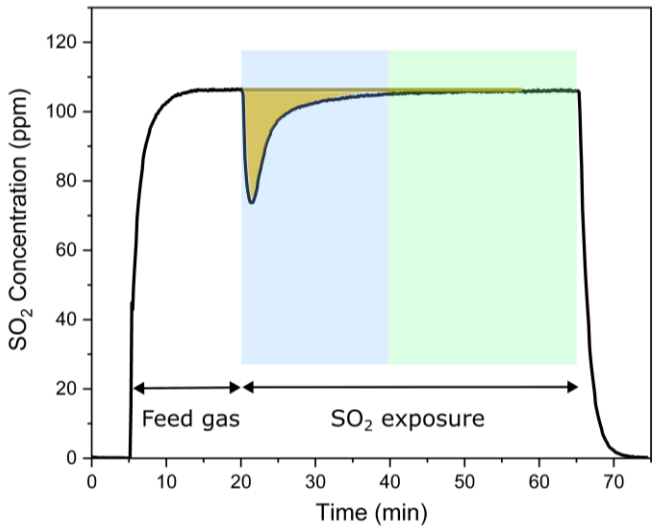

Figure II.2- The SO_2 uptake of Cu-CHA with Si/Al ratio of 6.7 during exposure to 100 ppm SO_2 in N_2 at 200 °C.

II.4 Results

II.4.1 Effect of SO_2 exposure on different Cu species

To determine the oxidation state of Cu for different Cu species, the d-d transitions in the 20000-8000 cm^{-1} interval in the DR UV-vis spectra were investigated. The light coloured lines in Figure II.3 are the spectra obtained for the different Cu^{I} and Cu^{II} species in Cu-CHA with Si/Al ratio of 6.7 before exposure to SO_2. The spectra for the Cu^{II} species show a clear absorption in

the d-d transition region (panels a and d), while those for the Cu^{I} species do not (panels b and c). The $[Cu^{II}_2(NH_3)_4O_2]^{2+}$ complex exhibits an adsorption in d-d region, centered at 13500 cm^{-1}, with slight variations in the position and shape compared to fw-Cu^{II} (Figure II.3d and a, respectively).[43] In summary, these spectra confirm the formation of well-defined Cu^{II} and Cu^{I} species, similarly to what observed by XAS after similar pre-treatments.[66]

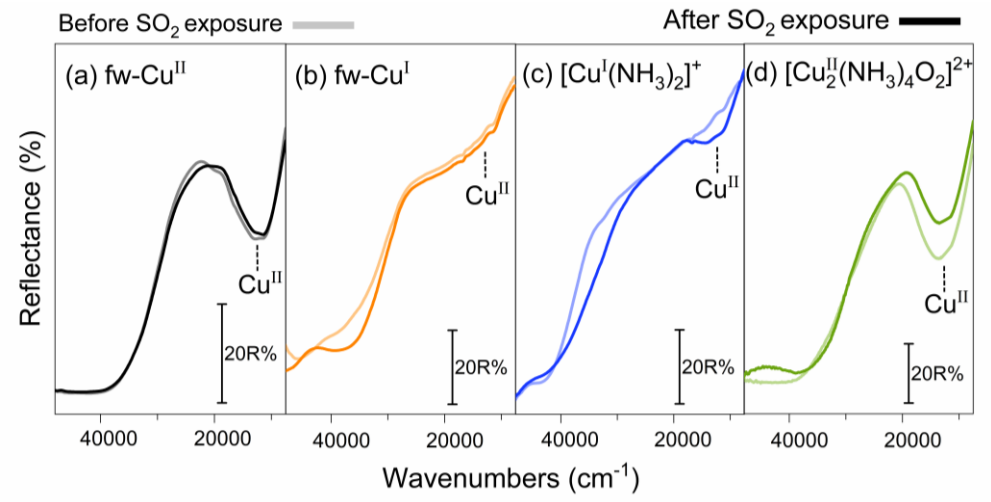

Figure II.3- Effect of SO_2 on different Cu species monitored by in situ DR UV-vis spectroscopy on Cu-CHA with Si/Al ratio of 6.7 before (light lines) and after SO_2 exposure (dark lines) at 200 °C.

The changes in the d-d transition upon SO_2 exposure reveal the different interaction of these four Cu species with SO_2. The dark coloured lines in Figure II.3 show the UV-vis spectra of the four Cu species after exposure to SO_2. For the $[Cu^{II}_2(NH_3)_4O_2]^{2+}$ complex, the fingerprint of Cu^{II} ions is affected, indicating an interaction of SO_2. The decrease in intensity indicates that some reduction of the Cu has taken place, in good agreement with earlier results obtained by X-ray absorption spectroscopy.[66] On the other hand, the spectra for the framework-bound species are not affected by the exposure to SO_2. Notice that the spectra of fw-Cu^{II} and $[Cu^{II}_2(NH_3)_4O_2]^{2+}$ are hardly distinguishable in the d-d region, but their response to SO_2 is clearly different. The spectrum of $[Cu^{I}(NH_3)_2]^{+}$ complex exhibits small changes, with a small portion of Cu^{II} being formed (Figure II.3c, dark coloured line). This change will be addressed in the Discussion section.

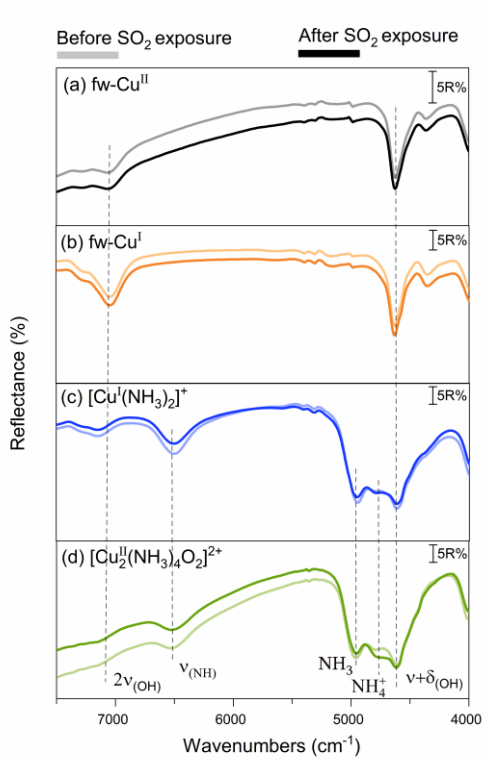

Figure II.4- Effect of SO_2 on different Cu species in the NIR region on sample Cu-CHA with Si/Al ratio of 6.7 before (light lines) and after SO_2 exposure (dark lines) at 200 °C.

The interaction of NH_3 ligands on Cu species was investigated in the near-infrared (NIR) region (Figure II.4c and d). After exposing the sample to NO/NH_3 to obtain $[Cu^{I}(NH_3)_2]^+$ and $[Cu^{II}_2(NH_3)_4O_2]^{2+}$ complexes, the near-infrared (NIR) region shows the vibrational modes of NH_3 coordinated to Cu ions and NH_4^+ formed by protonation from residual Brønsted sites.[30] More in detail, the band at 6510 cm^{-1} can be related to the overtone of the NH stretching modes of NH_3 and NH_4^+, with the corresponding stretching + bending combination modes at 4960 and 4730 cm^{-1}, respectively. These bands are absent in the NIR spectra of fw-Cu^{II} and fw-Cu^{I} (panels a and b, respectively) showing only the vibrational modes of silanols and Brønsted sites at 7050 and 4600 cm^{-1}.[76] After exposure to SO_2, all bands in NIR region were unchanged, except for the NH_4^+ band, which shows a slight increase in the $[Cu^{II}_2(NH_3)_4O_2]^{2+}$ complex (Figure II.4d). This indicates that the presence of the $[Cu^{II}_2(NH_3)_4O_2]^{2+}$ complex leads to NH_4^+ formation after SO_2 exposure.

Table II.1- SO_2 uptakes and corresponding S/Cu ratios for different Cu species after SO_2 exposure at 200 °C on Cu-CHA with Si/Al ratio of 6.7.

Cu state	fw-Cu^{II}	fw-Cu^{I}	$[Cu^{I}(NH_3)_2]^+$	$[Cu_2^{II}(NH_3)_4O_2]^{2+}$
SO_2 uptake ($\mu mol\ SO_2/g_{Catalyst}$)	30	7	27	101
S/Cu ratio	0.02	0.06	0.05	0.2

Having verified the higher sensitivity of the $[Cu_2^{II}(NH_3)_4O_2]^{2+}$ complex to SO_2, we have repeated the same protocols to measure the corresponding SO_2 uptakes and deactivation. The S/Cu ratio of catalysts was determined by measuring SO_2 uptakes after each pretreatment. The SO_2 uptake for the $[Cu_2^{II}(NH_3)_4O_2]^{2+}$ complex is higher (S/Cu = 0.2), compared to the other Cu species, in agreement with the changes observed in the UV-vis spectra. The amount of μmol of SO_2 uptakes per gram of catalyst and S/Cu ratio are in good agreement with what reported in Ref. [66] for the same catalyst (Table II.1).

The NH_3-SCR activity of the same Cu-CHA catalyst was measured at 200 °C before and after SO_2 exposure on the four states described above. Figure II.5 reports the calculated deactivation (II.3) as a function of SO_2 uptake, expressed as S/Cu ratio. The data show that the deactivation increases linearly with the SO_2 uptake. More in detail the lowest deactivation (7%) corresponds to the catalyst pretreated to obtain fw-Cu^{I}, followed by $[Cu^{I}(NH_3)_2]^+$ (15%) and fw-Cu^{II} (20%). The catalyst measured after formation of $[Cu^{II}_2(NH_3)_4O_2]^{2+}$complex exhibits the highest SO_2 uptake and deactivation (50%) compared to other species. This observation fits well with the measured UV-vis spectra, which indicates a significant reduction of Cu^{II} to Cu^{I} when SO_2 interacts with $[Cu^{II}_2(NH_3)_4O_2]^{2+}$ complexes. In summary, the catalyst exposing only fw-Cu^{I} sites can be expose to SO_2 without loss of activity, while the activity is decreasing more when the Cu species are divalent and/or coordinated by NH_3 ligands.

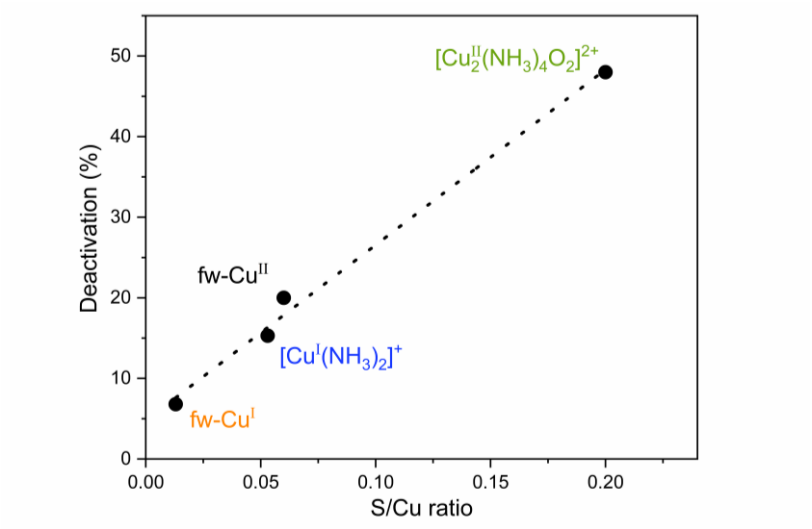

Figure II.5- Relation between deactivation and SO_2 uptake for the four different Cu species in Cu-CHA with Si/Al ratio of 6.7. SO_2 uptake was measured in 100 ppm SO_2 at 200 °C; deactivation was calculated by measuring NH_3-SCR activity in 500 ppm NO, 600 ppm NH_3, 10% O_2 and 5% H_2O at 200 °C, before and after SO_2 exposure.

II.4.2 Reducibility of the $[Cu^{II}_2(NH_3)_4O_2]^{2+}$ complex after SO_2 exposure followed by in situ DR UV-vis spectroscopy

The results discussed so far show that the Cu-CHA catalyst takes up more SO_2 after a pretreatment forming $[Cu^{II}_2(NH_3)_4O_2]^{2+}$ complexes, and this corresponds to the highest deactivation measured in this study. The deactivation is caused by a less efficient reduction of the $[Cu^{II}_2(NH_3)_4O_2]^{2+}$ complex by NO/NH_3 after SO_2 exposure. Because this reduction represents the reduction of part of the NH_3-SCR cycle, a less effective reduction of the $[Cu^{II}_2(NH_3)_4O_2]^{2+}$ complex leads to a slower NH_3-SCR reaction.[6,75] The change in reducibility of the $[Cu^{II}_2(NH_3)_4O_2]^{2+}$ complex species by SO_2 was measured by exposing this species to 500 ppm NO/600 ppm NH_3 at 200 °C, without and with SO_2 exposure. In Figure II.6, it is shown more time and gas composition for the procedure.

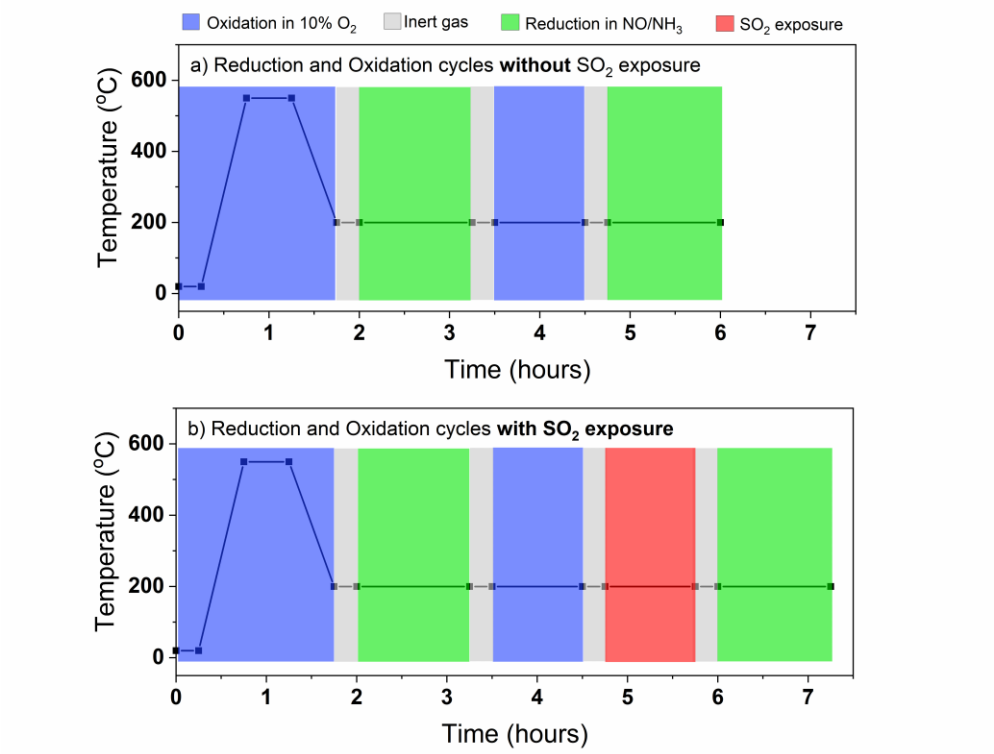

Figure II.6- Schematic representation of oxidation and reduction cycles a) without SO_2, and b) with SO_2 at 200 °C.

The complete $[Cu^{I}(NH_3)_2]^+/[Cu^{II}_2(NH_3)_4O_2]^{2+}/[Cu^{I}(NH_3)_2]^+$ redox cycle was followed by DR UV-Vis spectroscopy on Cu-CHA with Si/Al ratio of 6.7 (Figure II.7a). The data shows that after reaction with NO/NH_3, the $[Cu^{II}_2(NH_3)_4O_2]^{2+}$ complex is completely reduced to $[Cu^{I}(NH_3)_2]^+$ (red and blue spectra in Figure II.7a), in agreement with previous reports.[43] A reoxidation reproduced the original spectrum for the $[Cu^{II}_2(NH_3)_4O_2]^{2+}$ complex (green curve in Figure II.7a), indicating that all Cu can be reversibly reduced and oxidized. If the $[Cu^{II}_2(NH_3)_4O_2]^{2+}$ state is exposed to SO_2 a part of the Cu is reduced (green and yellow curve in Figure II.7b), in agreement with previous XAS measurements and Figure II.3d.[66,67] The subsequent reduction with NO/NH_3 (red curve in Figure II.7b) does not restore the initial $[Cu^{I}(NH_3)_2]^+$ state, indicating that a part of the Cu remains in a Cu^{II} state, and therefore, the Cu-CHA cannot be fully reduced to $[Cu^{I}(NH_3)_2]^+$ after exposure of $[Cu^{II}_2(NH_3)_4O_2]^{2+}$ to SO_2. This provides evidence for the less efficient reduction of Cu after exposure to SO_2, and the reaction of SO_2 with

$[Cu^{II}_2(NH_3)_4O_2]^{2+}$ complexes seem to remove a fraction of Cu^{II} sites from the redox Cu^{II}/Cu^{I} cycle.

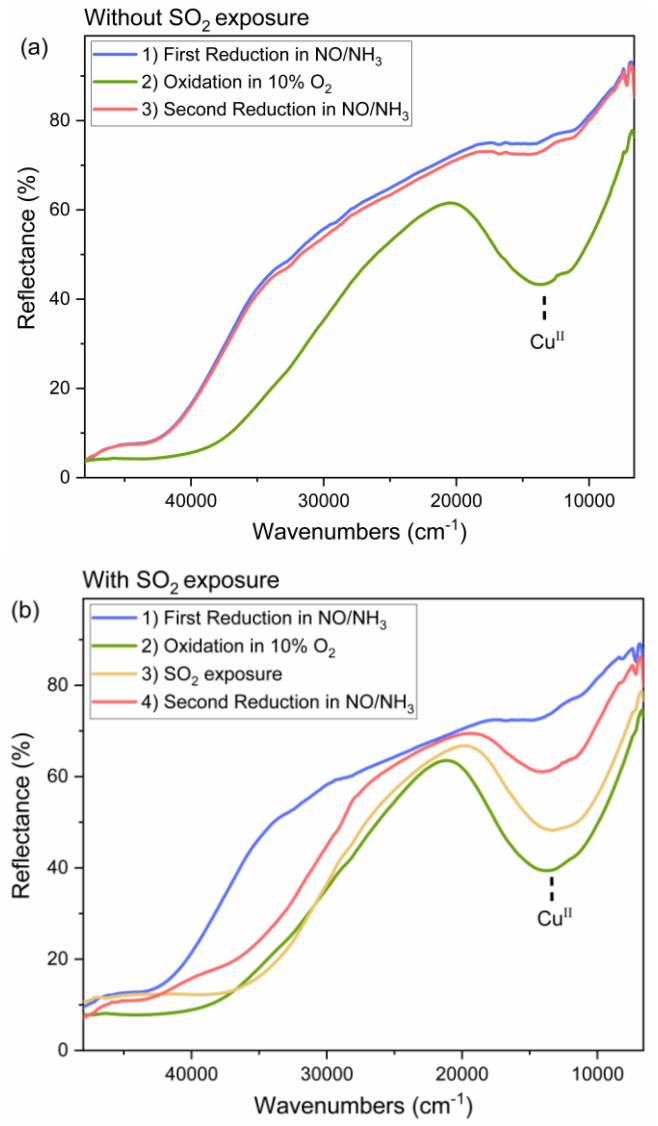

Figure II.7- Redox cycle of the $[Cu^{II}_2(NH_3)_4O_2]^{2+}$ complex in Cu-CHA with Si/Al ratio of 6.7 followed by DR UV-vis: formation of $[Cu^{I}(NH_3)_2]^{+}$, reaction with O_2 to form $[Cu^{II}_2(NH_3)_4O_2]^{2+}$ complex and subsequent reduction with NO/NH_3. b) as in a) with intermediate exposure of $[Cu^{II}_2(NH_3)_4O_2]^{2+}$ complex to SO_2, followed by NO/NH_3. All spectra measured at 200 °C.

II.4.3 Effect of Si/Al ratio on the reactivity of $[Cu^{II}_2(NH_3)_4O_2]^{2+}$ complex with SO_2

Having verified the higher reactivity of SO_2 with the $[Cu^{II}_2(NH_3)_4O_2]^{2+}$ complex with respect to other Cu states in Cu-CHA with Si/Al ratio of 6.7, we explored the same protocol as in Figure II.3d on other two Cu-CHA catalysts with the same Cu loading (3.2 wt%) and different Si/Al ratios (11 and 15). The UV-vis spectra measured before and after SO_2 interaction was converted into the Kubelka-Munk function, in order to make a semiquantitative comparison of the integrated area in the Cu^{II} d-d region.

Table II.2- Initial UV-vis area of $[Cu^{II}_2(NH_3)_4O_2]^{2+}$ complex and first-order rate constant at 200 °C for the different catalysts.

Si/Al ratio	UV-vis area of $[Cu^{II}_2(NH_3)_4O_2]^{2+}$ $\times 10^{-4}$ (cm^{-1})	Rate constant of fresh catalysts at 200 °C (mol NO. $g_{cat}^{-1}.h^{-1}$)
6.7	0.58	80.1
11	0.43	51.9
15	0.315	37.6

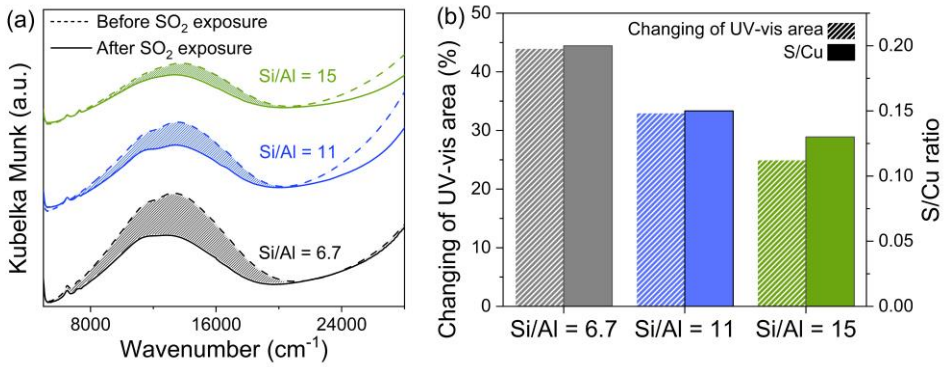

Figure II.8- Kubelka Munk converted DR UV-vis spectra of Cu-CHA zeolite with different Si/Al ratios (6.7, 11 and 15) and same loading (Cu = 3.2wt%) in the d-d region; spectra are vertically translated for clarity. b) Relative variation of the UV-vis area after SO_2 exposure and measured SO_2 uptake.

Before SO_2 exposure (solid lines in Figure II.8a) the measured area should be proportional to the amount of the formed $[Cu^{II}_2(NH_3)_4O_2]^{2+}$ complex. It is clear

from Figure II.8a and from the area values listed in Table II.2 (1st column) that the band intensity follows the Si/Al order 6.7 > 11> 15. This would imply an important effect of the catalyst Si/Al ratio (keeping constant the Cu loading) on the amount of formed $[Cu^{II}_2(NH_3)_4O_2]^{2+}$ complex. Interestingly, the same trend is followed by the first order kinetic constant measured at 200 °C on the fresh catalysts (2nd column in Table II.2) which is consistent with the hypothesis that the $[Cu^{II}_2(NH_3)_4O_2]^{2+}$ complex are relevant for the low temperature activity in the reaction (Figure II.9). In summary, a larger fraction of the Cu is present as the $[Cu^{II}_2(NH_3)_4O_2]^{2+}$ complex at low Si/Al ratio.

All catalysts were exposed to SO_2 to compare changes of UV-vis area and measure SO_2 uptakes. As previously discussed, the exposure of the $[Cu^{II}_2(NH_3)_4O_2]^{2+}$ complex to SO_2 causes a decrease in the intensity of Cu^{II} d-d transitions (Figure II.8, dashed lines). The relative variation in the spectral area (coloured area in Figure II.8) follows again the trend Si/Al 6.7 > 11 > 15. Thus, the catalyst showing the most abundant formation of $[Cu^{II}_2(NH_3)_4O_2]^{2+}$ complex is the most affected by SO_2 exposure. This is also reflected in the SO_2 uptake measured in the same conditions (reported as S/Cu ratio in Figure II.8b), which follows a similar trend.

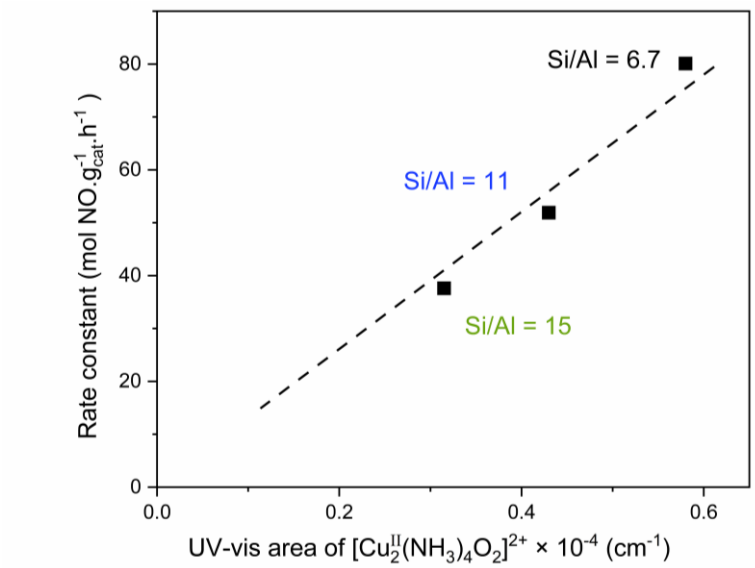

Figure II.9- Correlation between first-order rate constant versus initial UV-vis area of $[Cu^{II}_2(NH_3)_4O_2]^{2+}$ complex. The rate constant was calculated from catalytic activity measurements in 500 ppm NO, 600 ppm NH_3, 10% O_2 and 5% H_2O at 200 °C.

II.4.4 Repeated SO_2 exposure and NH_3-SCR catalytic tests

Cu-CHA with Si/Al ratio of 6.7 showed a deactivation around 50% after SO_2 exposure of the $[Cu^{II}_2(NH_3)_4O_2]^{2+}$ complex. After the same procedure, Cu-CHA with Si/Al ratio of 6.7, 11 and 15 show very similar deactivation values (50%, 57% and 53%, respectively) but different S/Cu ratios: 0.2, 0.15 and 0.13 for Cu-CHA with Si/Al ratios of 6.7, 11 and 15, respectively. To compare the SO_2 uptakes and deactivation for three catalysts, we thus carried out experiments to uptake more SO_2 and deactivate more catalysts. According to Figure II.2 (blue part), the catalysts SO_2 uptake takes place in the first 20 min of SO_2 exposure. By repeating the cycle of reduction in NO/NH_3 followed by oxidation to form the $[Cu^{II}_2(NH_3)_4O_2]^{2+}$ complex and SO_2 exposure, the SO_2 uptake increases gradually, and the total amount is measured by adding the SO_2 uptake during each exposure step. The catalytic activity was measured after each SO_2 exposure to calculate the deactivation. Totally, these steps reduction, oxidation, SO_2 exposure and measure of catalytic activity - were repeated six times (Figure II.10).

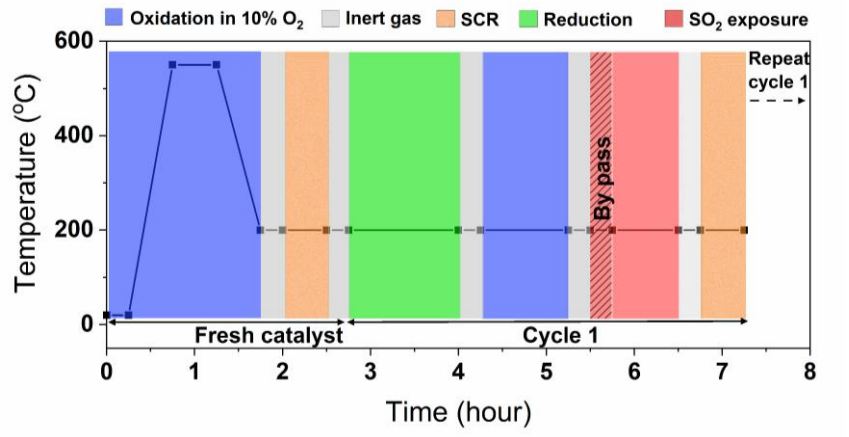

Figure II.10- Schematic representation of repeated SO_2 exposure procedure to measure SO_2 uptake during SO_2 exposure and deactivation.

In Figure II.11, the deactivation measured at 200 °C is plotted as a function of the SO_2 uptakes, expressed as S/Cu ratio. A good linearity is observed for each Si/Al ratio. As mentioned, all catalysts lose around 50% of their activity during the first cycle although the amount of SO_2 uptake is different. In the second cycle the deactivation increases around 75%, meaning that a further 50% is

lost with respect to the first poisoning cycle for all catalysts. This corresponds to an increase of S/Cu ratio which is only half of the initial S/Cu ratio for the three catalysts. Both deactivation and S/Cu ratio change less than 50% in the following cycles, eventually reaching a stable level after several cycles. This indicates that the deactivation behavior of the Cu-CHA catalysts through SO_2 exposure on the sensitive $[Cu^{II}_2(NH_3)_4O_2]^{2+}$ complex is different from beginning to the end, suggesting that complete deactivation of the catalyst is not achievable.

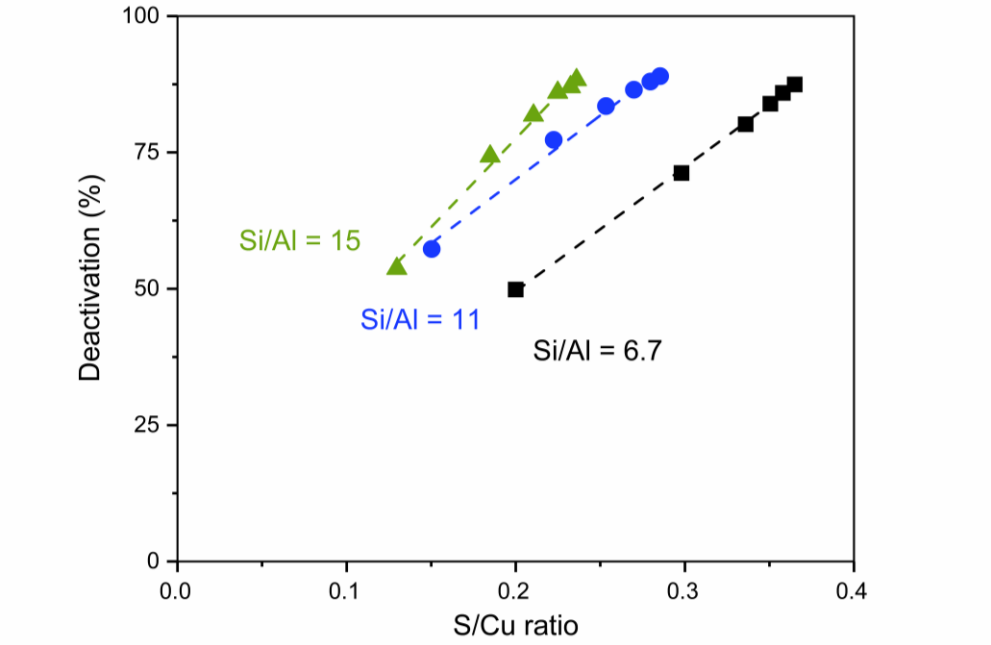

Figure II.11- The deactivation versus SO_2 uptake (S/Cu ratio) during repeated SO_2 exposure. NO conversion condition: 500 ppm NO, 600 ppm NH_3, 10% O_2 and 5% H_2O at 200 °C. SO_2 exposure condition: 100 ppm SO_2 at 200 °C, each point is related to one cycle.

II.5 Discussion

II.5.1 SO_2 reaction with $[Cu^{II}_2(NH_3)_4O_2]^{2+}$ complex causes Cu^{II}-sulfated formation and deactivation

DR UV-vis, SO_2 uptake and deactivation measurements confirm the sensitivity of the $[Cu^{II}_2(NH_3)_4O_2]^{2+}$ complex to SO_2 exposure. The $[Cu^{II}_2(NH_3)_4O_2]^{2+}$ complex is formed upon activation of O2 on by a pair of $[Cu^{I}(NH_3)]^{+}$ complexes, and therefore the reaction of SO_2 with

$[Cu^{II}_2(NH_3)_4O_2]^{2+}$ is a key step in the deactivation mechanism. It has been proposed that the SO_2 poisoning is more pronounced upon exposure to a typical NH_3-SCR feed gas ($NO/NH_3/O_2/H_2O$ mixture), as compared to a O_2/H_2O mixture. [59] This aligns well with the observation that SO_2 primarily interacts with the $[Cu^{II}_2(NH_3)_4O_2]^{2+}$ complex, because the formation of the $[Cu^{II}_2(NH_3)_4O_2]^{2+}$ complex requires the presence of both NO and NH_3, according to the NH_3-SCR reaction cycle. [43,46,47]

Moreover, we have shown by DR UV-vis that the catalyst cannot be completely reduced in NO/NH_3, closing the catalytic cycle, after SO_2 reaction with the $[Cu^{II}_2(NH_3)_4O_2]^{2+}$ complex. According to Molokova et al. SO_2 reaction with the $[Cu^{II}_2(NH_3)_4O_2]^{2+}$ complex causes the formation of a mixture of fw-Cu^I, $[Cu^I(NH_3)_2]^+$, a small amount of unreacted $[Cu^{II}_2(NH_3)_4O_2]^{2+}$ complex and a 'Cu^{II}-sulfated component', likely coordinated to NH_3 ligands.[66,81] This means that the band in the d-d region measured after SO_2 interaction is given by a fraction of (active) $[Cu^{II}_2(NH_3)_4O_2]^{2+}$ complex and by this Cu^{II}-sulfated component, which does not react efficiently with NO/NH_3 to close the catalytic cycle and is thus responsible for the measured deactivation.

Notably, the observation of NH_4^+ formation in the NIR region only after SO_2 exposure of $[Cu^{II}_2(NH_3)_4O_2]^{2+}$ complex could be related to the formation of some ammonium bisulfate $(NH_4)HSO_4$ as proposed by different authors.[48,56,82] However, the deactivation after SO_2 reaction with the $[Cu^{II}_2(NH_3)_4O_2]^{2+}$ complex is not compatible with an accumulation of ammonium bisulfate causing the physical blocking on the zeolite pores. This mechanism is not compatible with the observation that a small amount of SO_2 (S/Cu = 0.2) causes a deactivation of 50%.

II.5.2 Formation of $[Cu^{II}_2(NH_3)_4O_2]^{2+}$ complex and exposing SO_2 on catalysts with different Si/Al ratio

The first-order rate constant at 200 °C for three catalysts with identical Cu loading (3.2 wt%) exhibits a correlation with the obtained DR UV-vis spectra and corresponding calculated Kubelka-Munk area. It is reasonable to consider that the UV-vis area in the Cu^{II} d-d region after the described experimental procedure is associated with the capability of the catalysts to form

$[Cu^{II}_2(NH_3)_4O_2]^{2+}$ complex. This implies a correlation between the rate constant and the amount of formed $[Cu^{II}_2(NH_3)_4O_2]^{2+}$ complex, which can be monitored by DR UV-vis spectroscopy. This observation is in agreement with the hypothesis that the $[Cu^{II}_2(NH_3)_4O_2]^{2+}$ complex is the active sites in the low temperature NH_3-SCR reaction, so that the kinetic constant depends on its concentration (Figure II.9). The concentration of $[Cu^{II}_2(NH_3)_4O_2]^{2+}$ complexes and kinetic constant are higher for Cu-CHA with Si/Al ratio of 6.7. We can hypothesize that this is due to the higher negative charge in the framework induced by the presence of Al, which would favor the divalent oxidation state. Thus, maintaining Cu as Cu^I species within the zeolite cages becomes more challenging.

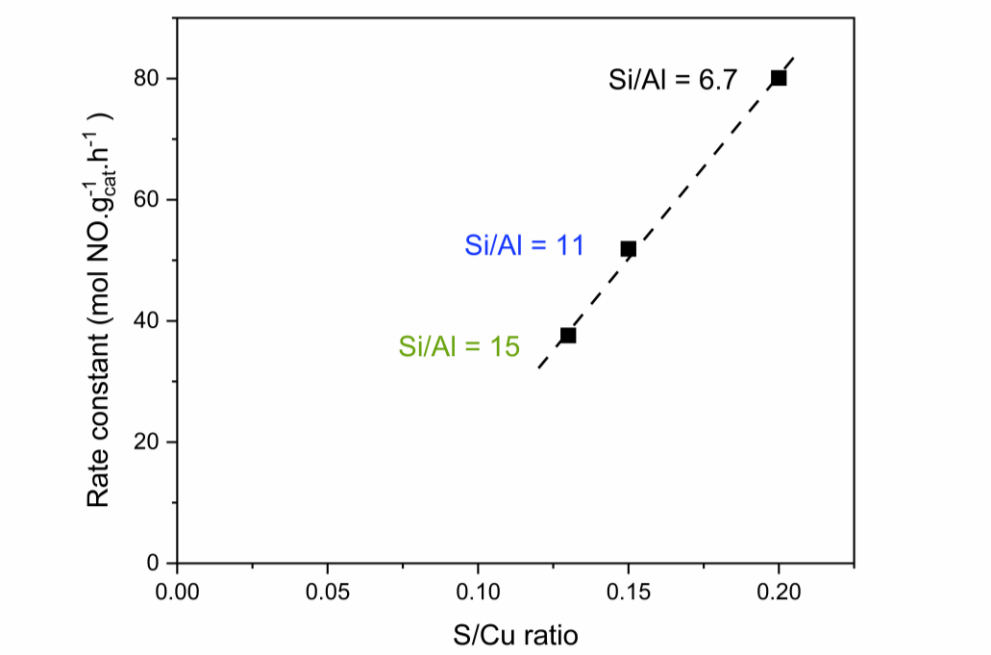

Figure II.12- Correlation between the first-order rate constant and SO_2 loading (S/Cu). The rate constant was calculated from catalytic activity measurements in 500 ppm NO, 600 ppm NH_3, 10% O_2 and 5% H_2O at 200 °C on fresh catalysts.

After SO_2 exposure of $[Cu^{II}_2(NH_3)_4O_2]^{2+}$ complex, all the catalysts showed a 50% decrease of activity after the first SO_2 exposure (Figure II.11), irrespective of the SO_2 uptake, which instead shows a linear correlation with the rate constant of fresh catalysts (Figure II.12).

II.5.3 Following the deactivation mechanism by SO_2 on catalysts with different Si/Al ratio

Notably, a small S/Cu ratio (0.2 for Cu-CHA with Si/Al ratio of 6.7) is capable of reducing the rate constant by 50%. Based on XAS data, coupled to the measurement of SO_2 uptake, Molokova et al. proposed a two-step mechanism where one single SO_2 molecule reacts with two $[Cu_2^{II}(NH_3)_4O_2]^{2+}$ complexes.[67] This, coupled to steric hindrance could explain the high impact on catalytic activity of a small SO_2 uptake.[48] The stoichiometry resulting from this mechanism is

$$II.4) \quad 2[Cu_2^{II}(NH_3)_4O_2]^{2+} + SO_2 \rightarrow 2[Cu^{I}(NH_3)_2]^{+} + fw - Cu^{I} + Cu^{II}SO_4Z$$

The sulfated species (Cu^{II}-SO_4Z) is characterized by a square-planer coordination of Cu with 4- ligands including oxygen and NH_3 as Z, as demonstrated by EXAFS and XANES analyse.[67] Based on this stoichiometry, we have considered as input for each catalyst the measured S/Cu ratio to calculate the fraction of formed Cu^{II}-sulfated and Cu^{I} species ($2Cu^{I}(NH_3)_2$ + fw-Cu^{I}), considering the rest of the Cu as unreacted $[Cu_2^{II}(NH_3)_4O_2]^{2+}$ (Table 3). For instance, an SO_2 uptake corresponding to S/Cu = 0.2 (Cu-CHA with Si/Al ratio of 6.7, Table II.3) would imply 20% Cu^{II}-sulfated components, 60% Cu^{I} species and 20% of the $[Cu_2^{II}(NH_3)_4O_2]^{2+}$ complexes. Thus, the UV-vis area in the d-d region measured in Cu-CHA with Si/Al ratio of 6.7 (Calibration sample) after SO_2 dosage would be due to 20% unreacted $[Cu_2^{II}(NH_3)_4O_2]^{2+}$ complexes plus 20% Cu^{II}-sulfated components. This assumption was used to estimate the relative absorption coefficient of Cu^{II}-sulfated component with respect to that of $[Cu_2^{II}(NH_3)_4O_2]^{2+}$. The obtained value (1.8) was then used to calculate the expected variation on Cu-CHA with Si/Al ratios of 11 and 15 based on the corresponding S/Cu ratios (Second column of Table II.3). The agreement between the calculated area variations and the measured ones (6^{th} and 5^{th} column of Table II.3) is striking, supporting the validity of the mechanism proposed in Ref. [67] for catalysts with three different Si/Al and S/Cu ratios.

Table II.3- Calculated percentage of Cu species formed in the three catalysts after SO_2 uptake based on the stoichiometry proposed in Ref [67] and measured S/Cu ratio, and corresponding measured and calculated variations in UV-vis area.

Si/Al ratio	Cu^{II} sulfated (S/Cu ratio)	$[Cu^{I}(NH_3)_2]^+$ and fw-Cu^{I}	$[Cu^{II}_2(NH_3)_4O_2]^{2+}$	UV-vis decrease (%)	
				Meas.	Calc.
6.7	0.2	0.60	0.20	44	-
11	0.15	0.45	0.40	33	33
15	0.12	0.36	0.52	25	26

The deactivation caused by SO_2 on the $[Cu^{II}_2(NH_3)_4O_2]^{2+}$ complex exhibits similar behavior across catalysts with different Si/Al ratios, although the SO_2 uptakes are different. The rate constant measurements indicate a 50% decrease in activity when SO_2 reacts with $[Cu^{II}_2(NH_3)_4O_2]^{2+}$ complex. It is interesting to notice that the activity of all catalysts further decreases of 50% in the second step of SO_2 exposure. This would suggest a mechanism where SO_2 affects half of the active $[Cu^{II}_2(NH_3)_4O_2]^{2+}$ complex in the first step, and half of the remaining $[Cu^{II}_2(NH_3)_4O_2]^{2+}$ complex in the second one. This does not happen in the following SO_2 exposure steps, which could be explained with the fact that the concentration of $[Cu^{II}_2(NH_3)_4O_2]^{2+}$ complex is too small, and the accessibility to SO_2 is limited by the high concentration of the Cu^{II}-sulfated compound in the zeolite pores.

As a further comment, from the stoichiometry proposed in eq.II.4, one SO_2 molecule would decompose two $[Cu^{II}_2(NH_3)_4O_2]^{2+}$ complexes, resulting in one inactive Cu^{II}-sulfated compound, two $[Cu^{I}(NH_3)_2]^+$ and one fw-Cu^{I}. This should result in a 25% decrease in activity for each SO_2, since the $[Cu^{I}(NH_3)_2]^+$ and fw-Cu^{I} sites should be still available for the NH_3-SCR reaction. Clearly, this is not in agreement with the deactivation measured in this work, suggesting that the poisoning mechanism is more complex.

II.5.4 O_2 sensitivity of Cu^I species on Cu-CHA catalysts

A small increase of Cu^I to Cu^{II} during SO_2 exposure of $[Cu^I(NH_3)_2]^+$ complex was observed (Figure II.3c). However, the spectrum of fw-Cu^I does not change after SO_2 exposure, showing that SO_2 does not react with Cu^I. Moreover, SO_2 has been shown to reduce Cu^{II} to Cu^I, meaning that the observed oxidation of Cu^I to Cu^{II} for $[Cu^I(NH_3)_2]^+$ complex cannot be related to the reaction with SO_2 itself, but could be related to the presence of small traces of oxygen stored in the sample. To explore this concept, the sensitivity of fw-Cu^I and $[Cu^I(NH_3)_2]^+$ species to O_2 was examined through pulse oxidation steps. Namely, the catalyst was exposed 10 times to 2% O_2/N_2 flow for 5 seconds after forming $[Cu^I(NH_3)_2]^+$ or fw-Cu^I species (Figure II.14a and b, respectively). Subsequently, the catalyst left in O_2 for 30 min to achieve complete oxidation (Figure II.13).

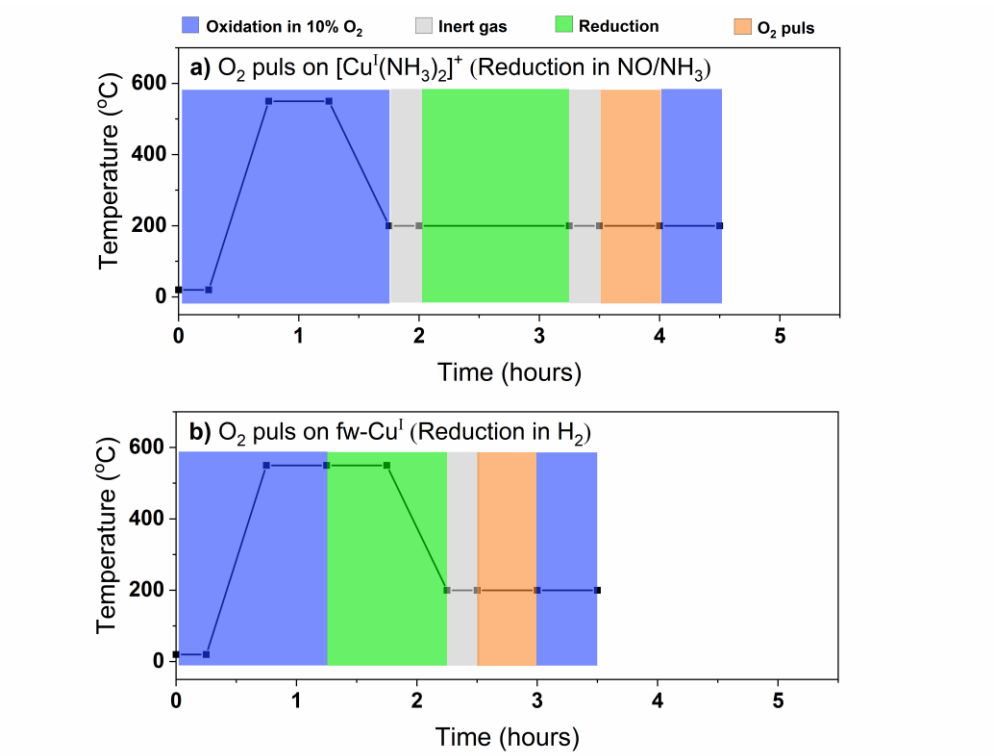

Figure II.13- Schematic representation of O_2 puls procedures on a) $[Cu^I(NH_3)_2]^+$ and b) fw-Cu^I at 200 °C.

Figure II.14 illustrates the changes in the spectra after each O_2 pulse, leading

to the formation of Cu^{II} species. It is evident that the mobile $[Cu^{I}(NH_3)_2]^+$ complex is more sensitive compared to the fw-Cu^{I} species. Indeed, the formation of $[Cu^{II}_2(NH_3)_4O_2]^{2+}$ complex has been related to the ability of a couple of mobile $[Cu^{I}(NH_3)_2]^+$ complexes to activate O_2, while the oxidation of fw-Cu^{I} ions is more difficult.[24,83,25] Nevertheless, both Cu^{I} species can be oxidized to Cu^{II} in fully oxidizing environments at 200 °C. Notably, the rate of oxidation and the final spectral shape differ, indicating the formation of two different Cu^{II} species.

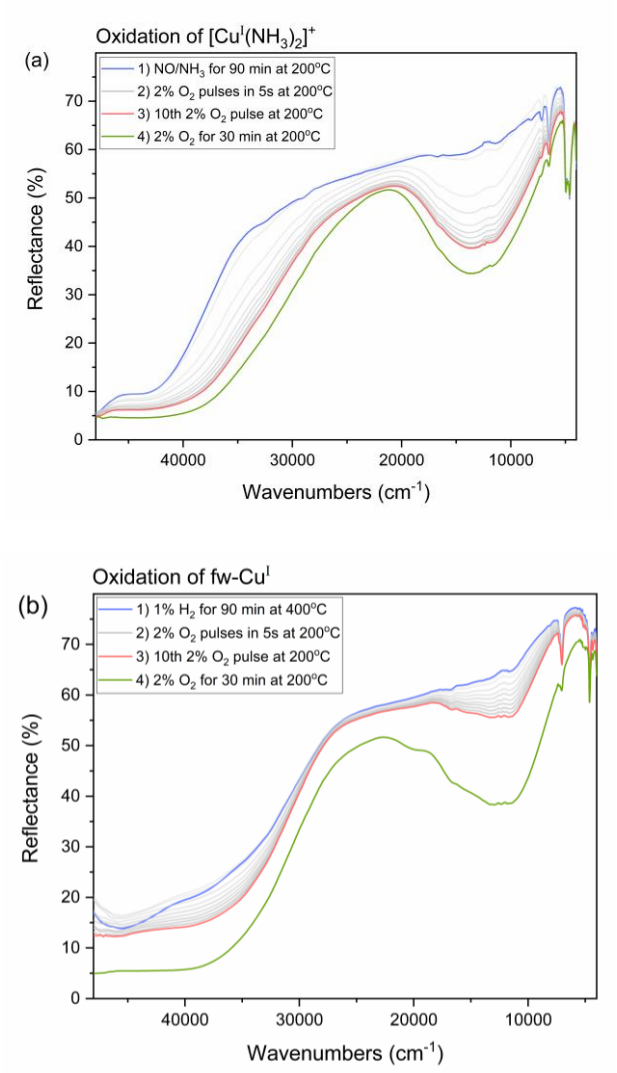

Figure II.14- DR UV-vis experiments: 5 s 2% O_2 pulses on a) $[Cu^{I}(NH_3)_2]^+$ and b) fw-Cu^{I} on Cu-CHA with Si/Al ratio of 6.7 at 200 °C.

These results indicate the high reactivity of $[Cu^{I}(NH_3)_2]^+$ to a small contamination or to the amount of oxygen stored in the catalysts in Cu_xO_y species.[66] Indeed, it suggests that the small amount of SO_2 uptake and deactivation after forming $[Cu^{I}(NH_3)_2]^+$ complex could be related to the presence of a small amount of $[Cu^{II}_2(NH_3)_4O_2]^{2+}$ complex.

II.6 Conclusions

In this study, we investigated the interaction of SO_2 with Cu-CHA catalysts with different Si/Al at 200 ºC, after specific pre-treatments to obtain well defined Cu^{I} and Cu^{II} species. DR UV-vis spectroscopy confirms the observation that SO_2 preferentially interacts with the $[Cu^{II}_2(NH_3)_4O_2]^{2+}$ complex, believed to be an important intermediate in the NH_3-SCR reaction at low temperature.

This interaction results in a reduction of Cu^{II} to Cu^{I} and in the formation of a Cu^{II}-sulfated compound, which cannot be reduced by NO/NH_3. This indicates that the Cu^{II}-sulfated compound is responsible for the observed loss of activity.

The Si/Al ratio of the zeolite affects the amount of formed $[Cu^{II}_2(NH_3)_4O_2]^{2+}$ complex, as measured by UV-vis spectroscopy, showing a correlation with the reaction rate measured at 200 °C, which is in the order 6.7 > 11 > 15. The same trend is observed for the SO_2 uptake measured after SO_2 interaction with the $[Cu^{II}_2(NH_3)_4O_2]^{2+}$ complex. However, the three catalysts show similar deactivation around 50 % after the first SO_2 exposure. Repeated SO_2 exposure cycles show a correlation between SO_2 accumulation and deactivation for the three catalysts, with both parameters gradually levelling off.

The measured changes in the UV-vis after SO_2 interaction with the $[Cu^{II}_2(NH_3)_4O_2]^{2+}$ complex is consistent with the formation of the Cu^{II}-sulfated compound following a reaction mechanism recently proposed.[67] This in turns indicates that the same reaction mechanism is taking place in the three catalysts, irrespective of the Si/Al ratio.

III Chapter III: Impact of water on SO_2 exposure of Cu-CHA catalyst in the NH_3-SCR reaction

III.1 Abstract

Cu-CHA zeolite catalysts exhibit different behaviors under wet and dry SO_2 exposure during deactivation in the NH_3-SCR reaction. To better understand the effect of SO_2 in the presence of H_2O, the catalyst was investigated under highly sensitive conditions, after the formation of the $[Cu^{II}_2(NH_3)_4O_2]^{2+}$ complex, exposure to SO_2, SO_2/O_2, SO_2/H_2O and $SO_2/O_2/H_2O$. *In situ* FT-IR spectroscopy, Temperature-programmed desorption (TPD), Raman spectroscopy, catalytic activity and SO_2 uptake measurements were carried out to compare the effects of SO_2 with H_2O. Different cycles of SO_2 exposure to the $[Cu^{II}_2(NH_3)_4O_2]^{2+}$ complex was carried out, showing a gradual increase in SO_2 uptake and deactivation, levelling off after a number of cycles. The presence of water in the feed causes an increase in SO_2 uptake and deactivation with respect to $SO_2 + O_2$, which is in turns higher than SO_2 alone. While uptake and deactivation level off after 5/6 cycles for SO_2 and SO_2/H_2O, these parameters do not increase significantly with subsequent cycles when O_2 is present. The highest uptake and deactivation are measured when both H_2O and O_2 are present in the feed with SO_2. At similar deactivation level, higher SO_2 uptake is observed in the presence of water. The *in situ* FTIR exhibit increased formation of NH_4^+ after SO_2/H_2O exposure with the same amount of SO_2 uptake compared to SO_2/O_2. Raman spectra reveal a combination of $(NH_4)_2SO_4$ and $CuSO_4$ species after different SO_2 exposure of the $[Cu^{II}_2(NH_3)_4O_2]^{2+}$ complex. Based on these observations, a mechanism is proposed in which SO_2/H_2O exposure deactivates one $[Cu^{II}_2(NH_3)_4O_2]^{2+}$ complex with one SO_2.

III.2 Introduction

The gases exiting the engine contain a lot of water vapor. In addition to this, one must add the percentage of water vapor produced upstream of the NH_3 - SCR catalyst during the oxidation of unburned hydrocarbons present in the exhaust gases. Thus, the SCR catalyst is exposed to water vapor with NOx and

NH_3 when the engine is running.[84] This affects catalytic activity with respect to dry conditions and can also cause deactivation by hydrothermal aging of the catalyst.[85,86] It is thus important to investigate how the presence of water in the feed affects the poisoning of the catalysts by SO_2.

The deactivation of Cu-zeolite catalysts in NH_3-SCR under wet SO_2 poisoning has been investigated, indicating the activity of the catalyst (consisting of 40 ppm SO_2, 14% O_2, 5% CO_2 and 4.5% H_2O) at 178 °C was decreased by 33% following SO_2 exposure at 200 °C, by 21% at 300 °C and by only 8% at 400 °C.[51] For the Cu-CHA catalyst, the effect of SO_x (30% SO_2/70% SO_3) under wet conditions exhibits a different trend, showing higher deactivation at 400 °C compared to 200 °C. This observation can be attributed to the formation of H_2SO_4, which is more likely to occur from the reaction of SO_3 and H_2O at 400 °C.[54] The formation of H_2SO_4 increased when H_2O was added to a mixture of 100 ppm SO_2/5% O_2, compared to dry SO_2 exposure at 200 °C.[87]

In the presence of ammonia during SO_2 exposure, ammonium sulfate species were formed at a higher rate compared to other species. The formation of ammonium sulfate under SO_2 exposure with SCR gas composition was more pronounced at 200 °C compared to 400 °C.[59] SO_2-TPD experiments exhibits a low temperature desorption of SO_2 at 428 °C for Cu/SSZ-13, which is higher than the desorption temperature for Cu-LTA (385 °C).[88] However, the S/Cu ratio for Cu-CHA was determined to be between 0.5-1 after SO_2 exposure, with a maximum deactivation observed on 95%.[52] There is no 1:1 correlation between deactivation and the S/Cu ratio under dry and wet SO_2 exposure at 200 °C. The small amount of SO_2 (10%-20%) deactivates the catalysts to 60%-80%.[53]

SO_2 exposure causes more severe deactivation under SCR conditions (NH_3/NO/O_2/H_2O) compared to exposure to SO_2/O_2/H_2O.[56] The effect of SO_2 on different Cu species formed during SCR conditions shows higher sensitivity of SO_2 to the $[Cu^{II}_2(NH_3)_4O_2]^{2+}$ complex.[66] The $[Cu^{II}_2(NH_3)_4O_2]^{2+}$ complex is widely accepted as an important intermediate in the NH_3-SCR oxidation-reduction cycles at low temperatures, which is formed by reaction of two $[Cu^{I}(NH_3)_2]^{+}$ complexes with O_2.[47,22] Two reaction mechanisms have been suggested for the reaction of SO_2 with the $[Cu^{II}_2(NH_3)_4O_2]^{2+}$ complex. In

one DFT based mechanism, SO_2 reacts with the $[Cu^{II}_2(NH_3)_4O_2]^{2+}$ complex to form a Cu^{II} sulfate species, which then reacts with NO and NH_3 to form N_2, H_2O and H_2SO_4. The formation of $(NH_4)HSO_4$ is then favored in the presence of H_2SO_4 and NH_3 as an acid-base reaction. The key point of this mechanism is that the presence of $(NH_4)HSO_4$ limits the mobility of the $[Cu^{I}(NH_3)_2]^{+}$ complexes and thus the activation of O_2 in the $[Cu^{II}_2(NH_3)_4O_2]^{2+}$ complex.[48]

This reaction mechanism is not in agreement with experimental results showing that the reaction of SO_2 with the $[Cu^{II}_2(NH_3)_4O_2]^{2+}$ complex causes a partial reduction of Cu^{II} to Cu^{I} species.[66] Moreover, the mechanism implies that deactivation should occur at relatively high SO_2 uptakes, which is at variance with experiments in the Chapter 2.[89] Another proposed mechanism involves the formation of Cu^{II} sulfate species, with Cu coordinated to four ligands, as proven by X-ray absorption spectroscopy. Based on the measured S/Cu uptake and on the speciation of Cu species measured by XANES after SO_2 interaction, two $[Cu^{II}_2(NH_3)_4O_2]^{2+}$ complexes react with one SO_2 to form two $[Cu^{I}(NH_3)_2]^{+}$ complexes, one fw-Cu^{I} and a Cu^{II} sulfate species. If the catalysts is exposed to SO_2/O_2, O_2 then oxidizes the two $[Cu^{I}(NH_3)_2]^{+}$ complexes to form more $[Cu^{II}_2(NH_3)_4O_2]^{2+}$ complexes, thereby increasing the effect of SO_2 exposure.[67]

In this work, we studied the effect of water on SO_2 exposure of Cu-CHA zeolite catalysts focusing on SO_2 uptake and deactivation. The catalyst was analyzed under SO_2, SO_2/O_2, SO_2/H_2O and $SO_2/O_2/H_2O$ exposures using *in situ* FTIR spectroscopy, TPD experiments, ex-situ Raman spectroscopy, catalytic activity and SO_2 uptake measurements. The catalyst displays higher SO_2 uptake after SO_2/H_2O exposure compared to SO_2/O_2 exposure at the same level of deactivation. *In situ* FTIR experiment shows an increase in NH_4^+ when dosing SO_2, which is higher after SO_2/H_2O exposure compared to SO_2/O_2. Based on the catalytic activity and spectroscopy results, the effect of water is analyzed trying to rationalize the data with a suggested mechanism of wet SO_2 poisoning.

III.3 Experimental

Cu-CHA zeolite catalysts were synthesized using the incipient wetness impregnation method. The Cu loading was maintained at 3.2 wt% for all

catalysts, with Si/Al ratios of 6.7 and 15.

FTIR spectra were collected in transmission mode with 4 cm^{-1} resolution using a Bruker N Invenio spectrometer equipped with a mercury cadmium telluride (MCT) cryodetector maintained at -196 ºC. The FTIR Sandwich cell described in Refs. [90,91] was placed inside the FTIR instrument for *in situ* spectroscopy measurements. The FTIR cell was connected to a gas setup allowing for flow control, and the analysis of the outlet was carried out by a Mass Spectrometer (MS) for selected experiments. 10 mg of catalysts were pressed into a self-supported disk. For all measurements, a background spectrum was collected and subtracted from all spectra. After assembling the sample and cell, the catalyst was heated in O_2 to 300 ºC with a ramp of 3 ºC/min, held 30 min at this temperature and then cooled to 200 ºC with the same temperature ramp. All subsequent procedures were performed at 200 ºC. The catalyst was reduced in 500 ppm NO/ 600 ppm NH_3 for 1 hour (30 min for cycles) and oxidized in 10% O_2 for 1 hour (45 min for cycles). The catalyst was then exposed to 30 ppm SO_2, 30 ppm SO_2 and 10% O_2 and 30 ppm SO_2 with 5% H_2O, independently. For cycle experiments, the catalyst was reduced and oxidized again as described after the SO_2 exposure step.

Raman spectra were collected using a Laser source with a wavelength of 266 nm (200 μW of power). All spectra were collected at 25 ºC in the range of 1000 - 4000 cm^{-1}. The Raman radiation was collected using a backscattering configuration and analyzed with a single-stage Czerny-Turner spectrometer (Andor Technology) featuring a 750 mm focal length and a holographic reflection grating with 1800 lines/mm and 250 nm ruling. Detection was performed using a back-thinned CCD cooled via a Peltier system (Andor Technology). The laser power delivered to the sample was approximately 0.1 mW. The final spectra were derived by averaging 12 separate measurements, each recorded over a duration of 5 minutes. All catalysts were measured *ex situ* after specific treatments, carried out on powders or on the pellet from *in situ* FTIR spectroscopy.

Catalytic activity and SO_2 uptake measurements were carried out using a U-shaped reactor. The gas setup was composed by several mass flow controllers to obtain the desired gas mixtures. The reactor outlet was analyzed by an FTIR

spectrometer. 5 or 10 mg of catalysts, meshed to 150 - 300 µm, were packed into the reactor and held on glass wool. The catalyst was heated to 550 °C in O_2 by a ramp rate of 5 °C/min and then cooled down to 200 °C to measure catalytic activity. To assess the catalytic activity of the fresh catalyst, it was exposed to 500 ppm NO, 600 ppm NH_3, 10% O_2, 5% H_2O in N_2 with a total flow of 13.5 NL/h and held for 20 min to calculate the conversion at 200 °C. The catalyst was then reduced in 800 ppm NO / 960 ppm NH_3 and oxidized in 10% O_2. Finally, the catalyst was exposed to 100 ppm SO_2, 100 ppm SO_2/10% O_2, 100 ppm SO_2/10% H_2O or 100 ppm SO_2/10% O_2/5% H_2O (likes the scheme of Figure II.10 with different conditions for the SO_2 exposure). The SO_2 uptake was determined by integration of the amount of SO_2 consumption during SO_2 exposure. The background SO_2 concentration (⁓ 100 ppm) was measured by bypassing the reactor for 15 min. The sample was exposed to the different SO_2 mixtures for 45 min to reach a stable background level. Additionally, the catalytic activity of deactivated samples was measured in the same conditions after SO_2 exposure in the different conditions mentioned above. The first-order rate constant of the catalyst was calculated as mentioned:

III.1) $$k = -\frac{F}{W} ln(1 - X)$$

and the deactivation of the catalyst was calculated based on:

III.2) $$Deactivation\ (\%) = \frac{k_{deactivated}}{k_{Fresh}} \times 100$$

Temperature programmed desorption (TPD) analysis was carried out to follow NH_3 and SO_2 desorption using the same setup as the catalytic measurements, with 50 mg of catalyst in the 150-300 µm sieve fraction based on dry weight. The catalyst was heated to 550 °C by a rate of 5 °C/min and held at this temperature for half an hour. The reactor was then cooled to 200 °C and the same procedure described for the *in situ* FTIR measurements was performed to form the Cu^{II} sulfate species. The catalyst was subsequently heated to 550 °C by a ramp rate of 3 °C/min to monitor NH_3 and SO_2 desorption. Additionally, SO_2 desorption was followed in the range of 200 to 550 °C.

III.4 Results

III.4.1 Catalytic activity and SO_2 uptake measurements

Repeated SO_2 exposure and deactivation measurements were carried out to investigate the behavior of Cu-CHA catalysts under different SO_2 exposure conditions through complete deactivation. In Figure III.1, the deactivation of Cu-CHA catalysts with 3.2 Cu wt% and a Si/Al = 6.7 is presented over six cycles under several conditions at 200 ºC. First, the catalyst was reduced in NO/NH_3 and oxidized in 10% O_2 (forming $[Cu^{II}_2(NH_3)_4O_2]^{2+}$ complex). Then, it was exposed to SO_2 (red curve), SO_2/O_2 (blue curve), SO_2/H_2O (orange curve) or $SO_2/O_2/H_2O$ (green curve) and the catalytic activity was subsequently measured at 200 °C.

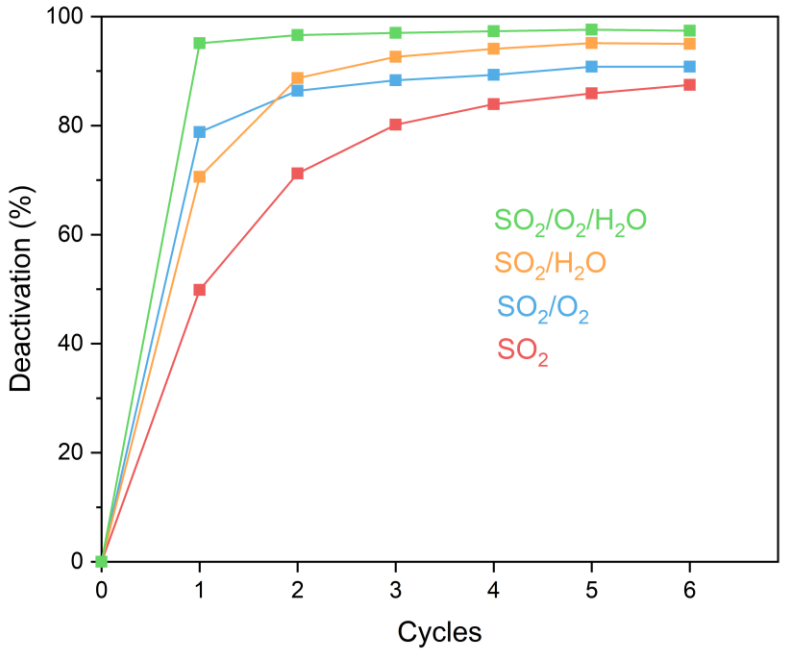

Figure III.1- Deactivation of Cu-CHA catalyst with 3.2 Cu wt% and Si/Al = 6.7 during six cycles after SO_2 exposure. The activity was measured in 500 ppm NO, 600 ppm NH_3, 10% O_2, 5% H_2O and N_2 as a balance with the total flow of 13.5 NL/h.

When the catalyst is exposed to only SO_2 the results are consistent with what discussed in Chapter II. Namely, deactivation is around 49% during the first cycle, indicating that half of the activity remained.[67,89] To achieve more deactivation, the catalyst was again reduced in NO/NH_3, oxidized in 10% O_2

and exposed to SO_2. Deactivation reaches around 75% after the second cycle, showing that SO_2 deactivates half of remaining active sites. However, the deactivation is less than half of the remaining active sites after the third cycle and stabilizes after six cycles.

The SO_2/O_2 exposure causes around 80% deactivation after the first cycle (Figure III.1, blue curve). After the second cycle, the deactivation becomes more or less stable. By adding water ($SO_2/O_2/H_2O$, green curve), the catalyst is deactivated close to 98% and becomes stable after only one cycle. This shows a severe deactivation compared to the first cycle of only SO_2 and SO_2/O_2 exposures. To better understand the effect of H_2O, the catalyst was exposed to SO_2/H_2O (Figure III.1, orange curve). The deactivation is higher than SO_2 alone and lower than SO_2/O_2 exposure after the first cycle, levelling off after the 3rd cycle. The final level of deactivation for SO_2/H_2O exposure becomes higher than both exposure to SO_2 only and SO_2/O_2, but lower with respect to $SO_2/O_2/H_2O$.

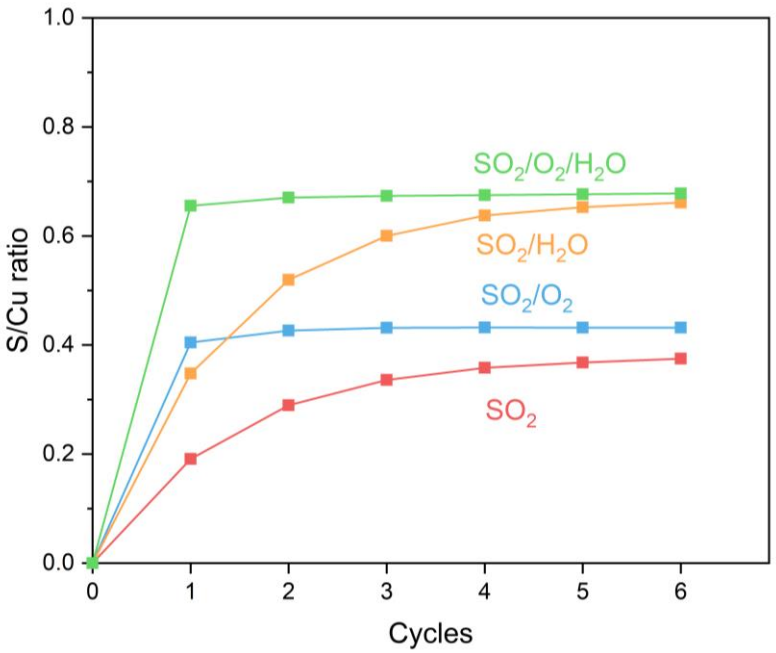

Figure III.2- SO_2 uptake of Cu-CHA catalyst with 3.2 Cu wt% and Si/Al = 6.7 during six cycles of SO_2 exposure.

In Figure III.2, the SO_2 uptake measured over the six cycles described above

is reported as S/Cu molar ratio. With SO_2 alone, an S/Cu ratio of 0.2 is reached after the first SO_2 exposure. The cumulative SO_2 uptake is approximately 0.3 after the second SO_2 exposure and gradually increases levelling off around 0.375. With SO_2/O_2 exposure, a S/Cu ratio around 0.4 is reached in the first step, very close to the final value of 0.43, which is 10% higher than the final level of the SO_2 alone exposure. The key point is that the trend of SO_2 uptake is similar to the deactivation behavior observed during the cycles (Figure III.1).

The total amount of SO_2 uptake increases with addition of H_2O to SO_2 and O_2 as measured by a S/Cu ratio of 0.65. This ratio reaches to a saturated level after one cycle. The uptake for $SO_2/O_2/H_2O$ exposure follows a similar trend to the SO_2/O_2 exposure. This indicates that the effect of O_2 can also be observed with SO_2/H_2O.[53] However, exposure to SO_2/H_2O shows that the S/Cu ratio does not stabilize after the first cycle. The SO_2 uptake trend is similar to the SO_2 alone, with approximately below a factor of two of the S/Cu ratio in each cycle. The deactivation trends for SO_2/H_2O and SO_2/O_2 exposures are similar after the third cycle; however, S/Cu ratio of SO_2/H_2O exposure is around 50% higher compared to SO_2/O_2 exposure.

III.4.2 Investigation of SO_2 exposure on Cu-CHA catalyst using *in situ* FTIR spectroscopy

The effect of water was monitored using *in situ* FTIR spectroscopy during the different steps of the process, that is i) pretreatment in O_2, ii) reduction with NO/NH_3 to form $[Cu^{I}(NH_3)_2]^+$ complexes, iii) reaction with O_2 to form $[Cu^{II}_2(NH_3)_4O_2]^{2+}$ complexes and iv) exposure to SO_2. Starting from the pre-treated catalyst, Figure III.3a shows the typical fingerprints of Brønsted acid sites at 3600 cm^{-1}.[68,92,93] Two bands at 900 cm^{-1} and 950 cm^{-1} are attributed to fw-Cu^{II} and fw-Cu^{II}(OH), respectively (Figure III.3c, black curve).[94,95]

Figure III.3c (green curve) shows the disappearance of Cu^{II} and $[Cu^{II}(OH)]^+$ bands after reduction in NO/NH_3. Additionally, the NH_3 and NH_4^+ bending modes appear at 1620 and 1430 cm^{-1}, respectively (Figure III.3b). This indicates that framework coordinated Cu species begin to dissolve in NH_3, forming mobile species as $[Cu^{I}(NH_3)_2]^+$ complexes.[96] The NH_3 and NH_4^+ stretching region (3300-2800 cm^{-1}) is observed instead of Brønsted sites in

Figure III.3a. The appearance of the NH_4^+ band is correlated with the consumption of Brønsted sites which are protonating NH_3. The area of the NH_4^+ band is lower for Cu-CHA with the Si/Al = 15, in agreement with the expected lower amount of Brønsted sites (Table III.1).

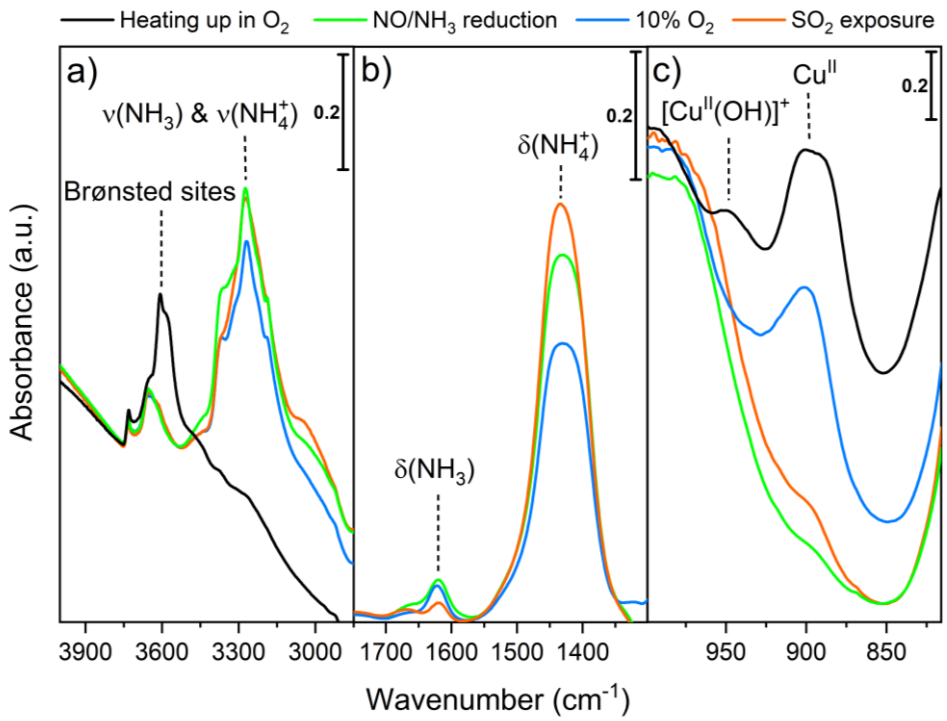

Figure III.3- IR spectra after i) pretreatment, ii) formation of $[Cu_I(NH_3)_2]^+$ complexes, iii) formation of $[Cu^{II}_2(NH_3)_4O_2]^{2+}$ complex and iv) SO_2 exposure for Cu-CHA catalyst with 3.2 Cu wt% and Si/Al = 6.7. Spectra in panel b) are background subtracted using the spectrum measured after heating up in O_2 as a reference.

The formation of $[Cu^{II}_2(NH_3)_4O_2]^{2+}$ complex under oxidation of the catalyst in 10% O_2 is shown in Figure III.3 (blue curve). The intensity of the NH_4^+ and NH_3 band decreases in Figure III.3b, while the intensity of Cu^{II} at 900 cm^{-1} increases (Figure III.3c). The shape of the latter peak slightly differs from the spectrum measured on the pretreated catalyst. Figure III.4 displays NH_3 desorption during the oxidation step, as monitored by Mass spectrometry, indicating that NH_3 is desorbed from the Cu-CHA catalyst during the oxidation. No significant changes are observed in the Bronsted bands, indicating that the decrease of NH_4^+ and release of NH_3 do not restore these

sites. The same behavior is observed for Cu-CHA with a high Si/Al ratio during the oxidation step for both NH_4^+, NH_3 and framework coordinated Cu^{II} bands. However, the relative decrease in the area of the NH_4^+ band in this case is around 9%, which is less compared to 27% for Cu-CHA catalyst with the low Si/Al ratio (Table III.1).

Table III.1- Spectral changes of NH_4^+ and framework-Cu^{II} in Cu-CHA catalysts with the same 3.2 Cu wt% and Si/Al = 6.7 and 15. The values were calculated by measuring the area of the corresponding bands.

Si/Al ratio	Area of NH_4^+ after reduction with NO/NH_3	NH_4^+ change after oxidation[b]	NH_4^+ change after SO_2 exposure[c]
6.7	49.6	- 27%	49%
15	17.5	- 9%	28%

[a] calculated as ratio of the corresponding areas; [b] percentage decrease with respect to the area measured in the reduction step; [b] percentage increase with respect to the previous oxidation step (that is formation of $[Cu^{II}_2(NH_3)_4O_2]^{2+}$ complex)

The effect of SO_2 exposure on the $[Cu^{II}_2(NH_3)_4O_2]^{2+}$ complex was investigated (orange curve in Figure III.3). The decrease in the intensity of NH_3 band is in agreement with the observation that the $[Cu^{II}_2(NH_3)_4O_2]^{2+}$ complex was broken after exposure to SO_2.[48,66,67,89] Additionally, the intensity of Cu^{II} band at 900 cm^{-1} decreases. The intensity of the NH_4^+ band increases, reaching a final intensity higher than what obtained after reduction in NO/NH_3 (see Table 1). This suggests that the total amount of NH_4^+ is greater than the NH_4^+ formed on Brønsted sites. The same trend is observed for Cu-CHA catalyst with a high Si/Al ratio. The changes in the NH_4^+ bands after SO_2 exposure for Cu-CHA with Si/Al = 6.7 and 15 are 49% and 28% with respect to the previous step (formation of $[Cu^{II}_2(NH_3)_4O_2]^{2+}$ complex) and 9.5% and 17% with respect to the amount of NH_4^+ related to Bronsted sites that is measured after the NO/NH_3 step), respectively (Table III.1).

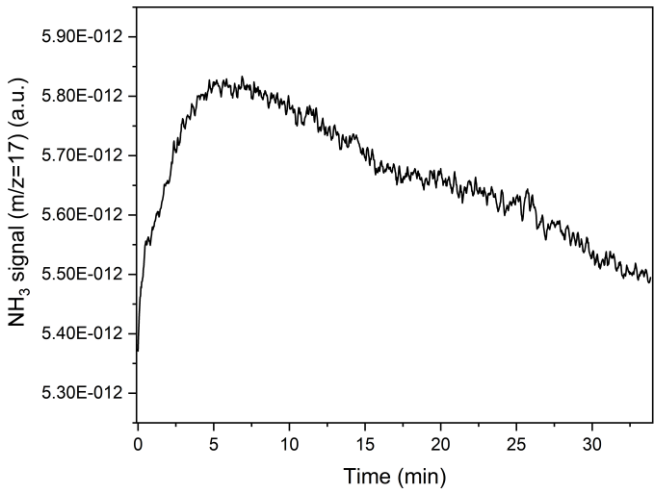

Figure III.4- Mass spectrometry of NH_3 desorption while forming $[Cu^{II}_2(NH_3)_4O_2]^{2+}$ complex for Cu-CHA catalyst with 3.2 Cu wt% and Si/Al = 6.7.

The evolution of the spectra was followed after a second reduction and oxidation cycle after SO_2 exposure, focusing on the two main regions of NH_4^+ and Cu^{II} bands (Figure III.5). Upon NO/NH_3 exposure, the intensity of the NH_3 band is completely restored, reaching a final intensity comparable to the first reduction step. However, the second reduction causes an increase in the NH_4^+ band which has a final intensity higher than after SO_2 exposure and the first reduction (Figure III.5a). The key point is that the second reduction occurs under the same conditions as the first reduction. The only difference is the SO_2 exposure of the $[Cu^{II}_2(NH_3)_4O_2]^{2+}$ complex. The NH_4^+ band decreases again after the oxidation reaching a higher intensity with respect to the same state before SO_2 exposure. Namely, the intensity of the NH_4^+ band increases of 16% after the second NO/NH_3 step with respect to the same step before SO_2, and of 29% after formation of the $[Cu^{II}_2(NH_3)_4O_2]^{2+}$ complex with respect to the same state before SO_2 (Table 2).

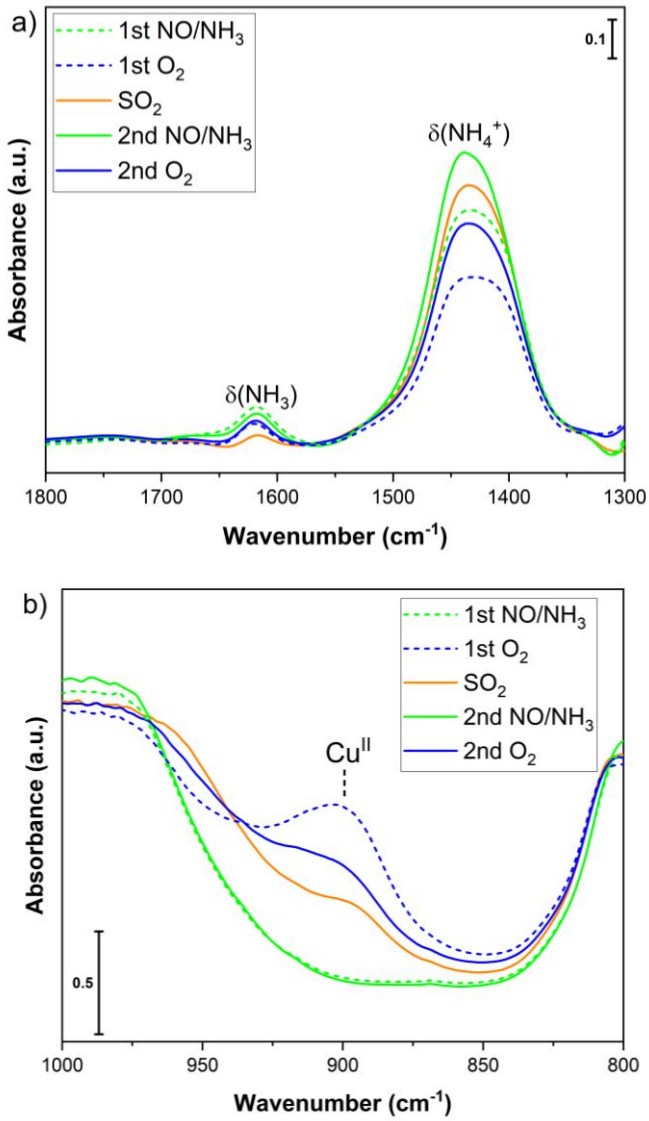

Figure III.5- Changes in the IR spectra in the a) NH_3 and NH_4^+ bending region and b) framework region followed through reduction/oxidation step before and after SO_2 exposure on Cu-CHA with 3.2 Cu wt% and Si/Al = 6.7.

In Figure III.5b, the changes in the Cu^{II} band at 900 cm^{-1} during the second reduction approximately match the spectra of the first reduction. However, the intensity of Cu^{II} band after the second oxidation is lower compared to the first oxidation. To assess the effect of SO_2 on the second cycle, the same experiment was conducted without SO_2 exposure for two cycles. In this case, all spectra of reduction and oxidation during first and second cycle are the

same in both spectral regions.

Table III.2- Changes in the area of NH_4^+ bands during SO_2 exposure and subsequent reduction and oxidation for Cu-CHA catalyst with 3.2 Cu wt% and Si/Al = 6.7.

Conditions	Change in NH_4^+ changes after SO_2 exposure[a]	Change in NH_4^+ between first and second reduction step	Change in NH_4^+ between first and second oxidation step
SO_2 only	49%	16%	29%
SO_2/O_2	45%	22%	39%
SO_2/H_2O	85%	33%	49%

[a] percentage increase with respect to the previous oxidation step (formation of $[Cu^{II}_2(NH_3)_4O_2]^{2+}$ complex)

Based on the analysis of IR spectra, specifically focusing on the intensity of the NH_4^+ band, the effect of SO_2/H_2O was investigated through two experiments following the same cycles described above exposing the catalyst to SO_2/H_2O and SO_2/O_2 between the two reduction and oxidation cycles (Figure III.6). The intensity of the NH_4^+ band after SO_2/O_2 exposure is similar to what observed after SO_2 (compare Figure III.5a and Figure III.6a and see Table III.2). However, the intensity of the NH_4^+ band after subsequent reduction and oxidation steps is higher with respect to what observed after SO_2. Namely, this results in an increase of 22 % and 39%, respectively (Table III.2).

Notably, for SO_2/H_2O exposure, the intensity of NH_4^+ band is approximately twice that of SO_2/O_2 exposure (Figure III.6 and Table III.2), even if they show the same SO_2 uptake (Figure III.2). The change in the area of the NH_4^+ band during the second reduction and oxidation after SO_2/H_2O exposure is higher compared to SO_2/O_2 exposure (33 and 49%, respectively, Table III.2). Additionally, the area of NH_4^+ band changes approximately twice as much compared to SO_2 exposure alone, which is consistent with the amount of SO_2 uptake.

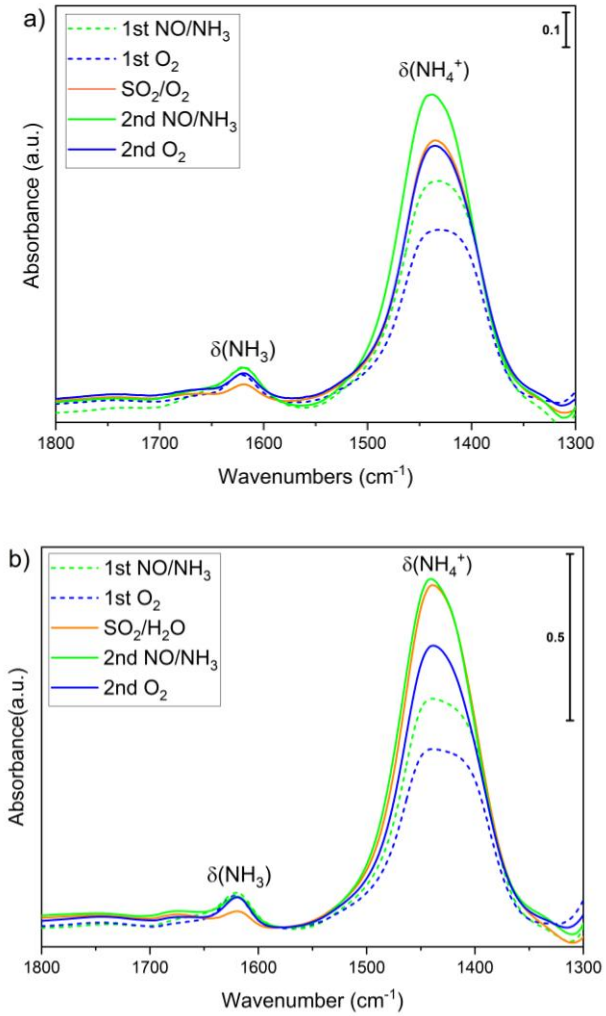

Figure III.6- Changes in the IR spectra in the NH_3 and NH_4^+ bending region followed through reduction/oxidation step before and after of a) SO_2/O_2 and b) SO_2/H_2O exposure on Cu-CHA with 3.2 Cu wt% and Si/Al = 6.7.

III.4.3 Probing the Temperature-programmed desorption (TPD) under dry and wet conditions

In Figure III.7, TPD experiments were investigated by increasing the temperature from 200 to 550 ºC after different pretreatments. In all experiments the catalyst was first exposed to NO/NH_3 followed by 10% O_2 as described for the IR studies, with a subsequent SO_2 (or SO_2/O_2, or SO_2/H_2O) exposure. Three additional experiments were carried out after the second reduction with NO/NH_3 after SO_2 exposure in different conditions. The

experiments were performed to monitor the desorption temperature and the amount of NH_3 which was present on the catalyst at 200 °C as NH_4^+ and NH_3 in the different conditions as monitored by IR.

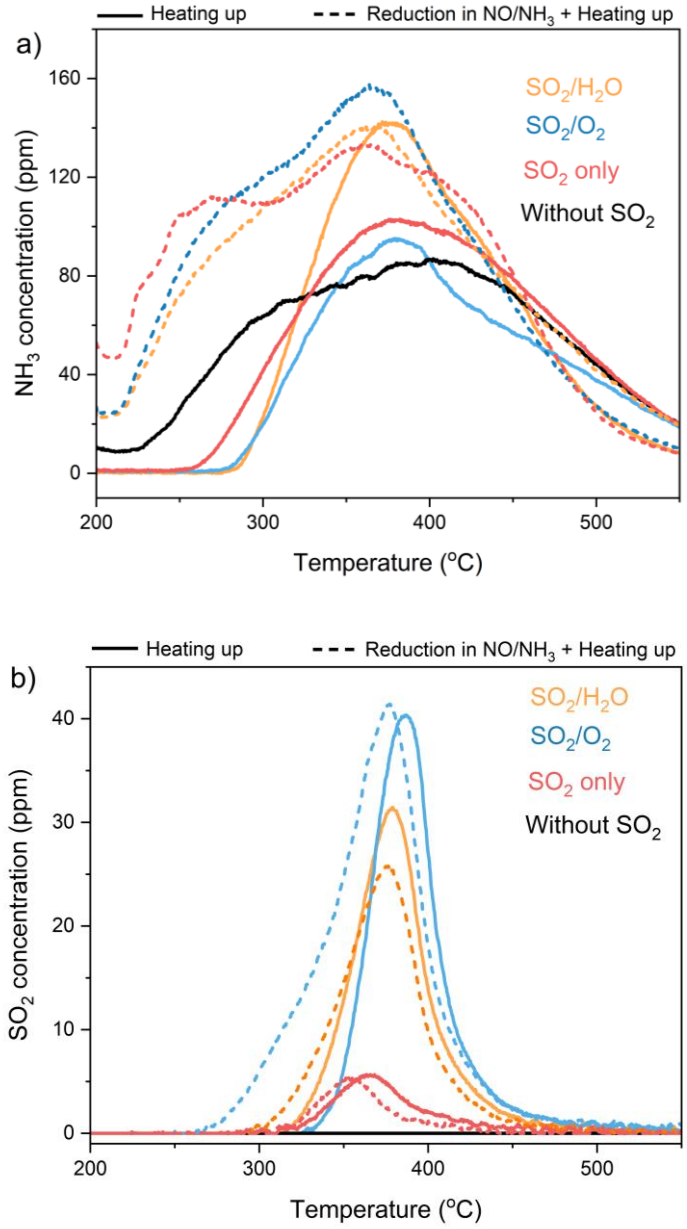

Figure III.7- TPD experiments of Cu-CHA catalysts with 3.2 Cu wt% and Si/Al = 6.7 under different SO_2 exposure after forming the $[Cu^{II}_2(NH_3)_4O_2]^{2+}$ complex.

Before analyzing the TPD profile after SO_2 exposure in different conditions, it is useful to consider the profile measured without SO_2 (black curve), which can be discussed on the basis of the abundant literature on NH_3-TPD. Typically, the NH_3-TPD profile of Cu-CHA is characterized by three desorption peaks; a low-temperature peak below 200 ºC, an intermediate-temperature peak at 250−350 ºC and a high-temperature peak at 400−500 ◦C. The low-temperature peak is generally assigned to NH_3 adsorbed to Lewis acid sites, whereas the peak at 400−500 ºC has been attributed to NH_3 adsorbed on Brønsted acid sites. NH_3 adsorbed at Cu-sites has been suggested to give rise to the intermediate-temperature peak at 250−350 ºC.[97–99] However, Chen et al. proposed, on the basis of first principle calculations that low-temperature peak (below 200 ºC) is assigned to NH_3 desorption from Lewis acid sites together with NH_3 desorption from a $[Cu^{II}(OH)(NH_3)_3]^+$ complex. The intermediate-temperature peak (250−350 ºC) is attributed to the decomposition of a linear $[Cu^{I}(NH_3)_2]^+$ complex and a residual from $[Cu^{II}(OH)(NH_3)_3]^+$. The high temperature peak is predicted to have contributions from Brønsted acid sites (NH_4^+), $[Cu^{I}(NH_3)]^+$ and $[Cu^{II}(NH_3)_4]^{2+}$.[69]

The NH_3 desorption profile reported in Figure III.7a resembles that measured after exposing a Cu-CHA catalyst to NH_3 at 200 °C, with a desorption peak around 250-350 °C and a more intense centered around 420 °C and extending above 500 °C.[69] A detailed assignment of the peaks through deconvolution is outside the scope of this work. However, it is important to remember that the reported TPD was carried out after formation of the $[Cu^{II}_2(NH_3)_4O_2]^{2+}$ complex, so that the assignment by Chen. et al. cannot be taken literally. We can only conclude that, due to the similarity of the profiles, the energy of interaction of NH_3 in the $[Cu^{II}_2(NH_3)_4O_2]^{2+}$ complex is similar to that of $Cu^{II}(NH_3)_3X$ (X = NH_3, OH-) complexes. We cannot exclude a contribution from a small fraction (around 10%) of unoxidized $[Cu^{I}(NH_3)_2]^+$ complexes.[44]

NH_3 desorption after SO_2 exposure shows the depletion of the component below 300 °C, so that the profile can be described as a main broad peak centered at 380 °C, which is probably due to the overlapping of two contributions, one related to NH_3 coordinated to Cu sites and one to NH_4^+. After SO_2/O_2 the desorption peak is still centered at 380 °C but loses a

component below 300 °C and some of the higher temperature desorption between 400 and 500 °C. On the other hand, NH_3 desorption peak is sharper with a maximum at 380 ºC for SO_2/H_2O exposure, losing components below 300 and above 450 °C with respect to SO_2 alone. The amount of desorbed NH_3 is comparable in the four experiments within the experimental error (Table III.3), indicating that no NH_3 is lost during the SO_2 exposure steps.

The amount of desorbed NH_3 increases after the second reduction in NO/NH_3 after SO_2 exposure (Table III.3), indicating that the capability of the catalyst to store NH_3 is increased after SO_2 poisoning. By assuming as a reference, the average value of NH_3 desorbed in the first 4 experiments (average of the first 4 entries of Table III.3, corresponding to 1002 ± 48 $\mu mol_{NH3}/g_{cat}$), we can estimate an increase in NH_3 storage capability around 12 % sending NO/NH_3 after SO_2 and around 35% after SO_2/O_2 or SO_2/H_2O, with an error around 5%. Thus, after exposure to SO_2 together with O_2 or H_2O, more NH_3 can be stored in the catalyst under these conditions.

Table III.3- Measured amount of NH_3 and SO_2 after reduction and oxidation for Cu-CHA catalyst with 3.2 Cu wt% and Si/Al = 6.7.

Conditions	Desorbed NH_3 $\mu mol_{NH3}/g_{cat}$	Desorbed SO_2 $\mu mol_{SO2}/g_{cat}$
No SO_2	956	-
SO_2 only	1033	20.5
SO_2/O_2	966	113.0
SO_2/H_2O	1053	94.5
NO/NH_3 after SO_2	1123	15.4
NO/NH_3 after SO_2/O_2	1364	161.0
NO/NH_3 after SO_2/H_2O	1324	86.7

What is interesting is the change in the shape of the desorption peak. All NH_3 desorption profiles show a main maximum slightly shifted with respect to the corresponding experiments without the second NO/NH_3 step. This is moving

from around 380 to 360 °C. An evident increase is observed for the three experiments below 300 °C, especially for the SO_2 only sample.

The corresponding SO_2 desorption profiles in the 200 – 550 °C range are reported in Figure III.7b. In the experiments where desorption was followed after SO_2 exposure (full lines) the measured amount follow the same trend observed in Figure III.2 (first cycle), that is $SO_2 << SO_2/H_2O < SO_2/O_2$ (see also Table III.3). When desorption is carried out after a subsequent NO/NH_3 treatment (dashed lines), we observe a slightly lower amount of SO_2 desorbed in the case of exposure to SO_2 and SO_2/H_2O, which could be considered within the experimental error. A higher SO_2 desorption is observed before and after the second NO/NH_3 treatment when the sample is exposed to SO_2/O_2. It is not clear if this is related to reproducibility issues, or if the exposure of the catalyst to NO/NH_3 after the formation of the Cu^{II}-sulfated complex causes the transformation of sulfated species. Indeed, the measured SO_2 desorbed amounts are lower with respect to the uptake of SO_2 measured in Table III.3. This is in agreement with the fact that SO_2 desorption after similar treatments has been measured to occur at temperatures higher than 550 °C.[66]

What is more interesting is the change in the maximum of the desorption peaks in the different experiments. First, the maximum of the SO_2 desorption peak moves from 366 to 380 °C and finally to 387 °C after exposure to SO_2, SO_2/H_2O and SO_2/O_2, respectively. This means that the sulfated species formed in the three experiments are different. Secondly, exposure of these sulfated species to NO/NH_3 causes a decrease in thermal stability. Namely, the maximum of the peak for SO_2 and SO_2/O_2 roughly decrease of 10 °C (from 366 to 355 °C and from 387 and 377 °C, respectively). The maximum of the peak measured after SO_2/H_2O is hardly affected, but a lower temperature tail is observed also in this case. These observations indicate a reaction between the sulfated species (involving ammonium and/or Cu ions) and the NO/NH_3 mixture.

As a final observation, the desorption temperatures measured in these experiments are different with what reported in Refs,[66,67] which have been measured with a different temperature ramp (10 °C/min vs 3 °C/min in this thesis work). However, we observe the same trend as in Ref,[68] regarding the

difference in desorption temperature of SO_2 in the catalysts treated to SO_2 and SO_2/O_2.

III.4.4 Following the effect of water on SO_2 exposure by Raman spectroscopy

Figure III.8 reports the Raman spectra measured on reference compounds, to help in the interpretation of the Raman spectra measured on Cu-CHA catalyst after the IR experiments described above. Three sulfates were measured, namely $(NH_4)_2SO_4$ and two $CuSO_4$, one hydrated $CuSO_4 \cdot 5H_2O$ and one theoretically anhydrous. These have been chosen as examples of sulfated species suggested to form during SO_2 exposure.[61,67,88] The spectrum of $CuSO_4 \cdot 5H_2O$ displays a significant peak at 984 cm^{-1}, attributed to the stretching vibration of SO_4^{2-}, denoted as $\nu_{sym}(SO_4^{2-})$ or ν_1 (A1 molecular symmetry in Td geometry).[100–102] A similar intense and sharp peak is observed in the spectrum of $(NH_4)_2SO_4$ at 975 cm^{-1} in agreement with the literature.[103,104] The same fingerprints were observed in a Cu-free H-CHA zeolite impregnated with 10 wt% of $(NH_4)_2SO_4$. The lower position of ν_1 for $(NH_4)_2SO_4$ is in agreement with the interpretation that this can be related to the differences of the polarizing power of cations. The higher dimension of the ammonium ion with respect to Cu would result in lower polarizing power, and a lower frequency of ν_1.[104,105]

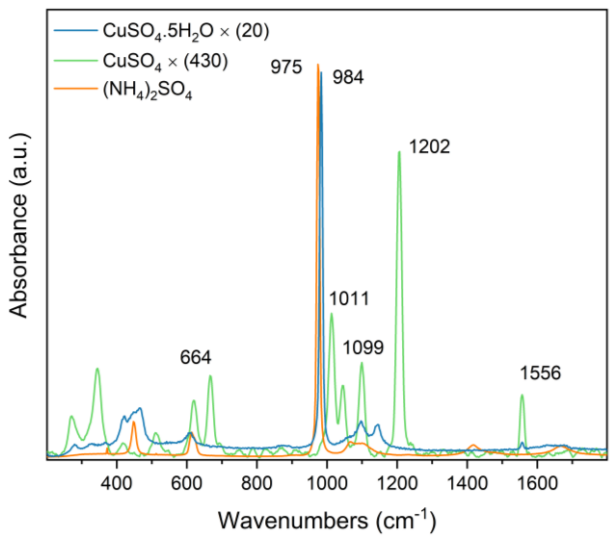

Figure III.8- Raman spectra of different sulfate references compounds. λex = 266 nm.

The spectrum of $CuSO_4$ shows several peaks of similar intensity at 664, 1011, 1099, 1202 and 1556 cm^{-1}, which does not fit with the literature spectra of anhydrous $CuSO_4$.[106,107] The spectrum more closely resemble that of monohydrate $CuSO_4$, in agreement with reports showing that the hydration level of $CuSO_4$ affects the spectral shape.[106,107] This observation is important, since it shows that the spectral shape (that is the splitting of SO_4^{2-} bands) does not only depends on the ion to which the sulfate is coordinated, but also (and importantly) by the geometry of SO_4^{2-}. This also means that both $(NH_4)_2SO_4$ and $CuSO_4$, if molecularly dispersed or interacting with the zeolite, could give different spectra with respect to the same compounds in their crystalline form (that is the reference spectra reported in Figure III.8).

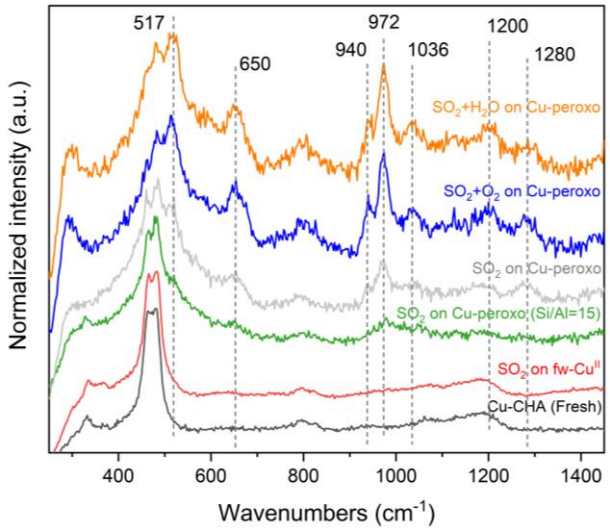

Figure III.9- Raman spectra of Cu-CHA catalysts with 3.2 Cu wt% and Si/Al = 6.7 (except green spectrum as Si/Al = 15) under different conditions. Ex situ spectra measured after the IR experiments described above. λex = 266 nm.

In Figure III.9, the Raman spectra measured on Cu-CHA catalyst after the IR experiments described above are reported. For comparison, the spectrum of fresh Cu-CHA is also reported. The spectrum measured after exposing to SO_2 framework coordinated Cu^{II} sites (that is without previous exposure to NO/NH_3 followed by O_2) does not show any peaks which can be associated to sulfated species. This is in agreement with the low SO_2 uptake and the

spectroscopic observation that in this case Cu sites are hardly affected.[66,89]

The spectrum after SO_2 exposure of the $[Cu^{II}_2(NH_3)_4O_2]^{2+}$ complex reveals several new peaks compared to fresh catalyst. The peak at 972 cm^{-1} is very close to the $\nu_{sym}(SO_4^{2-})$ peak observed on $(NH_4)_2SO_4$ and $CuSO_4 \cdot 5H_2O$. However, this peak is not the major one, as there are several other peaks at 650, 1036, 1280 cm^{-1}. The spectra of SO_2/O_2 and SO_2/H_2O exposures exhibit the same bands as the SO_2 exposure of the $[Cu^{II}_2(NH_3)_4O_2]^{2+}$ complex, but with higher intensity, in agreement with the higher SO_2 uptake measured. The multiplicity of bands observed could point to the fact that different sulfate species are present, that is both $(NH_4)_2SO_4$ and Cu-slphated species, such as the ones proposed by Molokova et al. and Bjerregaard et al.[48,67]

III.5 Discussion

III.5.1 Following the deactivation through cycles of SO_2/O_2 exposure

The cycles of SO_2 exposure, SO_2 uptake and catalytic activity measurements display how the catalysts can deactivate around 85%. The key point is that the catalysts reach the saturated level of deactivation based on the repeated reaction of SO_2 with the $[Cu^{II}_2(NH_3)_4O_2]^{2+}$ complex. It is interesting to comment on the observed trends before moving to discuss the effect of O_2. As mentioned in Chapter II, the activity of catalyst is decreased to 50 % after first SO_2 exposure. This can be related to the formation of two $[Cu^{I}(NH_3)_2]^{+}$ complexes and one Cu^{II} sulfated complex after reaction of one SO_2 molecule with two $[Cu^{II}_2(NH_3)_4O_2]^{2+}$ complex, as proposed in Ref Molokova et al.[67] In the second cycle two $[Cu^{I}(NH_3)_2]^{+}$ complexes formed can be oxidized and form a new $[Cu^{II}_2(NH_3)_4O_2]^{2+}$ complex. It means that it is feasible to recover one of the $[Cu^{II}_2(NH_3)_4O_2]^{2+}$ complex during cycles. Then, the second cycle shows the same situation with 50 % deactivation. Therefore, the total deactivation reaches around 75 %. However, the deactivation after the third cycle is lower than 50% of remaining activity. This can be related to the limitation in the activation of O_2 by two $[Cu^{I}(NH_3)_2]^{+}$ complexes to form the $[Cu^{II}_2(NH_3)_4O_2]^{2+}$ complex.[48] Therefore, the rest of cycles has the same trend and activity reaches a stable level.

When SO_2 exposure is carried out with O_2 on SO_2, a similar trend is observed.

However, both SO_2 uptake and catalytic measurements indicate that O_2 accelerates the reaction of SO_2 with the $[Cu^{II}_2(NH_3)_4O_2]^{2+}$ complex. As observed, SO_2 reduces a part of Cu ions in the $[Cu^{II}_2(NH_3)_4O_2]^{2+}$ complex to Cu^{I} species.[66,89] By adding O_2 to SO_2 exposure, the Cu^{I} ions formed by this reaction are oxidized to Cu^{II}. It means that the availability of the $[Cu^{II}_2(NH_3)_4O_2]^{2+}$ complex which is more sensitive to SO_2 is more compared to only SO_2 exposure.[67] In this case, SO_2 reacts more with Cu and the S/Cu ratio is close to the saturation level reached during only SO_2 exposure in the first cycle. The same holds for deactivation, which is close to saturation level already after the first exposure.

III.5.2 Investigation of the sulfated species by *in situ* FTIR spectroscopy and *ex situ* Raman spectroscopy

The *in situ* FTIR spectra measured while forming the $[Cu^{II}_2(NH_3)_4O_2]^{2+}$ complex and subsequent SO_2 exposure show several major changes in the NH_4^+ band. After NO/NH_3 exposure, both NH_3 and NH_4^+ are formed. The former is related to $[Cu^{I}(NH_3)_2]^+$, while the latter is due to the protonation of NH_3 by the Brønsted acid sites forming NH_4^+ cations coordinated to the negative charge from Al. The area of the NH_4^+ band was calculated by integration of this band for two catalysts with the same 3.2 Cu wt% and Si/Al = 6.7 and 15. The area measured on the former is three times higher than the latter, in agreement with the different Al content and corresponding Brønsted concentration.

After exposure to 10% O_2, the intensity of NH_4^+ is significantly decreased, particularly in sample with Si/Al = 6.7. A less important decrease in the NH_3 band is also observed. Mass spectrometry shows the release of NH_3 under this condition. It was not possible to estimate the amount of released NH_3 by the measurement carried out during the FTIR study, which was not optimized. However, MS measurements carried out independently on the same sample during XAS measurements carried out while acquiring the data reported in Refs Molokova et al, confirmed the evolution of NH_3 during this step. [66,67] Notice that this is at variance with what reported in Ref Negri et al, where a zeolite with higher Si/Al ratio (Si/Al = 15) was studied in similar conditions.[43]

In this step, $[Cu^{II}_2(NH_3)_4O_2]^{2+}$ complex is formed after oxidation of two

$[Cu^{I}(NH_3)_2]^+$ complexes.[22,42,43] The observed decrease in the NH_3 band could indicate that a portion of the Cu ions (unreacted $[Cu^{I}(NH_3)_2]^+$ or oxidized Cu^{II}) could lose NH_3 in the reaction and become framework coordinated. This hypothesis is in agreement with the increase of the band around 900 cm^{-1} assigned to fw-Cu^{II} sites (Figure III.3c), concomitant with the decrease of NH_3 and NH_4^+. In other words, this would indicate a solid state ion exchange between NH_4^+ and Cu^{II} ions. This would explain why the decrease in NH_4^+ intensity is not accompanied by a restoration of Bronsted sites. This procedure was repeated, sending again NO/NH_3 on the samples followed by oxidation, and the same changes were observed, indicating that the ion-exchange is reversible. An important aspect is that the change in NH_4^+ is less for catalysts with a high Si/Al ratio. This is in agreement with the hypothesis that we are observing an ion-exchange, which is favored at high Al contents.

The main focus of the *in situ* FTIR experiments was to investigate the effect of SO_2 exposure. Namely, I am focusing now on the observed decrease in NH_3 and increase in NH_4^+ bands. According to XAS results, the reaction of SO_2 with two $[Cu^{II}_2(NH_3)_4O_2]^{2+}$ complexes leads to the breaking of the complex and formation of two $[Cu^{I}(NH_3)_2]^+$ complexes, one fw-Cu^{I} and one Cu^{II} sulfated species, which could have some NH_3 ligands in the first coordination shell.[67] Based on the amount of desorbed NH_3 measured in this thesis (Table III.3), this process should not lead to release of NH_3. This suggests that some NH_3 desorbed from the $[Cu^{II}_2(NH_3)_4O_2]^{2+}$ complex during the reaction can appear as NH_4^+ which correlates with the FTIR observations. The difference between the changes in NH_3 and NH_4^+ can be attributed to different absorption coefficients.[108]

As mentioned, the NH_4^+ band increased significantly after SO_2 exposure, reaching a final intensity higher than after reduction in NO/NH_3. This indicates that the increase is not related to the protonation of NH_3 by Brønsted acid sites. One possible explanation is the formation of $(NH_4)_2SO_4$.[48,59–61] In this case, the increase of NH_4^+ should be correlated with SO_2 uptake. Comparing exposures to SO_2 and SO_2/O_2, the increase in NH_4^+ and NH_3 desorption were measured to be the same for both conditions. Notably, the S/Cu ratio is twice as high for SO_2/O_2 exposure compared to SO_2 exposure. This suggests that $(NH_4)_2SO_4$ is not the only product of the reaction between the

$[Cu^{II}_2(NH_3)_4O_2]^{2+}$ complex with SO_2 or SO_2/O_2.

When reduction in NO/NH_3 is carried out again after SO_2 exposure, the intensity of NH_4^+ band increases, showing a 16% increase in NH_4^+ area compared to the first reduction. Additionally, the intensity of the NH_4^+ band after the second oxidation is increased by 29% compared to the first oxidation (Table III.2). For SO_2/O_2 exposure, a similar trend is observed, with increases of 22% and 39% in the NH_4^+ area during the reduction and oxidation steps, respectively.

This data can be compared to the amount of NH_3 desorbed before SO_2 exposure and after a subsequent NO/NH_3 exposure (Table III.3). The amount of NH_3 stored on the sample after this step is higher in the samples exposed to SO_2/O_2 and SO_2/H_2O (around 35 %, considering the experimental error), with respect to the sample treated in SO_2 only (around 12%). The trend is similar to the measured SO_2 desorption (Table III.3). Interestingly, the increase of NH_4^+ in this step is in agreement with the mechanism proposed by Bjerregaard et. al where $(NH_4)_2SO_4$ or $(NH_4)HSO_4$ species are formed by reaction of NO and NH_3 with the intermediate formed after reaction of $[Cu^{II}_2(NH_3)_4O_2]^{2+}$ with SO_2.[48]

The Raman spectrum of the $[Cu^{II}_2(NH_3)_4O_2]^{2+}$ complex after SO_2 exposure displays several major peaks at 517, 650, 940, 972, 1036, 1200 and 1280 cm^{-1}. The spectra of the $(NH_4)_2SO_4$ reference shows an intense peak at 975 cm^{-1}, corresponding to the symmetric stretching of SO_4^{2-}, labeled as ν1. A similar spectrum is shown by $CuSO_4 \cdot 5H_2O$ with the intense peak ν1 high at 984 cm^{-1}. Both $(NH_4)_2SO_4$ and $CuSO_4 \cdot 5H_2O$ moieties in their crystalline form have a symmetric structure, resulting in a single ν1 major peak.[109] The small shift in the SO_4^{2-} peak for the two compounds is attributed to the polarizing effect of cations.[102] Based on these considerations, the peak at 972 cm^{-1} for SO_2 exposure of the $[Cu^{II}_2(NH_3)_4O_2]^{2+}$ complex could be related to the formation of $(NH_4)_2SO_4$. On the other hand, the peak at 940 cm^{-1} would imply a counterion smaller than Cu^{II}, to explain the higher polarizing effect on the frequency of ν1. We could tentatively explain it by an interaction with Cu^{I} ions.

The spectrum of $CuSO_4$ display several peaks, notably at 664 (asymmetric bending of SO_4^{2-}), 1011, 1099 and 1202 cm^{-1} (asymmetric stretching of SO_4^{2-}).[110,111] As mentioned above, this indicates a partial hydration of the salt used as a reference, which modifies the symmetry of the sulfate. Some of the bands of the reference resemble those observed after SO_2 exposure of the $[Cu^{II}_2(NH_3)_4O_2]^{2+}$ complex, without a perfect match. In particular, we mention the bands at 650, 1036, 1200 and 1280 cm^{-1}, which are absent (or very weak) in $(NH_4)_2SO_4$ salt. This suggests that a variety of sulfate species are present in the samples, both involving NH_4^+ and Cu ions in different environments. Work is in progress in the research group to better understand the observed spectra based on the DFT calculation of vibrational fingerprints of possible sulfate species present in the zeolite.

What is interesting is the increase in intensity of the Raman spectra moving from the sample with Si/Al = 6.7 treated with SO_2 to the SO_2/O_2 and SO_2/H_2O, which shows similar intensity, in agreement with the similar SO_2 uptake. Notice that there is no evident correlation between the intensity of the bands and the measured change in NH_4^+ intensity (Table III.1), confirming the hypothesis that the spectra are not mainly related to $(NH_4)_2SO_4$. By comparing the intensity of the spectra measured after SO_2 exposure on the zeolite with Si/Al = 15, it is clear that the Al content of the zeolite (and thus its Bronsted acid sites concentration) influences the formation of sulfate species. The S/Cu uptake measured on this sample in similar conditions was around 50% (ca 0.12) of that measured on our reference sample with Si/Al = 6.7. Finally, no sulfates are observed on the zeolite treated with SO_2 without prior formation of the $[Cu^{II}_2(NH_3)_4O_2]^{2+}$ complex, which showed a S/Cu ratio around 0.06.[89]

III.5.3 Investigation of the effect of H_2O compared to O_2 on SO_2 poisoning

The presence of H_2O during SO_2 exposure results in distinct SO_2 uptake and deactivation behavior compared to O_2 (Figure III.1 and Figure III.2, orange and blue, respectively), and to a trend similar to SO_2 alone for both parameters (orange and red curves). The incremental values of S/Cu ratio measured in the different conditions and different cycles are listed in Table III.4. In the first cycle the lowest uptake is measured with SO_2 alone (0.19), a similar value is

obtained for SO_2/O_2 and SO_2/H_2O (0.41 and 0.35) and the highest is obtained for $SO_2/H_2O/O_2$ (0.65). The same order is observed in the measured deactivation.

Table III.4- SO_2 uptake, expressed as Cu/S ratio, for each SO_2 exposure cycle in different conditions on Cu-CHA with Cu 3.2 wt% and Si/Al = 6.7 (data plotted as cumulative values in Figure III.2)

	Cycles						
Conditions	1st	2nd	3rd	4th	5th	6th	Total
SO_2	0.191	0.098	0.047	0.022	0.010	0.007	0.375
SO_2/O_2	0.405	0.022	0.005	0.001	0.000	0.000	0.432
SO_2/H_2O	0.348	0.172	0.081	0.038	0.015	0.009	0.661
$SO_2/O_2/H_2O$	0.655	0.015	0.003	0.001	0.002	0.001	0.678

The incremental SO_2 uptake decreases approximately 50% with respect to the previous cycle for repeated exposures for both SO_2 and SO_2/H_2O (two first lines of Table III.4), while very small uptakes are measured from the 2nd cycle when O_2 is present in the feed (3rd and 4th lines of Table III.4). After six cycles, the accumulated S/Cu ratios are in the order $SO_2 < SO_2/O_2 < SO_2/H_2O \cong SO_2/O_2/H_2O$. The level of deactivation follows at this point of the experiment the same order. Another interesting observation is the SO_2 uptake at the same level of deactivation in the different conditions. The deactivation after exposure to SO_2 alone at 6th cycle (87.5%), SO_2/O_2 at 2th cycle (86%) and SO_2/H_2O at 2rd cycle (88%) are approximately the same, however the accumulated S/Cu ratios are in the order SO_2 (0.375) < SO_2/O_2 (0.425) < SO_2/H_2O (0.52). This indicates that in the presence of H_2O a certain amount of SO_2 is less efficient in deactivating the catalyst.

The FTIR spectra provides further insights into the differences between the exposure conditions, considering only one step of SO_2 exposure. A significant increase in the NH_4^+ area—approximately double with respect to what observed for SO_2 or SO_2/O_2 exposures—is evident after SO_2/H_2O exposure (Table III.2). However, despite the substantial changes in the NH_4^+ area, the decrease in the area of adsorbed NH_3 is similar for SO_2 and SO_2/H_2O exposures

(Figure III.5 and Figure III.6). Interestingly, the increase in NH_4^+ area and NH_3 desorption after a second NO/NH_3 exposure (Table III.3) for SO_2/H_2O exposure is more pronounced than for SO_2/O_2, even though SO_2 uptake is comparable in both cases. This indicates that SO_2/H_2O exposure leads to enhanced NH_4^+ accumulation.

Additionally, significant changes in the NH_4^+ area are observed during the second reduction step. For SO_2/H_2O exposure, these changes are roughly double with respect to SO_2 alone, and higher with respect to SO_2/O_2, further highlighting the distinct effects of O_2 and H_2O during SO_2 poisoning. These results suggest that the interaction between SO_2 and H_2O promotes a stronger impact on NH_4^+ accumulation while maintaining comparable SO_2 uptake efficiency to other exposure conditions.

Based on the speciation of Cu species observed by XAS and the related SO_2 uptake, a two steps reaction mechanism between SO_2 and the $[Cu^{II}_2(NH_3)_4O_2]^{2+}$ complex was proposed.[67] In the reaction a sulfur intermediate (referred to as SO_aX) is formed after the reaction of the first SO_2 molecule with the $[Cu^{II}_2(NH_3)_4O_2]^{2+}$ complex (Eq.III.3). This intermediate can then react with another the $[Cu^{II}_2(NH_3)_4O_2]^{2+}$ complex to form the Cu^{II}-sulfated species (Eq.III.4).

$$III.3)\ [Cu^{II}_2(NH_3)_4O_2]^{2+} + SO_2 \rightarrow [Cu^{I}(NH_3)_2]^{+} + fw - Cu^{I} + SO_aX + \cdots$$

$$III.4)\qquad [Cu^{II}_2(NH_3)_4O_2]^{2+} + SO_aX \rightarrow [Cu^{I}(NH_3)_2]^{+} + Cu^{II}SO_4Z + \cdots$$

As a resulting stoichiometry one SO_2 can react with two $[Cu^{II}_2(NH_3)_4O_2]^{2+}$ complexes, forming two $[Cu^{I}(NH_3)_2]^{+}$ complexes, one fw-Cu^{I} and one Cu^{II}-sulfated species, as in Eq.III.5:

$$III.5)\ \ 2[Cu^{II}_2(NH_3)_4O_2]^{2+} + SO_2 \rightarrow 2[Cu^{I}(NH_3)_2]^{+} + fw - Cu^{I} + Cu^{II}SO_4Z$$

It can be thus hypothesized that in the case of SO_2/H_2O exposure, water can react with the SO_aX intermediate to form sulfated species not attached to Cu (like H_2SO_4, $HSO_4(NH_4)$ and/or $SO_4(NH_4)_2$, which is feasible at 200 ^oC).[48,67,112] Based on these considerations, the following mechanism can be proposed to explain the effect of H_2O:

III.6) $2[Cu_2^{II}(NH_3)_4O_2]^{2+} + 2SO_2 + 2H_2O \rightarrow 2[Cu^{I}(NH_3)_2]^{+} + [Cu_x^{II}O_y]^{2+} + 2(NH_4)_2SO_4$

This mechanism suggests that some Cu^{II} ions are reduced to $[Cu^{I}(NH_3)_2]^{+}$ complex during the reaction after the first SO_2 exposure. These $[Cu^{I}(NH_3)_2]^{+}$ could be re-oxidized to $[Cu_2^{II}(NH_3)_4O_2]^{2+}$ in the following step, to further react with SO_2. This would explain the gradual increase in SO_2 uptake in the subsequent stops, with a similar trend to SO_2 alone. On the contrary, in the presence of O_2 in the flow, the reaction of $[Cu^{I}(NH_3)_2]^{+}$ to $[Cu_2^{II}(NH_3)_4O_2]^{2+}$ followed by reaction with SO_2 has been shown to occur directly in the first step,[67] which would explain why the S/Cu uptake almost reach the maximum in the first step, without further significant increase in the repeated cycles.

The sulfate species formed after exposure to SO_2 and H_2O is likely $(NH_4)_2SO_4$, since no evidence for the presence of H_2SO_4 or HSO_4^- is observed by infrared.[Waller, johnson,Chih kai lin] In this process, SO_2 can disrupt a $[Cu_2^{II}(NH_3)_4O_2]^{2+}$ complex, producing one or two NH_4^+ cations. However, SO_2 alone interacts with only two of these complexes (Eq.III.5), forming a fewer number of NH_4^+ cations overall, in agreement with the changes observed in infrared, and summarized in Table III.2.

Additionally, when 50% more SO_2 is taken up during SO_2/H_2O exposure, the same level of catalytic deactivation occurs. This suggests that $(NH_4)_2SO_4$ has a limited impact on activity, despite it has been proposed that its accumulation inhibits the formation of $[Cu_2^{2+}(NH_3)_4O_2]^{2+}$ complexes. The remaining Cu^{2+} species after SO_2/H_2O exposure are identified as $[Cu_x^{2+}O_\gamma]^{2+}$ cores, without information on their ligands. Among these, a trans-μ-1,2-peroxo dicopper(II) ($[Cu_2^{2+}O_2]^{2+}$) species anchored to the framework, is proposed to be less active than the original $[Cu_2^{2+}(NH_3)_4O_2]^{2+}$ complexes under these conditions at 200 °C.[64,88,113]

III.6 Conclusion

The effect of H_2O on SO_2 poisoning of Cu-CHA zeolite catalyst has been investigated using *in situ* FTIR spectroscopy, TPD, Raman spectroscopy, deactivation and SO_2 uptake measurements. The catalytic activity and SO_2 uptake level off after several cycles of SO_2 exposure under different conditions. After the second cycles, the SO_2/H_2O exposure exhibits more SO_2

uptake compared to SO_2/O_2 at a similar deactivation level. In the presence of H_2O, a certain amount of SO_2 is less efficient in deactivating the catalyst. The TPD and *in situ* FTIR spectra show a higher amount of NH_4^+ formation after SO_2/H_2O exposure which can be attributed to the formation of $(NH_4)_2SO_4$ with Cu-sulfated species. The Raman results confirm the existence of different sulfate species after SO_2 exposure of the $[Cu^{II}_2(NH_3)_4O_2]^{2+}$ complex, indicating that $(NH_4)_2SO_4$ are not the only sulfated species in Cu-CHA catalyst under different conditions. The SO_2/H_2O exposure results in approximately twice the S/Cu ratio compared to SO_2 exposure in each cycle. Therefore, the proposed reaction mechanism suggests that the reaction of one SO_2 with one $[Cu^{II}_2(NH_3)_4O_2]^{2+}$ complex can form an intermediate which may react with H_2O to form $(NH_4)_2SO_4$. This indicates that the probability of $(NH_4)_2SO_4$ formation is higher in the presence of wet SO_2 exposure.

IV Chapter IV: Investigation of the SO_2 sensitivity of Cu-CHA catalyst in NH_3-SCR reaction

IV.1 Abstract

Copper-exchanged chabazite (Cu-CHA) catalysts are applied for selective catalytic reduction of NOx by ammonia (NH_3-SCR) in diesel exhausts. However, a limitation of Cu-CHA lies in its sensitivity to small amount of SO_2. To address this, we developed a formalism to describe the deactivation in terms of the sensitivity for SO_2 (simplified as SO_2 sensitivity, $d\tau/dn_{SO2}$) on Cu-CHA catalyst in NH_3-SCR reaction at 200 °C, without relying on kinetic assumptions. This formalism was applied to three Cu-CHA catalysts with different Cu loading (1.6 and 3.2 wt%) and Si/Al = 6.7 and 15. The Cu-CHA catalysts show a higher SO_2 sensitivity at the beginning of exposure to SO_2. A quadratic model reveals that activity decreases as a function of the uptake of SO_2 for all catalysts. Notably, the catalyst with high Cu loading and low Si/Al ratio exhibits a lower SO_2 sensitivity.

IV.2 Introduction

Cu-exchanged chabazite (Cu-CHA) zeolites are the state-of-the-art catalysts for the selective catalytic reduction of nitrogen oxides (NOx) by ammonia in presence of oxygen (O_2).[114,115] This reaction, in which the NOx reacts with ammonia to N_2 and H_2O, forms the basis of the current NOx emission control technologies applied in diesel vehicles. Cu-CHA materials have a good activity in the range 150-550 °C, and can tolerate exposures to temperatures over 700 °C,[7,21,116] which means that these materials are compatible with the harsh and dynamic conditions in an exhaust pipe.

The activity of Cu-CHA catalysts for NH_3-SCR, however, is sensitive to the presence of SO_2, in particular at temperatures below 300 °C.[51–53,59,117] Therefore, the application of Cu-CHA catalysts is recommended only in combination with ultra-low sulfur diesel fuel, and a proper operation of the catalyst to minimize the impact of SO_2.

A first explanation for the deactivation by SO_2 is that the formation of

ammonium sulfate or ammonium bisulfate under the conditions for NH_3-SCR makes the active centers inaccessible for the NO and NH_3 reactants.[56,61,118,119] An effective physical blocking of the active centers by deposition of ammonium sulfate or ammonium bisulfate requires large amounts of ammonium sulfates to be deposited in the catalysts. However, the catalytic activity of a Cu-CHA catalyst around 200 °C is reduced by about 80 % at S/Cu ratios of 0.2-0.3, indicating that deactivation is almost complete at a molar amount of SO_2 that is 4-5 times lower than the active Cu content.[52,53,120] Furthermore, V_2O_5/TiO_2 and Fe-zeolite based catalysts for NH_3-SCR show a significantly better tolerance for SO_2 under similar process conditions, in particular below 300 °C,[121,122] indicating that the formation of ammonium sulfate or ammonium bisulfate requires some influence of the catalyst. These observations seem inconsistent with a mechanism relying on blocking of the active centers and indicate that the SO_2-induced deactivation of Cu-CHA catalysts is a consequence of a direct interaction of SO_2 with the active Cu-centers.

Recently, it has been shown, that SO_2 preferably interacts with the $[Cu^{II}_2(NH_3)_4O_2]^{2+}$ complex (μ-η^2,η^2-peroxo diaminodicopper(II)-complex) in Cu-CHA catalysts, while Cu^I species show virtually no interaction with SO_2.[66,67,89] Below 300 °C, these $[Cu^{II}_2(NH_3)_4O_2]^{2+}$ complexes are formed upon oxidation of mobile $[Cu^I(NH_3)_2]^+$ species by oxygen.[22,42,43,46,123] The NH_3-SCR reaction proceeds via a reaction of NO with these $[Cu^{II}_2(NH_3)_4O_2]^{2+}$ complexes, and the reaction of SO_2 reduces the rate of this reaction with NO,[68] leading to the deactivation of the catalyst for NH_3-SCR. Because in this scenario, the catalyst deactivation involves the $[Cu^{II}_2(NH_3)_4O_2]^{2+}$ complexes, the deactivation is enhanced under process conditions that favor the formation of the $[Cu^{II}_2(NH_3)_4O_2]^{2+}$ complexes. This is supported by the observation that the uptake of sulfur upon exposing a Cu-CHA catalyst to SO_2 is significantly reduced, after reduction of the Cu to a Cu^I state, while it is enhanced in the presence of oxygen.[67,89]

The insight that the impact of SO_2 depends on the actual state of the Cu in the catalyst implies that the deactivation behavior of a catalyst does not only depend on the material properties of the catalyst, but also on the conditions the catalyst is exposed to. Therefore, a model describing the deactivation behavior

of Cu-CHA catalysts must also contain a record for the process conditions the catalyst has been exposed to.

In this Chapter, we construct a model to describe the deactivation of Cu-CHA catalysts by SO_2. In the model, the deactivation is described in terms of a decrease of the amount of active catalyst. This concept has been applied earlier to characterize the deactivation of zeolite catalysts used for the methanol-to-hydrocarbons reaction.[124,125] Foley et al. have categorized the deactivation behavior of catalysts in non-selective and selective deactivation.[124] Non-selective deactivation means that the catalyst becomes less active, without any further changes in the catalytic behavior. Deactivation by loss of active sites falls in this category. Therefore, for non-selective deactivation, it is possible to describe the activity at any point of the deactivation process in terms of a corresponding amount of fresh catalyst, effectively leading to a variable amount of catalyst as the deactivation progresses. With selective deactivation, the catalytic reaction or catalyst itself changes, such that the performance of the catalyst can no longer be described adequately as a loss of catalyst amount.[124] To model the deactivation of SO_2, we assume that SO_2 only leads to a loss of active Cu, without further changes to the NH_3-SCR reaction cycle, and have therefore used the non-selective approach.

A natural descriptor for the deactivation process would be the time, in analogy to the description of the deactivation of zeolites in the methanol-to-hydrocarbon reaction,[124,125] which then leads to a time-dependent amount of catalyst in the model. However, this leads to ambiguous results for the deactivation of Cu-CHA catalysts by SO_2. A better description of the deactivation is obtained by using the accumulated amount of SO_2 in the catalyst (n_{SO2}), and the deactivation model is adapted by directly replacing the time parameter with the accumulated amount of SO_2. Consequently, the deactivation model requires measurement of the conversion at different amounts of SO_2 for different ratios of the amount of catalyst and flow (W/F ratio in g_{cat}.h/mol). With this approach we obtain a quantification of the deactivation by SO_2, without further assumptions beyond the non-selective nature of the deactivation. The deactivation can then be related to the material properties of the catalyst.

In this study, we evaluate the deactivation from measurements of the NOx conversion at 200 ºC for different W/F ratios and different amounts of SO_2 in the catalyst. By applying the method to three Cu-CHA based catalysts with different Cu loading and Si/Al ratios, we obtain insight into the deactivation behavior of these catalysts, based on the uptake of SO_2 by these catalysts.

IV.3 Method for the deactivation measurement

An essential characteristic of catalyst deactivation is the change of the activity of a catalyst with time, possibly accompanied with a change in other properties, such as selectivity or reaction products. Applying this concept to the deactivation of Cu-CHA catalysts by SO_2, the deactivation is then described by the time of exposure to SO_2, at a well defined temperature and partial pressure of SO_2. In the following, we derive an expression for the deactivation in terms of SO_2 exposure time and show how this leads to ambiguous results. The ambiguity is then removed by exchanging the time variable with the accumulated amount of SO_2 in the catalyst.

In a deactivation measurement, the catalyst deactivation is observed as a change in the conversion during exposure to SO_2, while keeping the flow, the partial pressure of SO_2, and temperature constant. Following the concept as applied earlier for the methanol-to-hydrocarbon reaction over zeolite catalysts,[124,125] the change in conversion with exposure time to SO_2 is described by applying the chain rule for differentiation as follows:

$$\frac{dX}{dt_{SO_2}} = \frac{dX}{d\tau} \cdot \frac{d\tau}{dt_{SO_2}} = \frac{dX}{d\tau} \cdot \frac{1}{F}\frac{dW(t)}{dt_{SO_2}} \qquad \textit{IV.1)}$$

For a plug flow reactor, the derivative $dX/d\tau$ is the reaction rate, and thus Eq.IV.1 describes the deactivation by multiplication of the rate with a time-dependent factor $d\tau/dt_{SO2}$. In this article, we express the activity, or rate constant, in terms of the amount of catalyst, and therefore τ refers to a "contact time" expressed as the ratio of the amount of catalyst and flow (W/F). Introduction this definition of τ in the equation, the time-dependent term reflects a rate of change in catalyst amount as a description of the deactivation.

To determine the term $d\tau/dt_{SO2}$ from experimental data, Eq.IV.1 is rewritten as:

IV.2)

$$\frac{d\tau}{dt_{SO_2}} = \frac{\left[\frac{dX}{dt_{SO_2}}\right]}{\left[\frac{dX}{d\tau}\right]}$$

According to this approach, the right hand side of the equation contains the terms $d\tau/dt_{SO2}$ and $dX/d\tau$. The deactivation is then quantified as the ratio of the measured changes in conversion as a function of the exposure time to SO_2 and the measured rate of the fresh catalyst. In this way, a value for the term $d\tau/dt_{SO2}$ can be determined based on experimentally accessible data.

For the deactivation of Cu-CHA by SO_2, the SO_2 exposure time is an inappropriate descriptor for the deactivation process, as discussed here, because the SO_2 exposure causes a change in the state of the Cu on a time scale of minutes. Because the interaction of SO_2 with a Cu-CHA catalyst depends on the state of the catalyst, the impact of SO_2 exposure does not remain constant on the time scale of our measurement, which would be the requirement for using the exposure time as a descriptor. It has been shown that the SO_2 uptake takes place through a reaction of SO_2 with the $[Cu^{II}_2(NH_3)_4O_2]^{2+}$ complex, under the formation of some Cu^I species that does not react with SO_2.[66,67,89]

Consequently, if the Cu-CHA is prepared such that all Cu is present as the $[Cu^{II}_2(NH_3)_4O_2]^{2+}$ complex, exposure of the catalyst to SO_2 does not result in a complete saturation of the catalyst, or deactivation of the catalyst. A reoxidation and subsequent exposure to SO_2 will result in additional uptake of SO_2 and deactivation. Therefore, by repeating cycles of reduction, oxidation, and SO_2 exposure, a stepwise SO_2 uptake and deactivation occurs. This is further illustrated in Figure IV.1, which shows the measured NOx conversion and cumulative uptake of SO_2 in six consecutive cycles. Further extending the SO_2 exposure time in each cycle as shown in Figure IV.2 from 45 min by, for example, 1 hour, or shortening it by 30 min, does not affect the SO_2 uptake and measured NOx conversion, while the exposure time (t_{SO2}) changes. Therefore, an evaluation of τ/t_{SO2} according to Eq.IV.2 results in different values that depend on an arbitrarily chosen exposure time t_{SO2} in each cycle. Therefore, using the exposure time leads to ambiguous results for $d\tau/dt_{SO2}$.

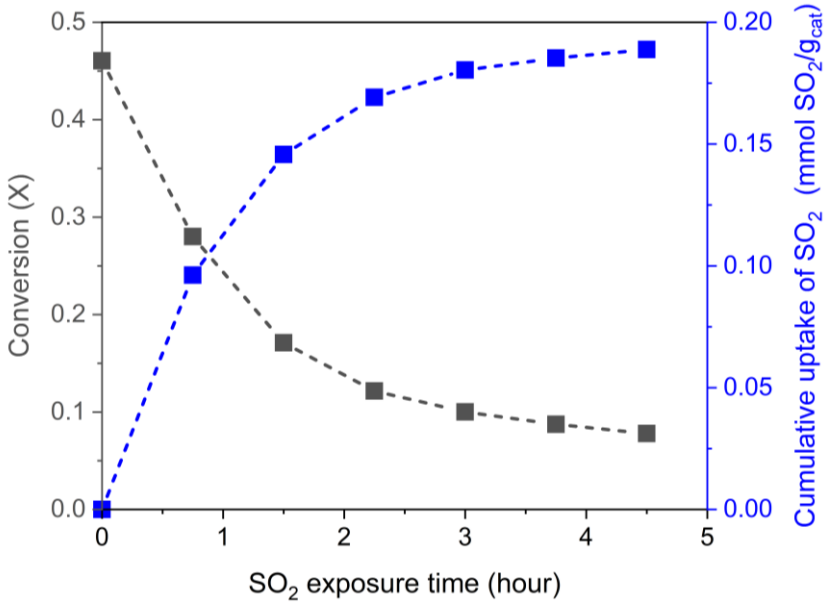

Figure IV.1- Measured conversion and accumulated SO_2 uptake in six consecutive SO_2 exposure cycles at 200 °C, Cu-CHA Catalyst with 3.2 Cu w% and Si/Al = 6.7.

Since the data in Figure IV.1 indicates that the decrease in conversion follows the SO_2 uptake, we have chosen the accumulated amount of SO_2 in the catalyst (n_{SO2}) as a descriptor for the deactivation process. Eq.IV.2 is adapted by replacing t_{SO2} with n_{SO2}, resulting in:

$$\frac{d\tau}{dn_{SO_2}} = \frac{\left[\frac{dX}{dn_{SO_2}}\right]}{\left[\frac{dX}{d\tau}\right]} \qquad IV.3)$$

The term $d\tau/dn_{SO2}$ represents a change in catalyst amount upon SO_2 uptake and can be interpreted as a sensitivity of a catalyst for SO_2. In this article, we use this as a parameter describing the SO_2 sensitivity of catalysts. The term $dX/d\tau$ refers to the rates measured for a fresh catalyst.

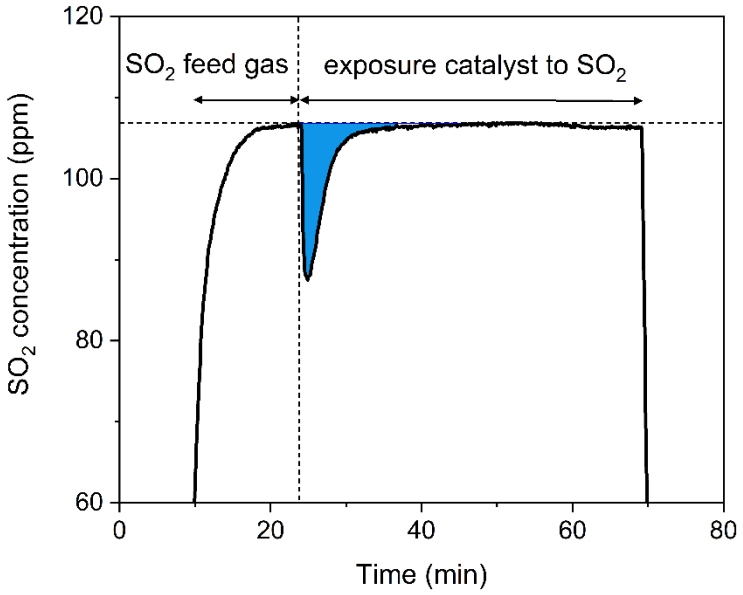

Figure IV.2- Measured SO_2 concentration during exposure to SO_2 at 200 °C for Cu-CHA Catalyst with 3.2 Cu wt% and Si/Al = 6.7. The blue area represents the uptake of SO_2.

IV.4 Experimental

The Cu-CHA catalysts used in this study are a Cu-CHA with 3.2 and 1.6 Cu wt% with a Si/Al = 6.7 and a 3.2 wt% Cu-CHA with Si/Al = 15. The catalysts were prepared by impregnation of the parent chabazite material with the appropriate amount of Cu-nitrate, followed by drying at 90 °C for 2 h, and calcination in air at 600 °C for 2 h.

To measure the deactivation in terms of the sensitivity for SO_2, the conversion of NOx is determined for different values of τ, and n_{SO2}. The measurements of the NOx conversion were conducted in a quartz U-tube powder reactor with a 4 mm inner diameter, using 5 or 10 mg catalyst (sieve fraction 150-300 µm). The reactor was connected to an FTIR spectrometer for gas composition analysis at the reactor outlet. Initially, the catalysts were heated to 550 °C in an atmosphere containing 10% O_2. The reactor was cooled to 200 °C to carry out the remaining procedure at this temperature. Subsequently, the activity of catalysts was measured using a gas mixture containing 500 ppm NO, 600 ppm NH_3, 5% H_2O and 10% O_2 at a total flow of 10, 11.1, 12.5, 14.3, 16.7 and 20 Nl/h. The flow values correspond to contact times τ = 0.0054, 0.0065, 0.0076,

0.0087, 0.0098 and 0.0108 g_{cat}.h/mol for a 5 mg sample and τ = 0.0112, 0.0134, 0.0157, 0.0179, 0.0201 and 0.0224 g_{cat}.h/mol for a 10 mg sample. The values for $dX/d\tau$ were determined based on these measurements.

After the activity measurements, the catalysts were prepared in different ways before the exposure to SO_2, in order to measure the dX/dn_{SO2}.

The different preparations were:

1. Reduction in NO/NH_3 followed by oxidation in 10% O_2, which results in the formation of the $[Cu^{II}_2(NH_3)_4O_2]^{2+}$ complex.[66]
2. Reduction in NO/NH_3, resulting in the formation of $[Cu^{I}(NH_3)_2]^{+}$ complex.[43,66]
3. Exposure to NH_3-SCR feed gas.

In general, five procedures are provided to calculate dX/dn_{SO2} under different conditions. After these preparations, the catalysts were exposed to 100 ppm SO_2/N_2 at 200 ºC for 45 min, followed by an activity measurement at different flows. For the first pretreatment (formation of the $[Cu^{II}_2(NH_3)_4O_2]^{2+}$ complex), the catalysts were exposed to two more different SO_2 exposure (SO_2/O_2 and $SO_2/NO/NH_3$) as well. The entire measurement consists of six consecutive cycles consisting of a preparation step, a SO_2 exposure step and a measurement of the catalytic activity. Contact time was set at 0.0166 g_{cat}.h/mol for catalysts with 1.6 Cu wt% and Si/Al = 6.7 as well as for catalysts with 3.2 wt% Cu and Si/Al = 15. For catalyst 3.2 Cu wt% and Si/Al = 6.7, the contact time was reduced to half this value (0.0076 g_{cat}·h/mol) by using half of the catalyst weight. The uptake of SO_2 in each sulfation step was determined by integration of the measured SO_2 concentration (see Figure IV.2), and the total amount of SO_2 is determined by addition of the SO_2 uptake in each individual SO_2 exposure step. From these measurements, the values for dX/dn_{SO2} were determined.

IV.5 Results

IV.5.1 Assessment of the SO_2 sensitivity in relation to the amount of SO_2

Figure IV.3 shows the experimental data needed to determine the deactivation behavior, according to the method described above (Eq.IV.3). Figure IV.3 shows the measured conversions for different contact times τ for the fresh Cu-CHA catalysts with 3.2 wt% Cu and Si/Al = 6.7 and 15 and Cu-CHA catalyst with 1.6 wt% Cu and Si/Al = 6.7. The measured data for the catalyst with 1.6 wt% Cu and Si/Al ratio = 6.7 and the catalyst with 3.2 wt% Cu and Si/Al = 15 can be approximated with a straight line, meaning that the conversion increases linearly with contact time. This indicates that the rate is approximately constant for all data points in the considered range of conditions. The same holds for catalyst with 3.2 wt% Cu and Si/Al = 15 at low contact time. However, the slope is higher, indicating that this catalyst is more active. At high contact time, the conversion of this catalyst exceeds that of other catalysts, reaching 0.6.

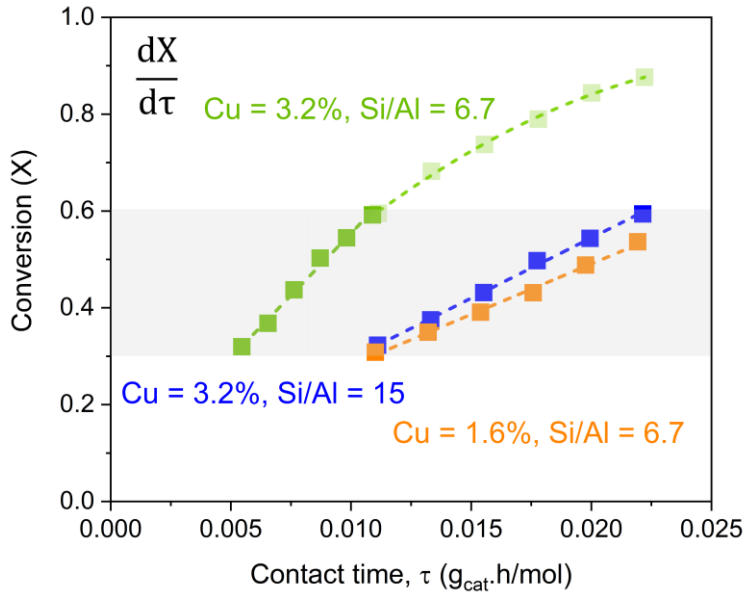

Figure IV.3- Fractional conversion at 200 °C versus contact time for the fresh Cu-CHA catalysts with 3.2 wt% Cu and Si/Al = 6.7 and 15 and Cu-CHA catalyst with 1.6 wt% Cu and Si/Al = 6.7. The grey section corresponds to the region from which the datapoints were selected for the calculation.

The amount of this catalyst was halved to determine the slope at lower contact times, since the curve flattens out at higher conversion levels. From these datapoints, the values for dX/dτ for all catalysts are determined by the calculation of the slope in the grey section. The slopes were determined to be

20.9 and 24.9 mol/g_{cat}.h for catalysts with 1.6 wt% Cu and Si/Al = 6.7 and catalyst with 3.2 wt% Cu and Si/Al = 15, respectively. For catalyst with 3.2 wt% Cu and Si/Al = 6.7, the slope is 51.4 mol/g_{cat}.h (Table IV.1).

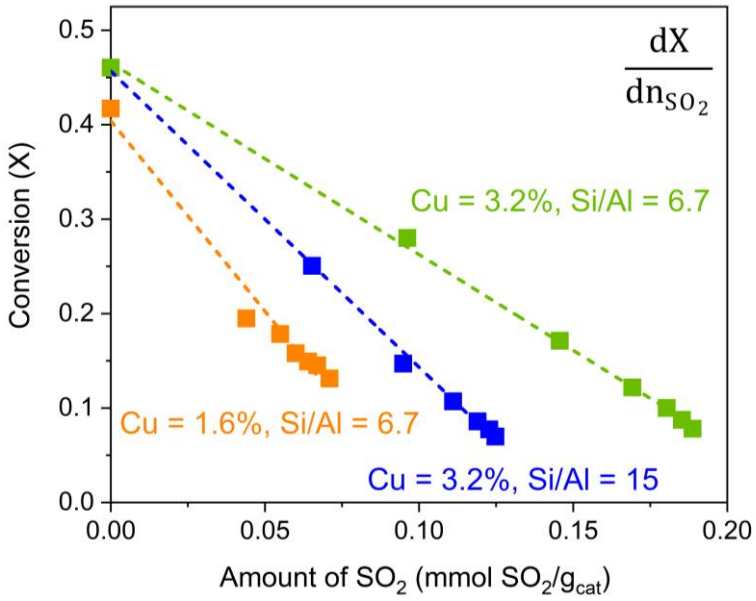

Figure IV.4- Fractional conversion versus the total amount of SO_2 uptake at contact time of 0.0166 g_{cat}.h/mol for catalyst with 1.6 wt% Cu and Si/Al = 6.7 and catalyst with 3.2 wt% Cu and Si/Al = 15 and contact time of 0.0076 g_{cat}.h/mol for catalyst with 3.2 wt% Cu and Si/Al ratio of 6.7.

Figure IV.4 shows the change in conversion as a function of the total uptake of SO_2, measured in a series of 6 cycles of reduction, oxidation, and SO_2 exposure. The SO_2 uptake measured along cycles increases in the series 1.6 Cu wt% & Si/Al = 6.7 < 3.2 Cu wt% & Si/Al = 15 < 3.2 Cu wt% & Si/Al = 6.7. This means that SO_2 uptake is favored at high Cu and Al contents. The datapoints are well described with a single straight line, indicating a constant value for the differential dX/dn_{SO2}. The key point is that both SO_2 uptake and decrease of conversion become very low after the first 3 cycles, being less than 5% of the first SO_2 uptake and conversion decrease. Both conversion and SO_2 uptakes level off for the three catalysts after fifth cycle through this SO_2 exposures. The dX/dn_{SO2} are -2.029, -3.134 and -4.033 $g_{cat}/mmol_{SO2}$ for catalysts with 3.2 Cu wt% and Si/Al = 6.7, 3.2 Cu wt% and Si/Al =15 and 1.6 Cu wt% and Si/Al = 6.7, respectively (Table II.1). Thus, the changes of conversion versus the SO_2 uptake are higher for the catalyst with low Cu and

high Al loading.

In Table IV.1, the SO_2 sensitivity ($d\tau/dn_{SO2}$) for the Cu-CHA catalysts was determined by dividing the calculated deactivation parameters dX/dn_{SO2} by the rate parameter $dX/d\tau$ (Eq.IV.3). The obtained $d\tau/dn_{SO2}$ values are negative due to the loss of catalyst weight caused by uptaking SO_2. At high Cu loading (3.2 wt%) $d\tau/dn_{SO2}$ is higher for the catalyst with high Si/Al ratio (-0.113 vs -0.040 g_{cat}^2.h/mol.mmolSO_2). However, it becomes more negative (-0.193) at low Si/Al and lower Cu content.

Table IV.1- Determined rate parameter, deactivation parameter and SO_2 sensitivity for three catalysts

Si/Al ratio	Cu cont. (wt%)	rate parameter, $dX/d\tau$ (mol/g_{cat}.h)	deactivation parameter, dX/dn_{SO2} (g_{cat}/mmol$_{SO2}$)	SO_2 sensitivity, $d\tau/dn_{SO2}$ (g_{cat}^2.h/mol. mmol$_{SO2}$)
6.7	2	20.9	-4.033	-0.193
6.7	4	51.4	-2.030	-0.040
15	4	24.9	-3.134	-0.113

IV.5.2 Construction of a deactivation model

The SO_2 sensitivity ($d\tau/dn_{SO2}$) was determined by measuring catalytic activity and SO_2 uptake after different pretreatments resulting in different Cu speciation and different SO_2-based mixtures (SO_2 alone, SO_2/O_2 and $SO_2/NO/NH_3$). The SO_2 uptake through 6 cycles varies as a function of the pretreatment as shown for the catalyst with 3.2 Cu wt% and Si/Al = 6.7 in Figure IV.5 and in Table IV.2.

A similar trend is observed when exposing the catalyst to SO_2 after NO/NH_3 pretreatment (brown), after forming the $[Cu^{II}_2(NH_3)_4O_2]^{2+}$ complex (blue), and after exposure to the SCR mixture (purple). In the three experiments the SO_2 uptake increases more during the first cycle and gradually levels off, resulting in a saturation curve. The SO_2 uptake after NO/NH_3 is much lower than the other two cases (total uptake of 0.050 mmol SO_2/g_{cat}). In the first cycle the

SO_2 uptake is slightly higher for SCR with respect to $[Cu^{II}_2(NH_3)_4O_2]^{2+}$ (0.109 vs 0.096 mmol SO_2/g_{cat}). However, after the first cycle the latter shows higher uptakes reaching a total after 6 cycles of 0.189 mmol SO_2/g_{cat}, which is higher than the SCR case (0.163 mmol SO_2/g_{cat}). The similar trend and SO_2 uptake measured for these two conditions are in agreement with the hypothesis that the $[Cu^{II}_2(NH_3)_4O_2]^{2+}$ complex is the active site in low temperature SCR, and that this is the most sensitive species to SO_2.

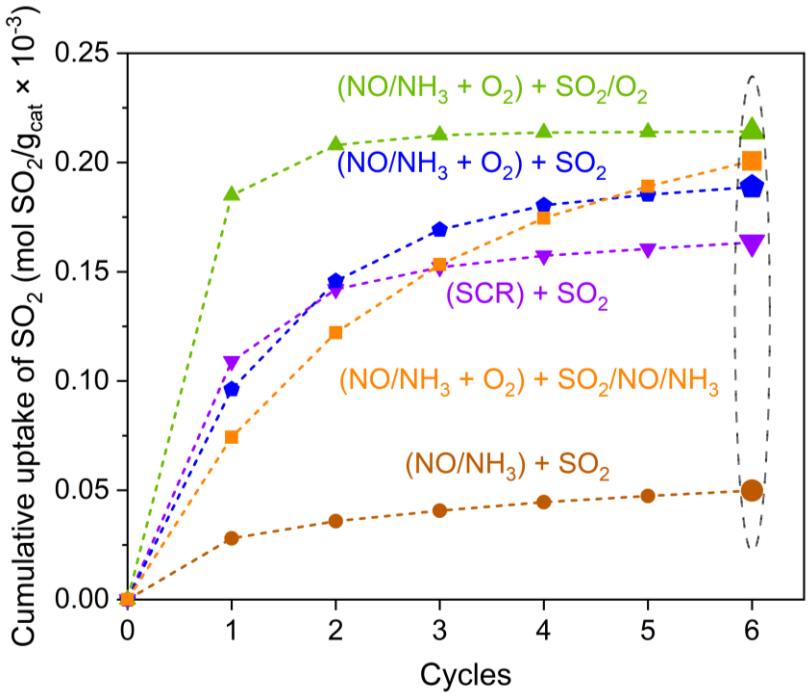

Figure IV.5- SO_2 uptakes measurements for Cu-CHA catalysts with 3.2 Cu wt% and Si/Al = 6.7 under different conditions at 200 °C.

The trend and amount of SO_2 after formation of the $[Cu^{II}_2(NH_3)_4O_2]^{2+}$ complex is also affected by the SO_2 conditions (SO_2 alone, SO_2/O_2 or $SO_2/NO/NH_3$). Namely, a saturation level is reached after two cycles by exposure to SO_2/O_2 (green curve). This could be explained by the oxidation of residual $[Cu^{I}(NH_3)_2]^{+}$ species after SO_2 exposure of the $[Cu^{II}_2(NH_3)_4O_2]^{2+}$ complex. This reaction would form a new $[Cu^{II}_2(NH_3)_4O_2]^{2+}$ complex which would then react with SO_2.[67] When exposure to SO_2 is carried out in the presence of NO/NH_3 (orange) the catalyst does not seem completely to reach a saturation

level after 6 cycles. The final uptake at this point is in the order SO_2 (0.189 mmol SO_2/g_{cat}) < $SO_2/NO/NH_3$ (0.201 mmol SO_2/g_{cat}) < SO_2/O_2 (0.214 mmol SO_2/g_{cat}).

Table IV.2- SO_2 uptake measured during 6 cycles of SO_2 exposure on catalyst with 3.2 Cu wt% and Si/Al = 6.7 after different pretreatments and different SO_2 mixtures.

Cycle	SO_2 uptake (mmol SO_2/g_{cat})				
	SCR	NO/NH_3	$[Cu^{II}_2(NH_3)_4O_2]^{2+}$		
	$+SO_2$	$+SO_2$	$+SO_2$	$+SO_2/O_2$	$+ SO_2/NO/NH_3$
1	0.109	0.028	0.096	0.185	0.074
2	0.142	0.036	0.146	0.208	0.122
3	0.152	0.041	0.169	0.213	0.153
4	0.157	0.045	0.180	0.214	0.175
5	0.161	0.047	0.185	0.214	0.189
6	0.163	0.050	0.189	0.214	0.201

According to the different procedures used to accumulate SO_2 in the catalyst, a different trend in the decrease of conversion (that is deactivation) *vs* SO_2 uptake is observed. This results in different dX/dn_{SO2} parameters depending on the used procedure. The SO_2 sensitivity ($d\tau/dn_{SO2}$)was then calculated for each procedure using the same $dX/d\tau$ of the fresh catalyst. This procedure has been carried out for the three catalysts with different compositions, to obtain the plots of $d\tau/dn_{SO2}$ *vs* SO_2 uptake (Figure IV.6). All catalysts have the highest SO_2 sensitivity ($d\tau/dn_{SO2}$) after reduction in NO/NH_3 and SO_2 exposure (● symbols). However, the catalysts with 1.6 Cu wt% and Si/Al = 6.7 and 3.2 Cu wt% and Si/Al=15 show the highest SO_2 sensitivity ($d\tau/dn_{SO2}$) (-0.259 and -0.274 g_{cat}^2.h/mol.mmol SO_2, respectively) at very low SO_2 uptake (0.017 and 0.031 mmmol SO_2/g_{cat}, respectively). By adding O_2 in the mixture of NO/NH_3 to have the SCR gas mixture, the SO_2 sensitivity ($d\tau/dn_{SO2}$) decreases (▼

symbols). In the case of the catalyst with 3.2 Cu wt% and Si/Al = 6.7 this corresponds to a noticeable increase in the total SO_2 uptake (0.163 mmol SO_2/g_{cat}), while the uptake is smaller for the other two catalysts (around 0.075 mmol SO_2/g_{cat}).

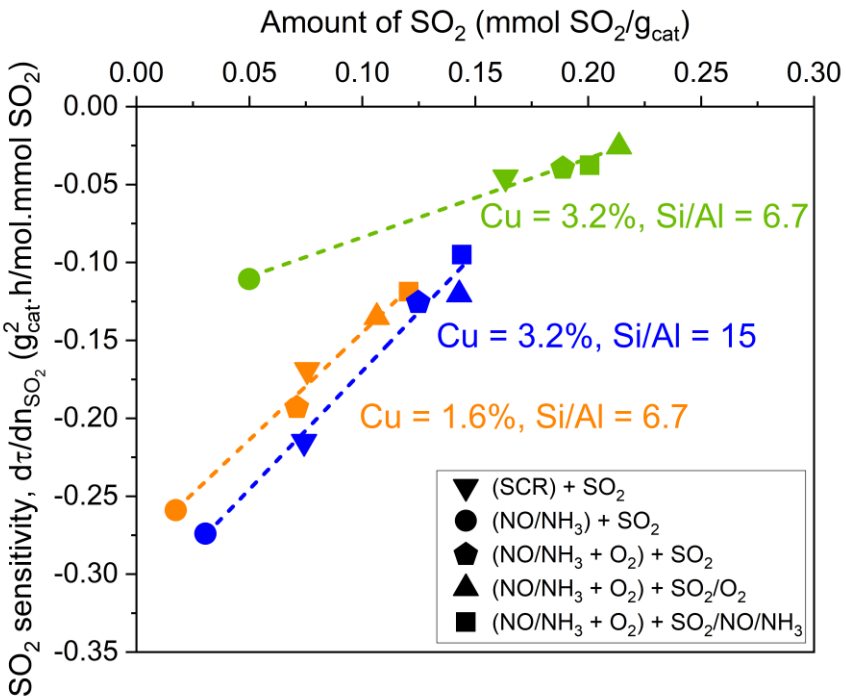

Figure IV.6- SO_2 sensitivity as a function of total SO_2 uptake after 6 cycles for three catalysts under different conditions.

The three catalysts show slightly different behaviors in the other tested conditions. For instance, while it has already been mentioned that for the catalysts with 3.2 Cu wt% and Si/Al = 6.7 the highest SO_2 uptake is obtained after exposing the $[Cu^{II}_2(NH_3)_4O_2]^{2+}$ complex to SO_2/O_2 (▲), the highest uptake is obtained after exposure of $[Cu^{II}_2(NH_3)_4O_2]^{2+}$ to $SO_2/NO/NH_3$ for the other two catalysts (■). Notwithstanding these differences, what is important to notice is that for all catalysts a linear correlation is observed between SO_2 sensitivity ($d\tau/dn_{SO2}$) and SO_2 total uptake. Interestingly, the higher the SO_2 uptake, the lower is the SO_2 sensitivity ($d\tau/dn_{SO2}$).

The resulting linear functions (Table IV.3) can be used to model the SO_2

sensitivity ($d\tau/dn_{SO2}$) as a function of the total amount of SO_2 uptake for three catalysts. The key point of the model is it is not based on any kinetic assumptions regarding the measurements and calculations to obtain these data points. All data were obtained based on a procedure that examines the conversion for a specific SO_2 uptake. The slope of the straight line of Cu-CHA catalyst with 3.2 Cu wt% and Si/Al = 15 is approximately 1.51, followed by 1.375 for 1.6 Cu wt% and Si/Al = 6.7 and a much lower value of 0.506 for the one with 3.2 Cu wt% and Si/Al = 6.7. This means that the first two catalysts experience a high sensitivity due to exposure to SO_2 (amount of SO_2), while the catalyst with high Cu loading and low Si/Al exhibits lower sensitivity when exposed to the same amount of SO_2 as the other catalysts.

Table IV.3- Calculated parameters of the slope, intercept and R-square of the linear function of three catalysts.

Si/Al ratio	Cu cont. (wt%)	Slope	Intercept	R-Square
6.7	1.6	1.375 ± 0.0926	-0.283 ± 0.0079	0.986
6.7	3.2	0.506 ± 0.0354	-0.131 ± 0.0061	0.985
15	3.2	1.510 ± 0.1145	-0.322 ± 0.0128	0.983

A deactivation model to correlate the contact time with the amount of SO_2 in the Cu-CHA catalyst was constructed by mathematical integration of the linear functions summarized in Table IV.3, using as boundary conditions the highest contact time (fresh catalysts) and the lowest contact time for each catalyst. Thus, quadratic equations were obtained for three catalysts (Figure IV.7). The Cu-CHA catalyst with 3.2 Cu wt% and Si/Al = 6.7 has a lower contact time at zero uptake (fresh catalyst) with respect to the other two since half of the weight of catalyst was used during measurements. As a result of the smaller slope of the linear function, the quadratic equation in Figure IV.7 for this catalyst shows that the change in contact time as a function of SO_2 is lower. The final level of three catalysts is different, depending on the final conversion uptake of the catalyst. This model allows to predict contact time as a function

of SO_2 uptake at given zeolite composition, without kinetic assumptions and only based on experimental data.

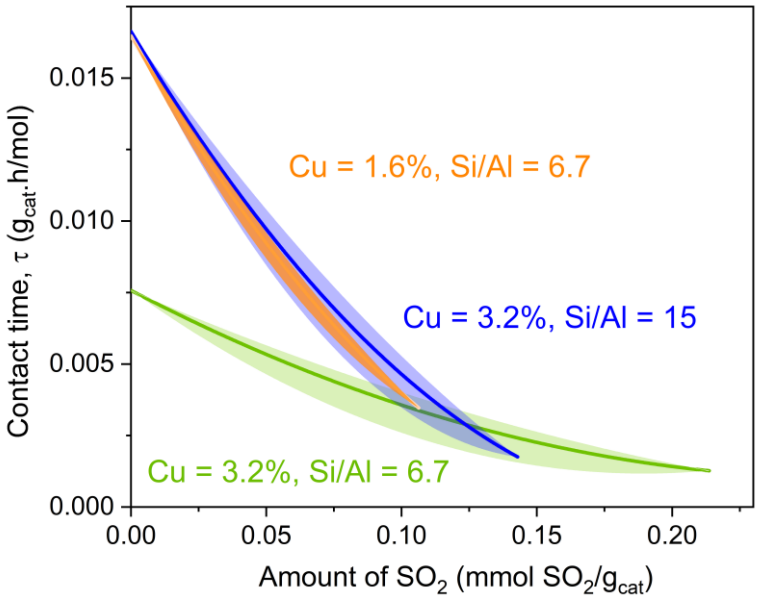

Figure IV.7- Deactivation models for three catalysts at 200 ºC. Quadratic equations obtained by integration of the linear equations summarized in Table IV.3. Shaded area represents the error calculated from the errors of slope and interception.

The quantification of NOx conversion as a function of the amount of SO_2 was calculated using the deactivation model and the rate of catalysts based on the data obtained at 200 ºC (Figure IV.3). In the deactivation models, all contact times were multiplied by the rate to determine the conversion. Notably, the conversion of the catalyst with respect to SO_2 does not follow a quadratic equation. The calculated conversion decreases more during the initial exposure to SO_2 for all three catalysts. A comparison of the calculated results with the experimental data is represented in Figure IV.8, demonstrating a fair agreement between the deactivation model and experimental observations. The experimental data were obtained using the total SO_2 uptake of all different SO_2 exposure.

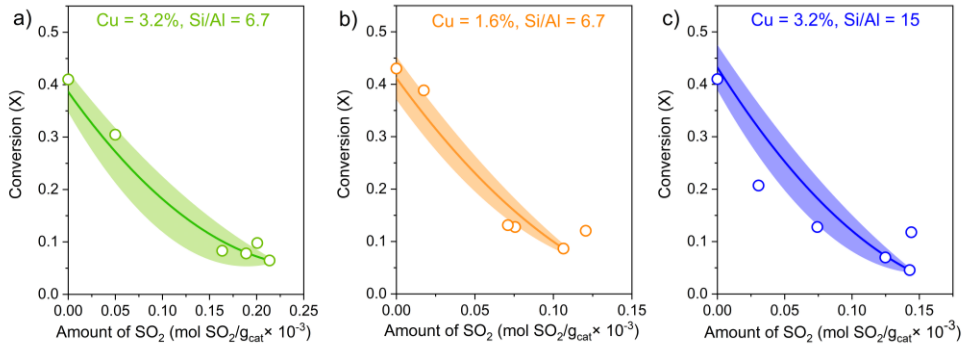

Figure IV.8- Comparison of the deactivation model with experimental measured data on three catalysts at 200 °C, including error for simulated model.

IV.6 Discussion

IV.6.1 Deactivation behavior with respect to SO_2 uptake

The SO_2 sensitivity ($d\tau/dn_{SO2}$) plotted in Figure IV.6 shows negative values since it indicates a decrease in the contact time with the respect to n_{SO2}. The contact time, expressed as the ratio of the weight of catalyst to the flow (W/F), determines the changes in the weight of catalyst under constant flow conditions.[125] The negative SO_2 sensitivity ($d\tau/dn_{SO2}$) indicates that the weight of the catalyst (which reflects the activity, or rate constant) decreases upon adding SO_2. The catalyst exhibited different SO_2 sensitivity ($d\tau/dn_{SO2}$) under different pretreatment and exposure to SO_2, allowing us to measure several changes in conversion as a function of SO_2 uptake. The total SO_2 uptake varies under different conditions as well. For instance, SO_2 exposure of the $[Cu^{II}_2(NH_3)_4O_2]^{2+}$ complex leads to reduction of Cu^{II} and formation of Cu^{II}-sulfate and Cu^{I}, which exhibit low reactivity towards SO_2.[66,67] The catalyst was pretreated again to form again Cu^{II} species, which become sensitive to SO_2, resulting in further uptake of SO_2. This cycle was repeated until reaching a point of no further SO_2 uptake (saturation level). The total SO_2 uptake represents the cumulative sum of each SO_2 uptake during each cycle. Plotting the SO_2 sensitivity ($d\tau/dn_{SO2}$) with respect to the total amount of SO_2 uptake shows a linear function for three catalysts with different composition (Figure IV.6). It is important to underline the fact that the procedure of adding SO_2 into the catalyst is not important and the observed trend clearly demonstrates this for three catalysts. The SO_2 sensitivity ($d\tau/dn_{SO2}$) decreases when the

catalysts are exposed to conditions favoring more SO_2 uptake. A small amount of loaded SO_2 deactivates the catalyst faster during the initial stages.[52,123] This means that activity significantly decreases with a small amount of SO_2.[53,66,89]

Based on the integration of the linear function, the relationship between contact time and the amount of SO_2 exhibits a quadratic behavior. In this case, the only assumption is that the catalytic activity can be presented as the activity of an equivalent amount of fresh catalyst. This shows that the reaction mechanism and parameters (such as reaction order, selectivity) do not change during the SO_2 exposure process. This can be rationalized as a non-selective deactivation, as proposed in Ref.[124]. The deactivation model shows that the contact time, which is proportional to the weight of the catalyst, and thus to activity, or rate constant, decreases upon the addition of more SO_2 in three catalysts (Figure IV.7). As mentioned, the deactivation of Cu-CHA catalysts by SO_2 may be attributed to two primary observations: formation of inactive Cu^{II}-sulfated species which implies the decrease of Cu active sites, or ammonium sulfated and bisulfated species causing the blocking of chabazite zeolite pores, that is limiting access of the reactants to the active sites. In the case of the physical blocking by ammonium sulfated species, Cu-CHA must accumulate a specific amount of sulfated species blocking the pores to reduce the activity. In this context, the ammonium sulfated species would hinder the reaction of feed gases by interaction with active Cu species over time. As mentioned, one ammonium sulfated species can stabilize the formation of the $[Cu^{II}_2(NH_3)_4O_2]^{2+}$ complex. Upon the addition of a second ammonium sulfate, the $[Cu^{II}_2(NH_3)_4O_2]^{2+}$ complex becomes destabilized.[48,123] In this case, the activity of catalysts should remain relatively constant at low SO_2 uptake before abruptly decreasing. However, the formation of Cu sulfated species could lead to another deactivation pathway. In this case, the catalyst deactivates with small amount of SO_2. After a while, the reactivity of Cu active sites toward SO_2 decreases and reaches to a constant level. It means that the reactivity of the catalyst with SO_2 is initially rapid but gradually slow down. This mechanism fits well with the quadratic model constructed in this work.

IV.6.2 Evaluating the effect of Cu loading and Si/Al ratio on SO_2 sensitivity

The Cu-CHA catalyst with high Cu loading and low Si/Al ratio exhibits a lower SO_2 sensitivity ($d\tau/dn_{SO2}$) under the same conditions compared to the other catalysts. This can be related to the mobility of the Cu species, which can play an important role during the low temperature NH_3-SCR reaction. The catalyst with low Cu loading has a lower possibility of forming the $[Cu^{II}_2(NH_3)_4O_2]^{2+}$ complex (the important Cu species for reducing NO) due to the reduced mobility of Cu species within the chabazite cell.[22] In this case, the concentration of Cu species as active sites can be quickly reduced by small SO_2 uptakes, while higher Cu loadings implies that higher uptakes are needed to react with all the $[Cu^{II}_2(NH_3)_4O_2]^{2+}$ complexes. Similarly, the catalyst with the higher Si/Al ratio (lower Al content) results in reduced mobility of Cu species, following the same mechanism of low Cu loading.[45,74] These observations further support the hypothesis that deactivation primarily occurs by interaction of SO_2 with the $[Cu^{II}_2(NH_3)_4O_2]^{2+}$ complexes.

IV.7 Conclusions

In this study, we applied a formalism to follow the deactivation in terms of the sensitivity for SO_2 (SO_2 sensitivity, $d\tau/dn_{SO2}$) of Cu-CHA catalysts in the low temperature NH_3-SCR reaction as a function of SO_2 uptake. Two parameters, dX/dn_{SO2} and $dX/d\tau$, were calculated based on conversion measurements without any kinetic assumption. Then, the SO_2 sensitivity ($d\tau/dn_{SO2}$) is calculated by dividing these two parameters. The SO_2 sensitivity ($d\tau/dn_{SO2}$) reflects the decrease in weight of catalysts (which is proportional to activity) by adding SO_2 to the catalyst.

The SO_2 sensitivity ($d\tau/dn_{SO2}$) changes under different conditions followed by different amount of the total SO_2 uptake. A linear function fits well the observed trend of the SO_2 sensitivity ($d\tau/dn_{SO2}$) *vs* amount of SO_2. The SO_2 sensitivity ($d\tau/dn_{SO2}$) is higher with less amount of SO_2. A quadratic equation, as the deactivation model, shows the change of activity by integration of this linear function with two boundary conditions (constant time for fresh catalyst and the minimum contact time). The deactivation model shows that activity is more affected at low SO_2 uptake. The Cu-CHA catalyst with 3.2 Cu wt% and

Si/Al = 6.7 shows more resistance than other catalysts to SO_2 exposure, which are characterized by lower Cu content at fixed Si/Al ratio and higher Si/Al ratio at the same Cu content. This can be related to the lower ability of these catalysts to form the $[Cu^{II}_2(NH_3)_4O_2]^{2+}$ complex, which is responsible for activity but is also highly sensitive to SO_2 exposure.

V Conclusions and Perspectives

This thesis has explored the effects of SO_2 on Cu-CHA zeolite catalysts in the NH_3-SCR reaction, focusing on their deactivation and sensitivity to SO_2. Through a combination of spectroscopy, SO_2 uptake measurements, and catalytic activity studies, the work has provided comprehensive insights into the role of Si/Al ratio, and environmental factors such as the presence of water, in determining the deactivation of catalysts. By developing a suitable formalism, the studies reveal the sensitivity of the deactivation to SO_2 in determining the performance of the catalyst by adding SO_2.

In **Chapter 2**, the interaction of SO_2 with Cu-CHA catalysts of varying Si/Al ratios was investigated at 200 °C. The study demonstrated that SO_2 selectively reacts with the $[Cu^{2+}{}_2(NH_3)_4O_2]^{2+}$ complex, leading to a 50% deactivation across all catalysts regardless of their Si/Al ratio. These results suggest that the mechanism of deactivation is consistent across different compositions. However, a correlation was observed between the Si/Al ratio and both the SO_2 uptake and NH_3-SCR activity. The catalysts with lower Si/Al ratios (6.7) exhibited higher activity and SO_2 uptake compared to those with higher ratios (15). This insight highlights the importance of optimizing the Si/Al ratio to enhance catalyst efficiency and resilience to SO_2 exposure.

In **Chapter 3**, the effect of water on SO_2 poisoning of Cu-CHA catalysts was explored. The presence of water in the feed significantly increased SO_2 uptake and deactivation levels compared to dry conditions. Notably, the combination of SO_2, water, and oxygen yielded the highest deactivation and SO_2 uptake levels. The findings indicate that water facilitates the formation of ammonium sulfate ($(NH_4)_2SO_4$) alongside Cu-sulfated species. Raman and FTIR spectroscopy confirmed the formation of diverse sulfate species under wet conditions, pointing to a mechanism where water promotes the reaction of one SO_2 with one $[Cu^{2+}{}_2(NH_3)_4O_2]^{2+}$ complex.

In **Chapter 4**, a formalism was developed to quantify the deactivation in terms of the sensitivity for SO_2 (simplified as SO_2 sensitivity, $d\tau/dn_{SO2}$) on Cu-CHA catalysts without relying on kinetic assumptions. The results demonstrated that catalysts with higher Cu loading (3.2 wt%) and lower Si/Al ratio (6.7) exhibited greater resistance to SO_2-induced deactivation compared to those

with lower Cu loading or higher Si/Al ratios. The SO_2 sensitivity was found to be highest at the initial stages of SO_2 exposure and to decrease over time, following a quadratic model. This model provides valuable insights into the behavior of Cu-CHA catalysts under different SO_2 uptakes.

The research conducted in this thesis underscores the complexity of SO_2-induced deactivation in Cu-CHA catalysts and provides actionable knowledge for improving catalyst design. By elucidating the effects of Si/Al ratio, water, and sensitivity of the deactivation to SO_2, the findings contribute to the development of more robust NH_3-SCR systems for diesel exhaust treatment.

Future research could further investigate the nature and structure of the sulfated species through advanced *in situ* spectroscopic techniques such as Raman and S L-edge X-ray absorption spectroscopy, coupled to DFT calculations. While this thesis has focused on controlled laboratory conditions, future studies could examine the SO_2 sensitivity of Cu-CHA catalysts in real-world diesel exhaust systems. Long-term durability tests under fluctuating temperatures, varying SO_2 concentrations, and dynamic water content are essential to evaluate the practical applicability of the understanding from this thesis. To complement experimental findings, computational modeling and simulations can offer atomistic insights into the mechanisms of SO_2/H_2O deactivation. Advanced modeling techniques can help predict the formation of deactivating species and identify potential pathways for the wet SO_2 poisoning.

VI References

1 M. Kampa and E. Castanas, *Environmental Pollution*, 2008, **151**, 362–367.

2 T. Selleri, A. D. Melas, A. Joshi, D. Manara, A. Perujo and R. Suarez-Bertoa, *Catalysts*, 2021, **11**, 404.

3 J. Sowman, S. Box, A. Wong, M. Grote, D. S. Laila, G. Gillam, A. J. Cruden, J. M. Preston and P. Fussey, in *IET Intelligent Transport Systems*, Institution of Engineering and Technology, 2018, vol. 12, pp. 521–526.

4 S. L. Anderson, P. L. T. Gabrielsson and C. U. I. Odenbrand, *Environmental and Energy Engineering*, 1994, **40**, 1911–1919.

5 I. Nova and E. Tronconi, *Fundamental and Applied Catalysis Urea-SCR Technology for deNOx After Treatment of Diesel Exhausts*, 2014.

6 S. Elkaee, S. Y. Kim, A. D. Phule, M. W. Uz Zaman, S. G. Lee, G. Park and J. Hwan Yang, *J Environ Chem Eng*, 2023, **11**, 111–131.

7 M. Moliner, C. Franch, E. Palomares, M. Grill and A. Corma, *Chemical Communications*, 2012, **48**, 8264–8266.

8 A. T. Smith, P. N. Plessow and F. Studt, *Journal of Physical Chemistry C*, 2021, **125**, 16508–16515.

9 E. Borfecchia, K. A. Lomachenko, F. Giordanino, H. Falsig, P. Beato, A. V. Soldatov, S. Bordiga and C. Lamberti, *Chem Sci*, 2015, **6**, 548–563.

10 T. V. W. Janssens, H. Falsig, L. F. Lundegaard, P. N. R. Vennestrøm, S. B. Rasmussen, P. G. Moses, F. Giordanino, E. Borfecchia, K. A. Lomachenko, C. Lamberti, S. Bordiga, A. Godiksen, S. Mossin and P. Beato, *ACS Catal*, 2015, **5**, 2832–2845.

11 A. Godiksen, F. N. Stappen, P. N. R. Vennestrøm, F. Giordanino, S. B. Rasmussen, L. F. Lundegaard and S. Mossin, *Journal of Physical*

Chemistry C, 2014, **118**, 23126–23138.

12 C. Negri, M. Signorile, N. G. Porcaro, E. Borfecchia, G. Berlier, T. V. W. Janssens and S. Bordiga, *Appl Catal A Gen*, 2019, **578**, 1–9.

13 H. Li, C. Paolucci, I. Khurana, L. N. Wilcox, F. Göltl, J. D. Albarracin-Caballero, A. J. Shih, F. H. Ribeiro, R. Gounder and W. F. Schneider, *Chem Sci*, 2019, **10**, 2373–2384.

14 A. Martini, E. Borfecchia, K. A. Lomachenko, I. A. Pankin, C. Negri, G. Berlier, P. Beato, H. Falsig, S. Bordiga and C. Lamberti, *Chem Sci*, 2017, **8**, 6836–6851.

15 C. Paolucci, A. A. Parekh, I. Khurana, J. R. Di Iorio, H. Li, J. D. Albarracin Caballero, A. J. Shih, T. Anggara, W. N. Delgass, J. T. Miller, F. H. Ribeiro, R. Gounder and W. F. Schneider, *J Am Chem Soc*, 2016, **138**, 6028–6048.

16 N. D. Nasello, N. Usberti, U. Iacobone, F. Gramigni, W. Hu, S. Liu, I. Nova, X. Gao and E. Tronconi, *ACS Catal*, 2023, **13**, 2723–2734.

17 W. Hu, T. Selleri, F. Gramigni, E. Fenes, K. R. Rout, S. Liu, I. Nova, D. Chen, X. Gao and E. Tronconi, *Angewandte Chemie - International Edition*, 2021, **60**, 7197–7204.

18 P. S. Hammershøi, C. Negri, G. Berlier, S. Bordiga, P. Beato and T. V. W. Janssens, *Catal. Sci. Technol.*, 2019, **9**, 2608–2619.

19 C. Paolucci, A. A. Verma, S. A. Bates, V. F. Kispersky, J. T. Miller, R. Gounder, W. N. Delgass, F. H. Ribeiro and W. F. Schneider, *Angewandte Chemie International Edition*, 2014, **53**, 11828–11833.

20 W. Hu, F. Gramigni, N. D. Nasello, N. Usberti, U. Iacobone, S. Liu, I. Nova, X. Gao and E. Tronconi, *ACS Catal*, 2022, 5263–5274.

21 F. Gao, E. D. Walter, M. Kollar, Y. Wang, J. Szanyi and C. H. F. Peden, *J Catal*, 2014, **319**, 1–14.

22 C. Paolucci, I. Khurana, A. A. Parekh, S. Li, A. J. Shih, H. Li, J. R. Di

Iorio, J. D. Albarracin-Caballero, A. Yezerets, J. T. Miller, W. N. Delgass, F. H. Ribeiro, W. F. Schneider and R. Gounder, *Science (1979)*, 2017, **357**, 898–903.

23 F. Gramigni, N. D. Nasello, N. Usberti, U. Iacobone, T. Selleri, W. Hu, S. Liu, X. Gao, I. Nova and E. Tronconi, *ACS Catal*, 2021, **11**, 4821–4831.

24 H. Falsig, P. N. R. Vennestrøm, P. G. Moses and T. V. W. Janssens, *Top Catal*, 2016, **59**, 861–865.

25 L. Chen, H. Falsig, T. V. W. Janssens and H. Grönbeck, *J Catal*, 2018, **358**, 179–186.

26 G. Deplano, A. Martini, M. Signorile, E. Borfecchia, V. Crocellà, S. Svelle and S. Bordiga, *Angewandte Chemie - International Edition*, 2021, **60**, 25891–25896.

27 M. Signorile, E. Borfecchia, S. Bordiga and G. Berlier, *Chem Sci*, 2022, **13**, 10238–10250.

28 A. M. Beale, I. Lezcano-Gonzalez, W. A. Slawinksi and D. S. Wragg, *Chemical Communications*, 2016, **52**, 6170–6173.

29 C. Negri, E. Borfecchia, M. Cutini, K. A. Lomachenko, T. V. W. Janssens, G. Berlier and S. Bordiga, *ChemCatChem*, 2019, **11**, 3828–3838.

30 F. Giordanino, E. Borfecchia, K. A. Lomachenko, A. Lazzarini, G. Agostini, E. Gallo, A. V. Soldatov, P. Beato, S. Bordiga and C. Lamberti, *Journal of Physical Chemistry Letters*, 2014, **5**, 1552–1559.

31 R. Millan, P. Cnudde, V. Van Speybroeck and M. Boronat, *JACS Au*, 2021, **1**, 1778–1787.

32 P. N. R. Vennestrøm, L. F. Lundegaard, C. Tyrsted, D. A. Bokarev, A. I. Mytareva, G. N. Baeva, A. Y. Stakheev and T. V. W. Janssens, *Top Catal*, 2019, **62**, 100–107.

33 A. Y. Stakheev, D. A. Bokarev, A. I. Mytareva, T. V. W. Janssens and P. N. R. Vennestrøm, *Top Catal*, 2017, **60**, 255–259.

34 M. L. Tsai, R. G. Hadt, P. Vanelderen, B. F. Sels, R. A. Schoonheydt and E. I. Solomon, *J Am Chem Soc*, 2014, **136**, 3522–3529.

35 F. Gao, D. Mei, Y. Wang, J. Szanyi and C. H. F. Peden, *J Am Chem Soc*, 2017, **139**, 4935–4942.

36 X. Wang, L. Chen, P. N. R. Vennestrøm, T. V. W. Janssens, J. Jansson, H. Grönbeck and M. Skoglundh, *ChemCatChem*, 2021, **13**, 2577–2582.

37 E. Borfecchia, C. Negri, K. A. Lomachenko, C. Lamberti, T. V. W. Janssens and G. Berlier, *React Chem Eng*, 2019, **4**, 1067–1080.

38 K. A. Lomachenko, E. Borfecchia, C. Negri, G. Berlier, C. Lamberti, P. Beato, H. Falsig and S. Bordiga, *J Am Chem Soc*, 2016, **138**, 12025–12028.

39 Y. Feng, T. V. W. Janssens, P. N. R. Vennestrøm, J. Jansson, M. Skoglundh and H. Grönbeck, *Journal of Physical Chemistry C*, 2024, **128**, 6689–6701.

40 A. R. Fahami, T. Günter, D. E. Doronkin, M. Casapu, D. Zengel, T. H. Vuong, M. Simon, F. Breher, A. V. Kucherov, A. Brückner and J. D. Grunwaldt, *React Chem Eng*, 2019, **4**, 1000–1018.

41 A. Oda, H. Shionoya, Y. Hotta, T. Takewaki, K. Sawabe and A. Satsuma, *ACS Catal*, 2020, **10**, 12333–12339.

42 L. Chen, T. V. W. Janssens and H. Grönbeck, *Physical Chemistry Chemical Physics*, 2019, **21**, 10923–10930.

43 C. Negri, T. Selleri, E. Borfecchia, A. Martini, K. A. Lomachenko, T. V. W. Janssens, M. Cutini, S. Bordiga and G. Berlier, *J Am Chem Soc*, 2020, **142**, 15884–15896.

44 A. Martini, C. Negri, L. Bugarin, G. Deplano, R. K. Abasabadi, K. A. Lomachenko, T. V. W. Janssens, S. Bordiga, G. Berlier and E.

Borfecchia, *Journal of Physical Chemistry Letters*, 2022, **13**, 6164–6170.

45 Y. Fu, W. Ding, H. Lei, Y. Sun, J. Du, Y. Yu, U. Simon, P. Chen, Y. Shan, G. He and H. He, *J Am Chem Soc*, 2024, **146**, 11141–11151.

46 L. Chen, T. V. W. Janssens, P. N. R. Vennestrøm, J. Jansson, M. Skoglundh and H. Grönbeck, *ACS Catal*, 2020, **10**, 5646–5656.

47 Y. Feng, X. Wang, T. V. W. Janssens, P. N. R. Vennestrøm, J. Jansson, M. Skoglundh and H. Grönbeck, *ACS Catal*, 2021, **11**, 14395–14407.

48 J. D. Bjerregaard, M. Votsmeier and H. Grönbeck, *J Catal*, 2023, **417**, 497–506.

49 Y. Zhang, Y. Peng, K. Li, S. Liu, J. Chen, J. Li, F. Gao and C. H. F. Peden, *ACS Catal*, 2019, **9**, 6137–6145.

50 S. A. Bates, A. A. Verma, C. Paolucci, A. A. Parekh, T. Anggara, A. Yezerets, W. F. Schneider, J. T. Miller, W. N. Delgass and F. H. Ribeiro, *J Catal*, 2014, **312**, 87–97.

51 Y. Cheng, C. Lambert, D. H. Kim, J. H. Kwak, S. J. Cho and C. H. F. Peden, *Catal Today*, 2010, **151**, 266–270.

52 P. S. Hammershøi, A. D. Jensen and T. V. W. Janssens, *Appl Catal B*, 2018, **238**, 104–110.

53 P. S. Hammershøi, Y. Jangjou, W. S. Epling, A. D. Jensen and T. V. W. Janssens, *Appl Catal B*, 2018, **226**, 38–45.

54 A. Kumar, M. A. Smith, K. Kamasamudram, N. W. Currier, H. An and A. Yezerets, *Catal Today*, 2014, **231**, 75–82.

55 J. Han, J. D. Bjerregaard, H. Grönbeck, D. Creaser and L. Olsson, *ACS Engineering Au*, 2024, **4**, 405–421.

56 K. Wijayanti, K. Leistner, S. Chand, A. Kumar, K. Kamasamudram, N. W. Currier, A. Yezerets and L. Olsson, *Catal Sci Technol*, 2016, **6**, 2565–2579.

57 L. Olsson, K. Wijayanti, K. Leistner, A. Kumar, S. Y. Joshi, K. Kamasamudram, N. W. Currier and A. Yezerets, *Appl Catal B*, 2016, **183**, 394–406.

58 D. W. Brookshear, J. G. Nam, K. Nguyen, T. J. Toops and A. Binder, *Catal Today*, 2015, **258**, 359–366.

59 K. Wijayanti, K. Xie, A. Kumar, K. Kamasamudram and L. Olsson, *Appl Catal B*, 2017, **219**, 142–154.

60 Y. Jangjou, Q. Do, Y. Gu, L. G. Lim, H. Sun, D. Wang, A. Kumar, J. Li, L. C. Grabow and W. S. Epling, *ACS Catal*, 2018, **8**, 1325–1337.

61 A. J. Shih, I. Khurana, H. Li, J. González, A. Kumar, C. Paolucci, T. M. Lardinois, C. B. Jones, J. D. Albarracin Caballero, K. Kamasamudram, A. Yezerets, W. N. Delgass, J. T. Miller, A. L. Villa, W. F. Schneider, R. Gounder and F. H. Ribeiro, *Appl Catal A Gen*, 2019, **574**, 122–131.

62 P. S. Hammershøi, A. L. Godiksen, S. Mossin, P. N. R. Vennestrøm, A. D. Jensen and T. V. W. Janssens, *React Chem Eng*, 2019, **4**, 1081–1089.

63 J. D. Bjerregaard, J. Han, D. Creaser, L. Olsson and H. Grönbeck, *Journal of Physical Chemistry C*, 2024, **128**, 4525–4534.

64 B. Ipek, M. J. Wulfers, H. Kim, F. Göltl, I. Hermans, J. P. Smith, K. S. Booksh, C. M. Brown and R. F. Lobo, *ACS Catal*, 2017, **7**, 4291–4303.

65 K. Wijayanti, K. Xie, A. Kumar, K. Kamasamudram and L. Olsson, *Appl Catal B*, 2017, **219**, 142–154.

66 A. Yu. Molokova, E. Borfecchia, A. Martini, I. A. Pankin, C. Atzori, O. Mathon, S. Bordiga, F. Wen, P. N. R. Vennestrøm, G. Berlier, T. V. W. Janssens and K. A. Lomachenko, *JACS Au*, 2022, **2**, 787–792.

67 A. Yu. Molokova, R. K. Abasabadi, E. Borfecchia, O. Mathon, S. Bordiga, F. Wen, G. Berlier, T. V. W. Janssens and K. A. Lomachenko, *Chem Sci*, 2023, **14**, 11521–11531.

68 A. Yu. Molokova, S. Davide, E. Borfecchia, F. Wen, S. Magliocco, S.

Bordiga, T. V. W. Janssens, K. A. Lomachenko and G. Berlier, *Catal Sci Technol*, 2024, **14**, 5989–5995.

69 L. Chen, T. V. W. Janssens, M. Skoglundh and H. Grönbeck, *Top Catal*, 2019, **62**, 93–99.

70 A. Wang and L. Olsson, *Nat Catal*, 2019, **2**, 566–570.

71 R. Gounder and A. Moini, *React Chem Eng*, 2019, **4**, 966–968.

72 Isabella Nova and Enrico Tronconi, *Emission Control Science and Technology*.

73 C. H. F. Peden, *J Catal*, 2019, **373**, 384–389.

74 S. H. Krishna, A. Goswami, Y. Wang, C. B. Jones, D. P. Dean, J. T. Miller, W. F. Schneider and R. Gounder, *Nat Catal*, 2023, **6**, 276–285.

75 C. Negri, A. Martini, G. Deplano, K. A. Lomachenko, T. V. W. Janssens, E. Borfecchia, G. Berlier and S. Bordiga, *Physical Chemistry Chemical Physics*, 2021, **23**, 18322–18337.

76 C. Negri, M. Signorile, N. G. Porcaro, E. Borfecchia, G. Berlier, T. V. W. Janssens and S. Bordiga, *Appl Catal A Gen*, 2019, **578**, 1–9.

77 E. Borfecchia, K. A. Lomachenko, F. Giordanino, H. Falsig, P. Beato, A. V. Soldatov, S. Bordiga and C. Lamberti, *Chem Sci*, 2015, **6**, 548–563.

78 K. A. Lomachenko, E. Borfecchia, C. Negri, G. Berlier, C. Lamberti, P. Beato, H. Falsig and S. Bordiga, *J Am Chem Soc*, 2016, **138**, 12025–12028.

79 C. Paolucci, I. Khurana, A. A. Parekh, S. Li, A. J. Shih, H. Li, J. R. Di Iorio, J. D. Albarracin-Caballero, A. Yezerets, J. T. Miller, W. N. Delgass, F. H. Ribeiro, W. F. Schneider and R. Gounder, *Science (1979)*, 2017, **357**, 898–903.

80 F. C. Meunier, *React Chem Eng*, 2016, **1**, 134–141.

81 S. L. Bergman, S. Dahlin, V. V. Mesilov, Y. Xiao, J. Englund, S. Xi, C. Tang, M. Skoglundh, L. J. Pettersson and S. L. Bernasek, *Appl Catal B*, 2020, **269**, 118722.

82 J. Du, X. Shi, Y. Shan, G. Xu, Y. Sun, Y. Wang, Y. Yu, W. Shan and H. He, *Catal Sci Technol*, 2020, **10**, 1256–1263.

83 L. Chen, H. Falsig, T. V. W. Janssens, J. Jansson, M. Skoglundh and H. Grönbeck, *Catal Sci Technol*, 2018, **8**, 2131–2136.

84 R. Gui, Q. Yan, T. Xue, Y. Gao, Y. Li, T. Zhu and Q. Wang, *J Hazard Mater*.

85 S. Singh, T. V. W. Janssens and H. Grönbeck, *Catal Sci Technol*, 2024, **14**, 3407–3415.

86 Y. R. Chen, L. Wei, A. Kumar, D. Wang and W. S. Epling, *Catal Sci Technol*, 2022, **12**, 6891–6902.

87 W. Su, Z. Li, Y. Zhang, C. Meng and J. Li, *Catal Sci Technol*, 2017, **7**, 1523–1528.

88 A. Wang and L. Olsson, *Chemical Engineering Journal*, 2020, **395**, 125048.

89 R. K. Abasabadi, T. V. W. Janssens, S. Bordiga and G. Berlier, *Catal Sci Technol*, 2024, **14**, 3076–3085.

90 S. Wuttke, P. Bazin, A. Vimont, C. Serre, Y. K. Seo, Y. K. Hwang, J. S. Chang, G. Férey and M. Daturi, *Chemistry - A European Journal*, 2012, **18**, 11959–11967.

91 S. Thomas, O. Marie, P. Bazin, L. Lietti, C. G. Visconti, M. Corbetta, F. Manenti and M. Daturi, *Catal Today*, 2017, **283**, 176–184.

92 P. M. Kester, J. T. Crum, S. Li, W. F. Schneider and R. Gounder, *J Catal*, 2021, **395**, 210–226.

93 L. J. Smith, A. Davidson and A. K. Cheetham, *Catal Letters*, 1997, **49**, 143–146.

94 J. H. Kwak, H. Zhu, J. H. Lee, C. H. F. Peden and J. Szanyi, *Chemical Communications*, 2012, **48**, 4758–4760.

95 S.-C. Wang, A. Al Abdulghani, E. Lebrón-Rodríguez, W.-S. Lo, H. Zhu, A. Moini, I. Petrovic, S. Prasad and I. Hermans, *ChemCatChem*, 2022, **14**, 1–20.

96 C. Paolucci, J. R. Di Iorio, W. F. Schneider and R. Gounder, *Acc Chem Res*, 2020, **53**, 1881–1892.

97 K. Leistner, K. Xie, A. Kumar, K. Kamasamudram and L. Olsson, *Catal Letters*, 2017, **147**, 1882–1890.

98 J. Luo, F. Gao, K. Kamasamudram, N. Currier, C. H. F. Peden and A. Yezerets, *J Catal*, 2017, **348**, 1–20.

99 I. Lezcano-Gonzalez, U. Deka, B. Arstad, A. Van Yperen-De Deyne, K. Hemelsoet, M. Waroquier, V. Van Speybroeck, B. M. Weckhuysen and A. M. Beale, *Physical Chemistry Chemical Physics*, 2014, **16**, 1639–1650.

100 D. Zengel, M. Stehle, O. Deutschmann, M. Casapu and J. D. Grunwaldt, *Appl Catal B*, 2021, **288**, 119991.

101 J. L. Dong, X. H. Li, L. J. Zhao, H. S. Xiao, F. Wang, X. Guo and Y. H. Zhang, *Journal of Physical Chemistry B*, 2007, **111**, 12170–12176.

102 K. Ben Mabrouk, T. Kauffmann, H. Aroui and F. Raman, *Journal of Raman Spectroscopy*, 2013, **44**, 1603–1608.

103 M. D. Fontana, K. Ben Mabrouk and T. H. Kauffmann, *Spectroscopic Properties of Inorganic and Organometallic Compounds*, 2013, **44**, 40–67.

104 K. Ben Mabrouk, T. H. Kauffmann, H. Aroui and M. D. Fontana, *Journal of Raman Spectroscopy*, 2013, **44**, 1603–1608.

105 N. Maubec, A. Lahfid, C. Lerouge, G. Wille and K. Michel, *Spectrochim Acta A Mol Biomol Spectrosc*, 2012, **96**, 925–939.

106 X. Fu, G. Yang, J. Sun and J. Zhou, *Journal of Physical Chemistry A*, 2012, **116**, 7314–7318.

107 E. Widjaja, H. H. Chong and M. Tjahjono, *Journal of Raman Spectroscopy*, 2010, **41**, 181–186.

108 B. Bridier, N. López and J. Pérez-Ramírez, *Dalton Transactions*, 2010, **39**, 8412–8419.

109 D. Liu and F. G. Ullman, *Journal of Raman Spectroscopy*, 1991, **22**, 525–528.

110 X. Fu, G. Yang, J. Sun and J. Zhou, *Journal of Physical Chemistry A*, 2012, **116**, 7314–7318.

111 L. Ge, A. Wang, X. Hu, J. Zhang, J. He, P. Wang, L. Han and D. Zhang, *Catal Sci Technol*, 2023, **13**, 4186–4196.

112 H. N. Sharma, Y. Sun and E. A. Glascoe, *Appl Catal B*, 2018, **220**, 348–355.

113 X. Wang, L. Chen, P. N. R. Vennestrøm, T. V. W. Janssens, J. Jansson, H. Grönbeck and M. Skoglundh, *ChemCatChem*, 2021, **13**, 2577–2582.

114 J. H. Kwak, R. G. Tonkyn, D. H. Kim, J. Szanyi and C. H. F. Peden, *J Catal*, 2010, **275**, 187–190.

115 U. Deka, A. Juhin, E. A. Eilertsen, H. Emerich, M. A. Green, S. T. Korhonen, B. M. Weckhuysen and A. M. Beale, *Journal of Physical Chemistry C*, 2012, **116**, 4809–4818.

116 D. W. Fickel and R. F. Lobo, *Journal of Physical Chemistry C*, 2010, **114**, 1633–1640.

117 X. Auvray, M. Arvanitidou, Å. Högström, J. Jansson, S. Fouladvand and L. Olsson, *Emission Control Science and Technology*, 2021, **7**, 232–246.

118 L. Zhang, D. Wang, Y. Liu, K. Kamasamudram, J. Li and W. Epling, *Appl Catal B*, 2014, **156–157**, 371–377.

119 Y. Jangjou, D. Wang, A. Kumar, J. Li and W. S. Epling, *ACS Catal*, 2016, **6**, 6612–6622.

120 S. Dahlin, C. Lantto, J. Englund, B. Westerberg, F. Regali, M. Skoglundh and L. J. Pettersson, *Catal Today*, 2019, **320**, 72–83.

121 M. Iwasaki, *Mechanistic aspect of NO–NH3–O2 reacting system.*, Springer New York, New York, NY, 2014, vol. 1.

122 B. B. Hansen, P. S. Hammershøi, F. H. Fagerberg, S. I. Hansen, X. B. Sjøgren, P. N. R. Vennestrøm, A. D. Jensen and T. V. W. Janssens, *Emission Control Science and Technology*, 2024, **10**, 204–12.

123 T. V. W. Janssens, E. Borfecchia, K. Lomachenko, H. Gronbeck and G. Berlier, *ChemCatChem*, 2024, **16**, 1–20.

124 B. L. Foley, B. A. Johnson and A. Bhan, *ACS Catal*, 2019, **9**, 7065–7072.

125 T. V. W. Janssens, *J Catal*, 2009, **264**, 130–137.

VII Publications

Abasabadi RK, Janssens TV, Bordiga S, Berlier G. Probing the effect of the Si/Al ratio in Cu-CHA zeolite catalysts on SO_2 exposure: in situ DR UV-vis spectroscopy and deactivation measurements. Catalysis Science & Technology. 2024; 14, 3076-3085.

DOI: 10.1039/D4CY00129J

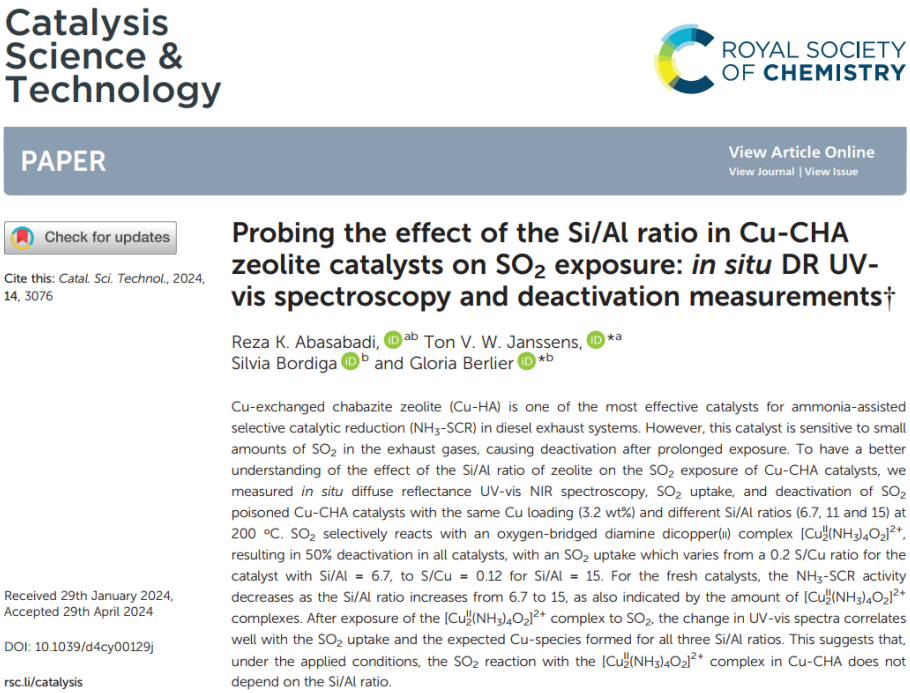

Catalysis Science & Technology

ROYAL SOCIETY OF CHEMISTRY

PAPER

View Article Online
View Journal | View Issue

Check for updates

Cite this: *Catal. Sci. Technol.*, 2024, 14, 3076

Probing the effect of the Si/Al ratio in Cu-CHA zeolite catalysts on SO_2 exposure: *in situ* DR UV-vis spectroscopy and deactivation measurements†

Reza K. Abasabadi, [ab] Ton V. W. Janssens, [*a] Silvia Bordiga [b] and Gloria Berlier [*b]

Received 29th January 2024,
Accepted 29th April 2024

DOI: 10.1039/d4cy00129j

rsc.li/catalysis

Cu-exchanged chabazite zeolite (Cu-HA) is one of the most effective catalysts for ammonia-assisted selective catalytic reduction (NH_3-SCR) in diesel exhaust systems. However, this catalyst is sensitive to small amounts of SO_2 in the exhaust gases, causing deactivation after prolonged exposure. To have a better understanding of the effect of the Si/Al ratio of zeolite on the SO_2 exposure of Cu-CHA catalysts, we measured *in situ* diffuse reflectance UV-vis NIR spectroscopy, SO_2 uptake, and deactivation of SO_2 poisoned Cu-CHA catalysts with the same Cu loading (3.2 wt%) and different Si/Al ratios (6.7, 11 and 15) at 200 °C. SO_2 selectively reacts with an oxygen-bridged diamine dicopper(II) complex $[Cu^{II}_2(NH_3)_4O_2]^{2+}$, resulting in 50% deactivation in all catalysts, with an SO_2 uptake which varies from a 0.2 S/Cu ratio for the catalyst with Si/Al = 6.7, to S/Cu = 0.12 for Si/Al = 15. For the fresh catalysts, the NH_3-SCR activity decreases as the Si/Al ratio increases from 6.7 to 15, as also indicated by the amount of $[Cu^{II}_2(NH_3)_4O_2]^{2+}$ complexes. After exposure of the $[Cu^{II}_2(NH_3)_4O_2]^{2+}$ complex to SO_2, the change in UV-vis spectra correlates well with the SO_2 uptake and the expected Cu-species formed for all three Si/Al ratios. This suggests that, under the applied conditions, the SO_2 reaction with the $[Cu^{II}_2(NH_3)_4O_2]^{2+}$ complex in Cu-CHA does not depend on the Si/Al ratio.

Molokova AY, Abasabadi RK, Borfecchia E, Mathon O, Bordiga S, Wen F, Berlier G, Janssens TV, Lomachenko KA. Elucidating the reaction mechanism of SO_2 with Cu-CHA catalysts for NH3-SCR by X-ray absorption spectroscopy. Chemical Science. 2023;14(41):11521-31.

DOI: 10.1039/D3SC03924B

My contribution was in the measurement of X-ray absorption spectroscopy (XAS) at the S K-edge, and X-ray emission spectroscopy (XES) of Cu-CHA catalysts at ID 26, ESRF (European Synchrotron Radiation Facility).

Chemical Science

ROYAL SOCIETY OF CHEMISTRY

EDGE ARTICLE

View Article Online
View Journal | View Issue

Check for updates

Cite this: *Chem. Sci.*, 2023, **14**, 11521

All publication charges for this article have been paid for by the Royal Society of Chemistry

Elucidating the reaction mechanism of SO_2 with Cu-CHA catalysts for NH_3-SCR by X-ray absorption spectroscopy†

Anastasia Yu. Molokova, [ab] Reza K. Abasabadi, [bc] Elisa Borfecchia, [b] Olivier Mathon,[a] Silvia Bordiga, [b] Fei Wen,[d] Gloria Berlier, [b] Ton V. W. Janssens [*c] and Kirill A. Lomachenko [*a]

The application of Cu-CHA catalysts for the selective catalytic reduction of NO_x by ammonia (NH_3-SCR) in exhaust systems of diesel vehicles requires the use of fuel with low sulfur content, because the Cu-CHA catalysts are poisoned by higher concentrations of SO_2. Understanding the mechanism of the interaction between the Cu-CHA catalyst and SO_2 is crucial for elucidating the SO_2 poisoning and development of efficient catalysts for SCR reactions. Earlier we have shown that SO_2 reacts with the $[Cu_2^{II}(NH_3)_4O_2]^{2+}$ complex that is formed in the pores of Cu-CHA upon activation of O_2 in the NH_3-SCR cycle. In order to determine the products of this reaction, we use X-ray absorption spectroscopy (XAS) at the Cu K-edge and S K-edge, and X-ray emission spectroscopy (XES) for Cu-CHA catalysts with 0.8 wt% Cu and 3.2 wt% Cu loadings. We find that the mechanism for SO_2 uptake is similar for catalysts with low and high Cu content. We show that the SO_2 uptake proceeds *via* an oxidation of SO_2 by the $[Cu_2^{II}(NH_3)_4O_2]^{2+}$ complex, resulting in the formation of different Cu^I species, which do not react with SO_2, and a sulfated Cu^{II} complex that is accumulated in the pores of the zeolite. The increase of the SO_2 uptake upon addition of oxygen to the SO_2-containing feed, evidenced by X-ray adsorbate quantification (XAQ) and temperature-programmed desorption of SO_2, is explained by the re-oxidation of the Cu^I species into the $[Cu_2^{II}(NH_3)_4O_2]^{2+}$ complexes, which makes them available for reaction with SO_2.

Received 28th July 2023
Accepted 2nd October 2023

DOI: 10.1039/d3sc03924b

rsc.li/chemical-science

Martini A, Negri C, Bugarin L, Deplano G, Abasabadi RK, Lomachenko KA, Janssens TV, Bordiga S, Berlier G, Borfecchia E. Assessing the influence of zeolite composition on oxygen-bridged diamino dicopper (II) complexes in Cu-CHA deNO x catalysts by machine learning-assisted X-ray absorption spectroscopy. The Journal of Physical Chemistry Letters. 2022 Jun 28;13(26):6164-70.

DOI: 10.1021/acs.jpclett.2c01107

I contributed by performing the *in situ* DR UV-Vis spectroscopy of Cu-CHA catalysts at Department of Chemistry, University of Turin.

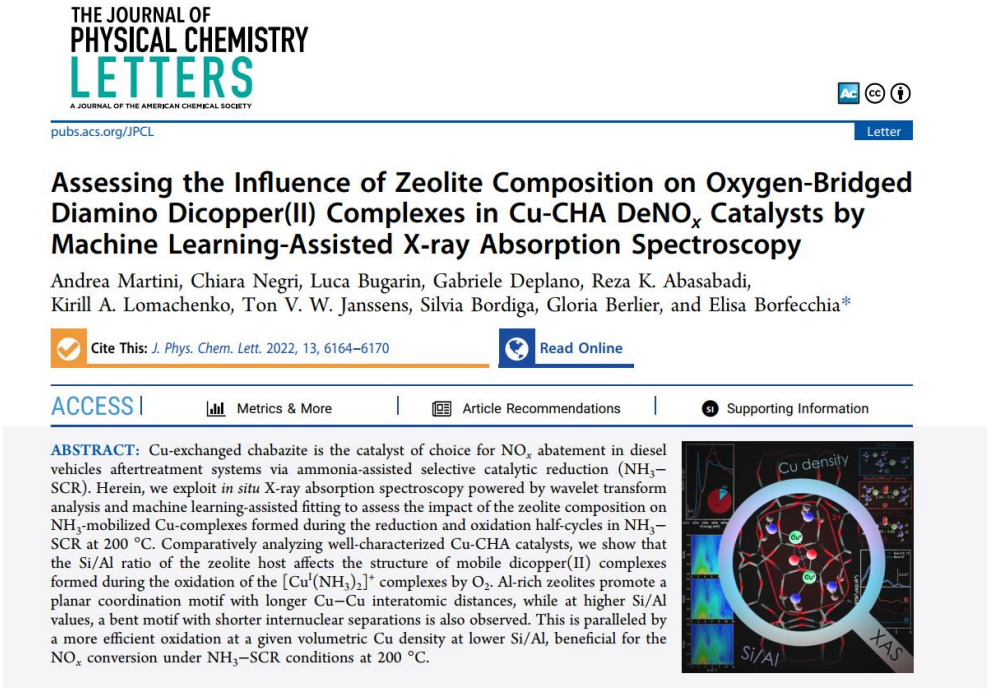

THE JOURNAL OF PHYSICAL CHEMISTRY LETTERS

A JOURNAL OF THE AMERICAN CHEMICAL SOCIETY

pubs.acs.org/JPCL Letter

Assessing the Influence of Zeolite Composition on Oxygen-Bridged Diamino Dicopper(II) Complexes in Cu-CHA DeNO$_x$ Catalysts by Machine Learning-Assisted X-ray Absorption Spectroscopy

Andrea Martini, Chiara Negri, Luca Bugarin, Gabriele Deplano, Reza K. Abasabadi, Kirill A. Lomachenko, Ton V. W. Janssens, Silvia Bordiga, Gloria Berlier, and Elisa Borfecchia*

Cite This: *J. Phys. Chem. Lett.* 2022, 13, 6164−6170 Read Online

ACCESS | Metrics & More | Article Recommendations | Supporting Information

ABSTRACT: Cu-exchanged chabazite is the catalyst of choice for NO_x abatement in diesel vehicles aftertreatment systems via ammonia-assisted selective catalytic reduction (NH_3−SCR). Herein, we exploit *in situ* X-ray absorption spectroscopy powered by wavelet transform analysis and machine learning-assisted fitting to assess the impact of the zeolite composition on NH_3-mobilized Cu-complexes formed during the reduction and oxidation half-cycles in NH_3−SCR at 200 °C. Comparatively analyzing well-characterized Cu-CHA catalysts, we show that the Si/Al ratio of the zeolite host affects the structure of mobile dicopper(II) complexes formed during the oxidation of the $[Cu^I(NH_3)_2]^+$ complexes by O_2. Al-rich zeolites promote a planar coordination motif with longer Cu−Cu interatomic distances, while at higher Si/Al values, a bent motif with shorter internuclear separations is also observed. This is paralleled by a more efficient oxidation at a given volumetric Cu density at lower Si/Al, beneficial for the NO_x conversion under NH_3−SCR conditions at 200 °C.

VIII Presentation at Conferences

- R. K. Abasabadi, A. Y. Molokova, K. A. Lomachenko, P. N. R. Vennestrøm, F. Wen, T. V. W. Janssens, S. Bordiga, E. Borfecchia, G. Berlier. Following SO_2 poisoning of Cu^{I} and Cu^{II} on CHA zeolites for the NH_3-SCR reaction: an *in situ* UV-Vis study. **The 20th International Zeolite Conference (IZC2022)**, Valencia-Spain, 3rd to 8th July, 2022. (Poster)

- R. K. Abasabadi, A. Y. Molokova, K. A. Lomachenko, P. N. R. Vennestrøm, F. Wen, T. V. W. Janssens, S. Bordiga, E. Borfecchia, G. Berlier. Investigation of SO_2 poisoning of Cu species on CHA zeolites by Diffuse Reflectance UV-VIS NIR spectroscopy. **The 20th National Congress on Catalysis (GIC 2022)**, Riccione, Italy, 11th to 14th September, 2022. (Oral)

- R. K. Abasabadia, A. Y. Molokova, K. A. Lomachenko, P. N. R. Vennestrøm, F. Wen, T. V. W. Janssens, S. Bordiga, E. Borfecchia, G. Berlier. Effect of the Si/Al ratio on SO_2 poisoning of Cu-CHA zeolites studied by in situ DR UV-Vis spectroscopy and deactivation measurements. **The 7th International Congress on Operando Spectroscopy (Operando VII)**, Grindelwald-switzerland, 7th to 11th May, 2023. (Poster)

- R. K. Abasabadi1, P. N. R. Vennestrøm, F. Wen, S. Bordiga, E. Borfecchia, G. Berlier, T. V. W. Janssens. In situ SO_2 poisoning and deactivation measurements of Cu exchanged zeolite catalysts in NH_3-SCR reaction, **The 15th European Congress in Catalysis (EuropaCAT 2023)**, Prague, Czech Republic, 27th August to 1st September, 2023. (Oral)